NAVAL POSTGRADUATE SCHOOL
Monterey, California

THESIS

SOLID ROCKET MOTOR PLUME PARTICLE SIZE MEASUREMENTS USING MULTIPLE OPTICAL TECHNIQUES IN A PROBE

by

John R. Manser

March, 1995

Thesis Advisor: David W. Netzer

Approved for public release; distribution is unlimited.

DISCLAIMER NOTICE

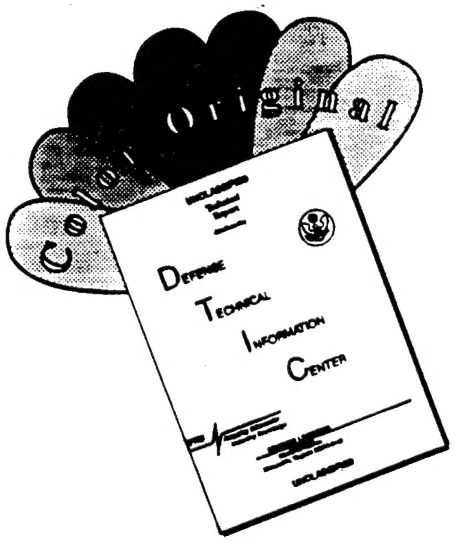

THIS DOCUMENT IS BEST QUALITY AVAILABLE. THE COPY FURNISHED TO DTIC CONTAINED A SIGNIFICANT NUMBER OF COLOR PAGES WHICH DO NOT REPRODUCE LEGIBLY ON BLACK AND WHITE MICROFICHE.

REPORT DOCUMENTATION PAGE

Form Approved OMB No. 0704-0188

1. AGENCY USE ONLY *(Leave blank)*	2. REPORT DATE	3. REPORT TYPE AND DATES COVERED
	March 1995	Master's Thesis

4. TITLE AND SUBTITLE
SOLID ROCKET MOTOR PLUME PARTICLE SIZE MEASUREMENTS USING MULTIPLE OPTICAL TECHNIQUES IN A PROBE

5. FUNDING NUMBERS
F04611-94-X-0516

6. AUTHOR(S)
Manser, John R.

7. PERFORMING ORGANIZATION NAME(S) AND ADDRESS(ES)
Naval Postgraduate School
Monterey CA 93943-5000

8. PERFORMING ORGANIZATION REPORT NUMBER

9. SPONSORING/MONITORING AGENCY NAME(S) AND ADDRESS(ES)
Air Force Phillips Laboratory, Edwards AFB, CA

10. SPONSORING/MONITORING AGENCY REPORT NUMBER

11. SUPPLEMENTARY NOTES
The views expressed in this thesis are those of the author and do not reflect the official policy or position of the Department of Defense or the U.S. Government.

12a. DISTRIBUTION/AVAILABILITY STATEMENT
Approved for public release; distribution unlimited

12b. DISTRIBUTION CODE

13. ABSTRACT *(maximum 200 words)* An experimental investigation to measure particle size distributions in the plume of sub-scale solid rocket motors was conducted. A phase-Doppler particle analyzer (PDPA) in conjunction with three-wavelength extinction measurements were used in a specially designed particle collection probe in an attempt to determine the entire plume particle size distribution. In addition, a laser ensemble particle sizer was used for comparative data. The PDPA and Malvern distributions agreed in the observed modes near 1 and 4.5 mm diameter (d). Scanning Electron Microscope (SEM) pictures of collected particles were in good agreement with the measured Malvern Sauter Mean diameter (d_{32}) of 2.59 mm. Data analysis indicate that less than 3% of the total mass of the particles was contained in particles with diameter $d < 0.5$ mm. Therefore, the PDPA, which can typically measure particles down to a minimum diameter of 0.5 mm with a dynamic range (d_{max}:d_{min}) of 50:1, can be used by itself to determine the particle size distribution. Multiple wavelength measurements were found to be very sensitive to inaccuracies in the measured transmittances.

14. SUBJECT TERMS	15. NUMBER OF PAGES
Particle Sizing, Solid Rocket Motors, Aluminum Oxide	111
	16. PRICE CODE

17. SECURITY CLASSIFICATION OF REPORT	18. SECURITY CLASSIFICATION OF THIS PAGE	19. SECURITY CLASSIFICATION OF ABSTRACT	20. LIMITATION OF ABSTRACT
Unclassified	Unclassified	Unclassified	UL

NSN 7540-01-280-5500

Standard Form 298 (Rev. 2-89)
Prescribed by ANSI Std. 239-18

Approved for public release; distribution is unlimited.

SOLID ROCKET MOTOR PLUME PARTICLE
SIZE MEASUREMENTS USING MULTIPLE
OPTICAL TECHNIQUES IN A PROBE

John R. Manser
Lieutenant, United States Navy
B.S., United States Naval Academy, 1986

Submitted in partial fulfillment
of the requirements for the degree of

MASTER OF SCIENCE IN ASTRONAUTICAL ENGINEERING

from the

NAVAL POSTGRADUATE SCHOOL
March 1995

Author: _____
John R. Manser

Approved by: _____
David W. Netzer, Thesis Advisor

_____
Oscar Biblarz, Second Reader

_____
Daniel J. Collins, Chairman
Department of Aeronautics and Astronautics

ABSTRACT

An experimental investigation to measure particle size distributions in the plume of sub-scale solid rocket motors was conducted. A phase-Doppler particle analyzer (PDPA) in conjunction with three-wavelength extinction measurements were used in a specially designed particle collection probe in an attempt to determine the entire plume particle size distribution. In addition, a laser ensemble particle sizer was used for comparative data. The PDPA and Malvern distributions agreed in the observed modes near 1 and 4.5 μm diameter (d). Scanning Electron Microscope (SEM) pictures of collected particles were in good agreement with the measured Malvern Sauter Mean diameter (d_{32}) of 2.59 μm. Data analysis indicate that less than 3% of the total mass of the particles was contained in particles with diameter $d < 0.5$ μm. Therefore, the PDPA, which can typically measure particles down to a minimum diameter of 0.5 μm with a dynamic range (d_{max}:d_{min}) of 50:1, can be used by itself to determine the particle size distribution. Multiple wavelength measurements were found to be very sensitive to inaccuracies in the measured transmittances.

TABLE OF CONTENTS

I. INTRODUCTION 1

II. BACKGROUND 5

A. PARTICLE SIZE DISTRIBUTIONS 5

B. NUMBER, SURFACE/AREA, AND VOLUME/MASS DISTRIBUTIONS 6

C. SAUTER MEAN DIAMETER D_{32} 7

D. LOG-NORMAL DISTRIBUTION FUNCTION 8

E. EXACT SOLUTION FOR THE LOG-NORMAL F(D) 11

F. MULTIPLE-WAVELENGTH EXTINCTION TECHNIQUE 13

III. EQUIPMENT DESCRIPTION & SETUP 19

A. ROCKET MOTOR 19

1. Propellants 20

2. Igniter 22

3. Nozzle 23

B. PROBE AND TUBES 24

C. WHITE LIGHT SOURCE AND DIODES 25

D. PDPA SYSTEM 26

E. DEFLECTOR 28

F. DATA ACQUISITION SOFTWARE & HARDWARE 28

G. MALVERN 2600 30

H. VIDEO CAMERA 30

IV. EXPERIMENTAL PROCEDURES 33

A. PHASE 1 FIRINGS 34

1. AC-14 10/24/94 34

2. AC-14 11/23/94 35

3. AC-14 12/8/94 35

4. AC-14 1/18/95 36

5. AC-14 2/8/95 36

B. PHASE 2 FIRINGS 37

1. PS-1 2/23/95 37

2. PS-1 2/25/95 37

3. PS-1 2/27/95 38

4. PS-1 3/1/95 38
5. PS-1 3/2/95 39
6. PS-1 3/3/95 39
7. PS-1 3/4/95 39
8. PS-1 3/5/95 39
9. PS-1 3/6/95 40
10. PS-1 3/7/95 40
V. RESULTS & DISCUSSION 43
A. MOTOR 43
B. EXPECTED RESULTS 44
C. MALVERN 46
D. PDPA 48
E. THREE-WAVELENGTH EXTINCTION 50
F. SEM ANALYSIS 53
VI. CONCLUSIONS 55
APPENDIX A. MICROPEP OUTPUT 57
APPENDIX B. PROBE DRAWINGS 61
APPENDIX C. MIE CODE "MIESCAT3.FOR" 65
APPENDIX D. MACRO FOR LOTUS 1-2-3 RELEASE 4 73
APPENDIX E. MIE CODE "MIESCAT6.FOR" 75
APPENDIX F. LINEAR INTERPOLATION IN LOTUS 1-2-3 RELEASE 4 ...83
APPENDIX G. DATA PRINTOUTS, PLOTS, AND TABLES 85
LIST OF REFERENCES 97
INITIAL DISTRIBUTION LIST 99

LIST OF FIGURES

1. Plot of Equations (2.11), (2.12), and (2.13) as PDF #1, #2, and #3 respectively. .. 11
2. Extinction Coefficients for Three Wavelengths. 16
3. Average Extinction Coefficients for Three Wavelengths and a Log-Normal Distribution. 16
4. Average Extinction Coefficient Ratios for Three Wavelengths and a Log-Normal Distribution. 17
5. Sub-Scale Motor. 19
6. Expected Ideal Pressure-Time Trace for PS-1. 24
7. Spectrum of Oriel Hg-Xe Light Source. 26
8. Equipment Setup for PDPA and Three-Wavelength Measurements. 28
9. LABTECH Notebook Data Acquisition and Experiment Control Program for PDPA and Three-Wavelength Extinction Measurements. 29
10. Malvern Data from PS-1 Firing 3/7/95. 85
11. PDPA Data from PS-1 Firing 3/2/95. 86
12. PDPA Data from PS-1 Firing 3/3/95. 88
13. PDPA Data from PS-1 Firing 3/4/95. 89
14. LABTECH Notebook Data Acquisition Program Plot of PS-1 Firing 2/25/95. ... 90
15. Normal Plot of PS-1 Firing 2/25/95. 91
16. Bare Light (No Probe) PS-1 Firing 3/5/95. 92
17. PS-1 Firing 3/6/95. 93
18. MATLAB Distribution Plots for "Small Particles". 94
19. Scanning Electron Microscope Pictures of Al_2O_3 Collected in the Probe. 95

LIST OF TABLES

1. Test Propellant AC-14 Specifications. 21
2. Operational Propellant PS-1 Specifications. 22
3. Nozzle Selection. 23
4. Summary of PS-1 Firings Used for Data Reduction. 43
5. Three-Wavelength Extinction Results. 51

I. INTRODUCTION

Solid rocket motors have used aluminum as a metallic fuel in composite and composite-modified double-base propellants for many years. Typically, 5 - 20 % of the mass of the propellant is contained in crystalline aluminum particles mixed with approximately 70 % ammonium perchlorate (AP) as an oxidizer. The remaining percent of the mass is contained in binders, plasticizers, or burning rate catalysts. Metallic fuels help performance as measured by an increased specific impulse I_{sp}. When metallic fuels combust, they react with the oxidizer and form metal oxides. For aluminum, the product oxide is Al_2O_3, also called alumina. These compounds are initially in the liquid phase at the high temperatures in the motor chamber, but then become solid with the temperature drop through the nozzle and into the plume.

In aluminized propellants the physical process of combustion has been under investigation for over thirty years. However, the generally accepted theory is as follows: An AP/binder flame starts the process. The 20 - 30 μm aluminum particles melt at 933 K on the propellant surface and sinter together forming much larger agglomerates but an oxide shell forms around the agglomerate and inhibits further combustion until the oxide's melting point is reached at 2327 K. These agglomerates detach the surface and enter the flame zone. There the oxide shell melts, allowing inner aluminum to vaporize as well as form more oxide. An oxide "cap" forms on one side. Thus, clouds of burning agglomerates, burning unagglomerated droplets, and product oxide droplets exist in the motor. When the droplets burn, the vaporized aluminum forms smoke oxide (diameters < 2 μm) that streams around the agglomerate. The larger droplets with their oxide cap form 5 - 150 μm residual oxide. Thus, any particle size distribution in the motor is expected to be bimodal. [Ref. 1-3]

As the particles pass through the nozzle various processes occur. Collision coalescence can cause larger particles to form, whereas, shattering produces just the opposite. It has been both measured and modeled that the larger particles entering the

exhaust nozzle cannot make the rapid turn at the throat, resulting in their being concentrated more along the plume centerline. The smaller particles are capable of turning with the gas flow and have been observed throughout the plume cross-section. Losses occur due to two-phase flow of liquid or solid particles and gas in the nozzle. These can be further defined in terms of thermal and velocity lag losses which vary with the size of particles. Thus, knowledge of the particle size distribution is important to determine these losses.

Besides determining losses, there are other reasons why particle size information is desired. Plume signature and flowfield codes, such as the SIRRM and SPF, require this information. Tactically, the Al_2O_3 in a missile plume makes the plume very opaque and visible, therefore leading to missile detection, tracking, and potentially targeting. For example, when viewing a Space Shuttle launch from several miles away, the plume emission of the Shuttle Rocket Booster (SRB)'s is highly visible but the huge columns of aluminum oxide exhaust are unforgettable. Size distribution information is also important for determining the available particle damping in the motor, slag formation, heat transfer, and nozzle flow computations [Ref. 1]. For example, Blomshield [Ref. 4] conducted dry combustion bomb experiments with SRB propellants containing different manufacturer's AP to evaluate the variation of the resulting Al_2O_3 size distribution between them and their impact on slag formation in the SRB's. This work was done as a result of the pressure anomaly during STS-54.

The properties of aluminum oxide are important for use with different particle sizing techniques and calculations. The optical properties of alumina, such as the index of refraction, are important for use in optical techniques as well as the previously mentioned computer codes. In the plume, both liquid and solid alumina can exist due to the range of temperature. The density of Al_2O_3 varies with temperature and phase. Reed [Ref. 2, p.9] lists the following two formulae for liquid and solid alumina respectively:

$$\rho_L = 2.98 - (1.13 \times 10^{-3})(T - 2327) \qquad \text{liquid} \tag{1.1}$$

$$\rho_S = 4.00 - (1.16 \times 10^{-4})T \qquad \text{solid} \tag{1.2}$$

where ρ is density in g/cc and T is temperature in K. Salita [Ref. 3, Figure 13] provides a plot of the variation of aluminum and alumina densities with temperature as well as their ratio. Regarding the complex index of refraction ($m = n - ik$), Reed [Ref. 2] reviewed others' results indicating a range for the Al_2O_3 n from 1.65 to 1.76. The complex part k, which is the index of absorption, has shown high variability but is almost zero for the solid phase in the plume. The liquid phase has a much higher k around 0.5 - 1.0 x 10^{-4} .

The Naval Postgraduate School (NPS) has been conducting research in the area of solid rocket motor particle sizing both in the motor and in the plume using various techniques for several years. Optical techniques have received the most attention since they offer the potential for obtaining particle information without disturbing the flow, i.e., they are non-intrusive. However, collection probes are sometimes required to limit the sample volume because the plume is too opaque for forward scattering measurements. Various optical techniques have been applied individually in different regions of the motor and plume. Each technique has a limited particle size measurement range. The present investigation used a phase-Doppler particle analyzer (PDPA) in conjunction with a three-wavelength extinction measurement in an attempt to determine the entire plume particle size distribution. In addition, a laser ensemble particle sizer was used for comparative data. The phase-Doppler and three-wavelength extinction measurements were made simultaneously in a particle collection probe. A composite propellant with 20% aluminum was used in a sub-scale motor to provide the particle-laden plume.

II. BACKGROUND

A. PARTICLE SIZE DISTRIBUTIONS

Particle size is usually represented by the diameter (in microns) of an equivalent size spherical particle. For a collection of particles, size information is often given in the form of a size or frequency distribution where frequency is plotted against particle diameter.

There are various types of frequency distributions depending upon the parameter of interest. Typically, this is number or mass and the distribution is termed either a number or mass distribution. Frequency is another loose term that can represent several things. For example, a number distribution could use frequency to mean actual number, normalized number, or number percent for a given diameter.

Due to experimental limitations, frequency is determined empirically for diameter intervals where diameter D is a continuous random variable. Other terms synonymous with diameter intervals are classes, class intervals, or size bins. The middle diameter in each class is sometimes called the class mark.

Classification of data leads to representation using a special type of bar chart known as a histogram. It uses adjacent rectangles where the base of each rectangle is along the abscissa and represents the minimum to maximum diameters of the particles in that class. The height of each rectangle corresponds to the ordinate and represents the frequency of the particles in that class. For histograms the frequency is usually given per diameter. For example, a number distribution would have as frequency the number percent in each class divided by the class width. The area of each rectangle then represents the number percent in the class. This is a very useful form because a probability density function (PDF) $p(d)$ can be fit to the histogram.

Synonymous terms for probability density function are probability function, density function, or distribution function. The PDF can be visualized as the smooth curve resulting from connecting the mid-points of the tops of the rectangles as the widths of the

rectangles (class widths) approach zero. The area under a PDF equals 1 or 100%, meaning the probability P that the diameter is between -∞ and +∞ is 100%. Symbolically $P(-\infty < D < +\infty) = 1$, or mathematically

$$\int_{-\infty}^{+\infty} p(D)\,dD = 1 \tag{2.1}$$

Since there are no particles with diameters less than zero, the lower limit can be set to zero. Similarly, the probability P that the diameter is between two arbitrary sizes *a* and *b* is just the area under the curve from *a* to *b* or

$$P(a < D < b) = \int_{a}^{b} p(D)\,dD \tag{2.2}$$

When the lower limit of the integral above is zero then the integral represents the probability P that the diameter is less than *b*. This has a special name: the cumulative probability function or cumulative distribution function *f*. For a distribution of particles, replacing *b* with *d*, this function *f*(*d*) represents the percent (or fraction) of particles less than diameter *d*. Mathematically,

$$f(d) = P(D \le d) = \int_{0}^{d} p(D)\,dD \tag{2.3}$$

B. NUMBER, SURFACE/AREA, AND VOLUME/MASS DISTRIBUTIONS

Some particle sizing techniques count particles and therefore determine a number distribution directly. Others, such as sieving, separate particles based upon their surface area, volume, or weight. Thus it is paramount to know what distribution a given technique will yield and to be able to compare these different distributions. Additionally, the total number, surface area, volume, mass, or weight of the particles in the distribution are used for comparison and analysis. When actual values are of interest as opposed to percent (e.g., number instead of number %), then the distribution function often differs from the PDF by a factor of the total parameter of interest (e.g., total number of particles

in the distribution). Take, for example, the number distribution $N(d) = N$ x PDF where N is the total number of particles in the distribution. The PDF is the number percent per diameter, and $N(d)$ is the number per diameter. Integration of $N(d)$ over all D results in N. Integration of $N(d)$ from d_1 to d_2 yields the number of particles between d_1 and d_2. Since the surface area of a sphere is πd^2, the surface or area distribution $S(d)$ corresponding to $N(d)$ is $S(d) = N(d)$ x πd^2 where $S(d)$ is the area per diameter. Similarly, the volume distribution $V(d)$ corresponding to $N(d)$ is $V(d) = N(d)$ x $\pi d^3 / 6$ where $V(d)$ is the volume per diameter. For a constant particle density, the mass distribution looks the same as the volume distribution and differs numerically by a factor representing the density. Corresponding area and volume or mass PDF's can be found by dividing $S(d)$ and $V(d)$ by S and V the total area and volume of particles in the distribution, respectively. The constants S and V can be found by integrating $S(d)$ and $V(d)$ over all D. Since $S(d)$ and $V(d)$ only differ from their corresponding PDF's by constants they have the same shape as the PDF's, just different values.

C. SAUTER MEAN DIAMETER D_{32}

Various diameters are used to compare distributions. They are referred to as mean, average, or equivalent diameters. Just as the different distributions are equivalent to $N(d)$ times d raised to some power, the mean diameters can be represented for a continuous distribution as

$$d_{pq} = \frac{\int_0^\infty N(D) D^p dD}{\int_0^\infty N(D) D^q dD} \tag{2.4}$$

or for a discrete distribution as

$$d_{pq} = \frac{\Sigma N(d) d^p \Delta d}{\Sigma N(d) d^q \Delta d} \tag{2.5}$$

where $N(d)$ is the number per class width Δd [Ref. 5]. One widely used mean diameter is the Sauter or Volume-Surface mean diameter d_{32}.

D. LOG-NORMAL DISTRIBUTION FUNCTION

In certain cases, such as ground particles, the histogram has a Gaussian or normal distribution shape when the frequency is plotted versus the logarithm of the diameter. When plotted on a linear scale the distribution is skewed or stretched to the right. Such a distribution is said to be log-normal.

Like a Gaussian or normal distribution, the log-normal distribution can be characterized by two parameters, the first quantifying the central tendency and the second determining the spread about this center. For a Gaussian distribution, these two parameters are the mean diameter d_m (or arithmetic mean d_{10}) and the standard deviation σ. Similarly, for a log-normal distribution these parameters are the geometric mean diameter d_g and the geometric standard deviation σ_g. Two other diameters are sometimes used to describe central tendency: the median and the mode. The median splits the distribution in two by number of samples. In probability terms, if all the N sampled particles are put in order of increasing size and assigned a number, called the rank (from one to N), then the median diameter is that of the particle with rank $(N + 1)/2$. On the other hand the diameter with the highest frequency, i.e., the peak of the distribution, is termed the mode diameter. The number of peaks can be specified by referring to the distribution as monomodal, bimodal, or trimodal. It is important to note that d_m is also the median and the mode diameter for a normal distribution. However, for a log-normal distribution d_g is also the median diameter, but is neither the mode nor the mean. For a log-normal distribution:

$$d_M = d_g \exp(-\ln^2 \sigma_g) \tag{2.6}$$

$$d_m = d_g \exp(0.5 \ln^2 \sigma_g) \tag{2.7}$$

where d_M is the mode diameter and d_m is the mean diameter [Ref. 6].

For a log-normal distribution of particles, the other representative distributions (i.e., number, surface area, or volume/mass) are also log-normal with the same σ_g. However, each distribution has a different d_g. To differentiate between them it helps to use an additional subscript. For example, d_{gn} refers to a number distribution whereas d_{gm} refers to a mass distribution. In some sources, count with a subscript *c* is used instead of number. The Hatch-Choate Equations relate the various d_g's. One of these is

$$d_{gn} = d_{gm}\exp\left[-3\ln^2(\sigma_g)\right] \tag{2.8}$$

The following relation is also helpful in relating the various mean diameters to d_g.

$$d_{pq} = d_{gm}\exp\left[\frac{p+q-6}{2}\ln^2(\sigma_g)\right] \tag{2.9}$$

$$= d_{gn}\exp\left[\frac{p+q}{2}\ln^2(\sigma_g)\right] \tag{2.10}$$

Since different distributions are of interest to different researchers, rather than discussing several d_g's it is easier to use a mean diameter such as d_{32}. Note: one aspect of d_{32} can be counterintuitive. As one might expect for a given d_{gn}, as σ_g increases the number distribution is skewed more to the right and d_{32} increases. However, if d_{32} is held constant and σ_g increased d_{gn} *decreases* and the number distribution shifts *left*, becoming less skewed to the right. The mass geometric mean d_{gm}, however, still increases and the volume/mass distribution is more skewed to the right.

Sometimes log-normal distributions are plotted on log-probability paper since $f(d)$ plots as a straight line with slope σ_g. The geometric mean d_g is readily identified since it corresponds to an ordinate value of 0.5 or 50%. All the distributions, i.e., number, area, and volume, plot as parallel lines. If the distribution is bimodal rather than monomodal, then it has an s-shape between the two lines making up the individual modes. The

drawback to the log-probability plot is its unavailability in standard plotting software such as spreadsheets. According to the MathWorks however, such a plotting function is available for MATLAB in their Statistics Toolbox.

Several forms of the log-normal distribution function are presented in the literature. Three forms are listed below:

$$p(d) = \frac{1}{\sqrt{2\pi}\,\sigma_g d} \exp\left\{-\left[\frac{\ln(d/d_g)}{\sqrt{2}\,\sigma_g}\right]^2\right\} \tag{2.11}$$

$$p(d) = \frac{1}{\sqrt{2\pi}\,\log(\sigma_g) d} \exp\left\{-\left[\frac{\log(d/d_g)}{\sqrt{2}\,\log(\sigma_g)}\right]^2\right\} \tag{2.12}$$

$$p(d) = \frac{1}{\sqrt{2\pi}\,\ln(\sigma_g) d} \exp\left\{-\left[\frac{\ln(d/d_g)}{\sqrt{2}\,\ln(\sigma_g)}\right]^2\right\} \tag{2.13}$$

Some sources use a version of one of the three equations above without the d in the denominator. [Ref. 6-10]

It is therefore important to determine the correct form. Three criteria are used to check them:

1. Integration of the PDF (area under the curve) from $d = 0$ to $+\infty$ must equal one (i.e., $f(+\infty) = 1$).
2. Using $f(d)$, the ratio of $d_{84\%}$ (d where $f(d) = 0.84$ or 84%) over $d_{50\%}$ (d where $f(d) = 0.50$ or 50%) must equal σ_g.
3. The function must behave as depicted in references for different values of d_g and σ_g.

MATLAB can be used for analysis. The functions QUAD and QUAD8 performed numerical integration, although an exact solution for $f(d)$ is available for Equations (2.11) and (2.13) as described in the next section. Figure 1 shows a plot of Equations (2.11) to (2.13). All three equations without the d in the denominator fail criterion 1. However, it should be noted that some sources integrate the PDF with respect to $\ln(d)$ vice d. This is

the same as integrating a PDF, with a d in the denominator, with respect to d since $d[\ln(D)] = (1/D)dD$ in differential form. As is, Equation (2.12) fails criterion 1 as is readily apparent by inspecting the figure. Equation (2.11) fails criterion 2. Equations (2.11) and (2.12) fail criterion 3. Equation (2.13) passes all criteria and thus was used in the analytical work. Note however that Equation (2.11) is a PDF and fits in as Kerker [Ref. 6, p. 357] describes "a family of logarithmically skewed distributions". [Ref. 6]

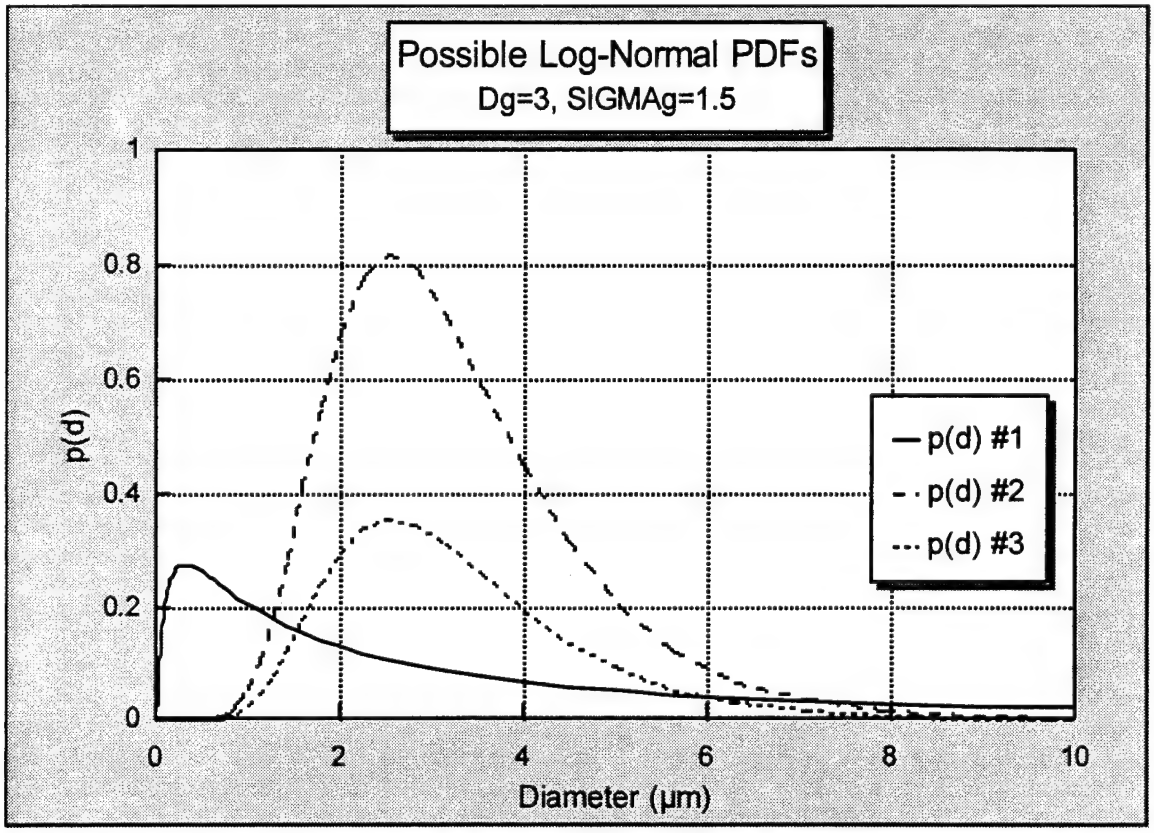

Figure 1. Plot of Equations (2.11), (2.12), and (2.13) as PDF #1, #2, and #3 respectively.

E. EXACT SOLUTION FOR THE LOG-NORMAL F(D)

The general form of the log-normal distribution function is

$$p(d) = \frac{1}{\sqrt{2\pi}\,\beta d} \exp\left\{-\left[\frac{\ln(d)-\alpha}{\sqrt{2}\,\beta}\right]^2\right\} \qquad (2.14)$$

where β and α are constants [Ref. 10]. Most often, for solid rocket motor particle sizing $\beta = \ln(\sigma_g)$ and $\alpha = \ln(d_g)$ as in Equation (2.13). Although numerical integration techniques can be used to obtain an approximate $f(d)$, there is an exact solution using the error function erf(x).

$$\operatorname{erf}(x) \triangleq \frac{2}{\sqrt{\pi}} \int_0^x \exp(-t^2)\, dt \tag{2.15}$$

and using Equations (2.3) and (2.14)

$$f(d) = \int_0^d \frac{1}{\sqrt{2\pi}\,\beta D} \exp\left\{-\left[\frac{\ln(D)-\alpha}{\sqrt{2}\,\beta}\right]^2\right\} dD \tag{2.16}$$

By letting

$$t = \frac{\ln(D)-\alpha}{\sqrt{2}\,\beta} \tag{2.17}$$

then

$$dt = \frac{1}{\sqrt{2}\,\beta D}\, dD \tag{2.18}$$

and the limits of integration are

$$t = \lim_{D\to d}\left[\frac{\ln(D)-\alpha}{\sqrt{2}\,\beta}\right] = \frac{\ln(d)-\alpha}{\sqrt{2}\,\beta} \qquad \text{upper limit} \tag{2.19}$$

$$t = \lim_{D\to 0}\left[\frac{\ln(D)-\alpha}{\sqrt{2}\,\beta}\right] = -\infty \qquad \text{lower limit} \tag{2.20}$$

Therefore,

$$f(d) = \int_{-\infty}^{\frac{\ln(d)-\alpha}{\sqrt{2}\,\beta}} \frac{1}{\sqrt{\pi}} \exp(-t^2)\,dt \tag{2.21}$$

$$= \frac{1}{\sqrt{\pi}} \int_{-\infty}^{0} \exp(-t^2)\,dt + \frac{1}{\sqrt{\pi}} \int_{0}^{\frac{\ln(d)-\alpha}{\sqrt{2}\,\beta}} \exp(-t^2)\,dt \tag{2.22}$$

Since

$$\int_{-\infty}^{+\infty} \exp(-t^2)\,dt = \sqrt{\pi} \tag{2.23}$$

and $\exp(-t^2)$ is an even function, i.e., symmetric about the ordinate, then

$$\frac{1}{\sqrt{\pi}} \int_{-\infty}^{0} \exp(-t^2)\,dt = \frac{1}{\sqrt{\pi}} \int_{0}^{+\infty} \exp(-t^2)\,dt = \frac{1}{2} \tag{2.24}$$

Using this and the definition of the error function, then

$$f(d) = \frac{1}{2} + \frac{1}{2}\,\mathrm{erf}\left[\frac{\ln(d)-\alpha}{\sqrt{2}\,\beta}\right] = \frac{1}{2}\left\{1 + \mathrm{erf}\left[\frac{\ln(d)-\alpha}{\sqrt{2}\,\beta}\right]\right\} \tag{2.25}$$

[Ref. 11]. Thus for solid rocket motor particle sizing

$$f(d) = \frac{1}{2}\left\{1 + \mathrm{erf}\left[\frac{\ln(d/d_g)}{\sqrt{2}\,\ln(\sigma_g)}\right]\right\} \tag{2.26}$$

F. MULTIPLE-WAVELENGTH EXTINCTION TECHNIQUE

Cashdollar [Ref. 12] discusses the use of light extinction measurements for extracting particle size distribution parameters. Light entering a cloud of particles is absorbed, scattered, and transmitted. Transmittance T is the ratio of transmitted intensity to incident intensity. Light extinction is the sum of absorption and scattering. When Mie theory is applied to light scattered by single spherical particles the extinction coefficient Q can be determined as a function of wavelength λ, particle diameter d, and complex

index of refraction $m = n - ik$ (k is the absorption index). Bouguer's law provides the transmittance through a monodisperse (single size) distribution of particles:

$$T = \exp\left[-\left(\frac{3QC_mL}{2\rho d}\right)\right] \tag{2.27}$$

where

T = transmittance
Q = dimensionless extinction coefficient
C_m = mass concentration of particles (mass of particles per volume of gas)
L = path length through the cloud of particles
ρ = particle density
d = particle diameter

The volume concentration of particles C_v (volume of particles per volume of gas) can be related to C_m by

$$C_v = \frac{C_m}{\rho} \tag{2.28}$$

To obtain accurate values for extinction, it is necessary to have the detector not see forward scattered light. An approximation for the required detector viewing half angle $\theta_{\frac{1}{2}}$ to satisfy this requirement is [Ref. 12]

$$\theta_{\frac{1}{2}} \leq 7.0\frac{\lambda}{d} \tag{2.29}$$

Dobbins revised the Bouguer transmission law to apply to a polydisperse system (many sizes) [Ref. 12]:

$$T = \exp\left[-\left(\frac{3\bar{Q}C_mL}{2\rho d_{32}}\right)\right] \tag{2.30}$$

where $\bar{Q}$ is the average extinction coefficient, found for a continuous distribution by

$$\bar{Q} = \frac{\int_0^\infty Q(D)N(D)D^2 dD}{\int_0^\infty N(D)D^2 dD} \tag{2.31}$$

or for a discrete distribution by

$$\bar{Q} = \frac{\Sigma Q(d)N(d)d^2 \Delta d}{\Sigma N(d)d^2 \Delta d} \tag{2.32}$$

Since $\bar{Q}$ depends upon the distribution, then for a log-normal distribution it is a function of d_{32}, σ_g, λ, and m. Taking the natural logarithm of both sides of Equation (2.30) and ratioing two equations for different wavelengths results in

$$\frac{\ln T(\lambda_1)}{\ln T(\lambda_2)} = \frac{\bar{Q}(\lambda_1)}{\bar{Q}(\lambda_2)} \tag{2.33}$$

This is the basis of the multiple-wavelength technique. Transmittances for different wavelengths of light passing through the same volume of particles over identical path lengths are experimentally measured. A Mie code is used to generate $\bar{Q}$'s for the set wavelengths and for various values of d_{32}, σ_g, and m. Then, using Equation (2.33) the ratios can be compared and further iterations performed as necessary to determine the best values of d_{32}, σ_g, and m. The more wavelengths used the more ratios to compare and, presumably, the more accurate the method. The number of ratios for a set of n wavelengths is equal to the sum of integers less than n (e.g., for six wavelengths there are $1 + 2 + 3 + 4 + 5 = 15$ ratios). Note that the number of independent ratios is only $n - 1$ (e.g., five for six wavelengths). The accuracy of the method is also increased by spreading the wavelengths across the spectrum [Ref. 13]. To determine d_{32}, σ_g, and $m = n - ik$ (4 variables) a minimum of four independent ratios are required. Figures 2, 3, and 4 show plots of the Mie code Q's, $\bar{Q}$'s, and $\bar{Q}$ ratios for the three wavelengths used in the experiments and an assumed log-normal distribution. Notice from Figure 4 that as d_{32} increases the $\bar{Q}$ ratios flatten out. For this reason the technique does not work for distributions with lots of mass in large particles.

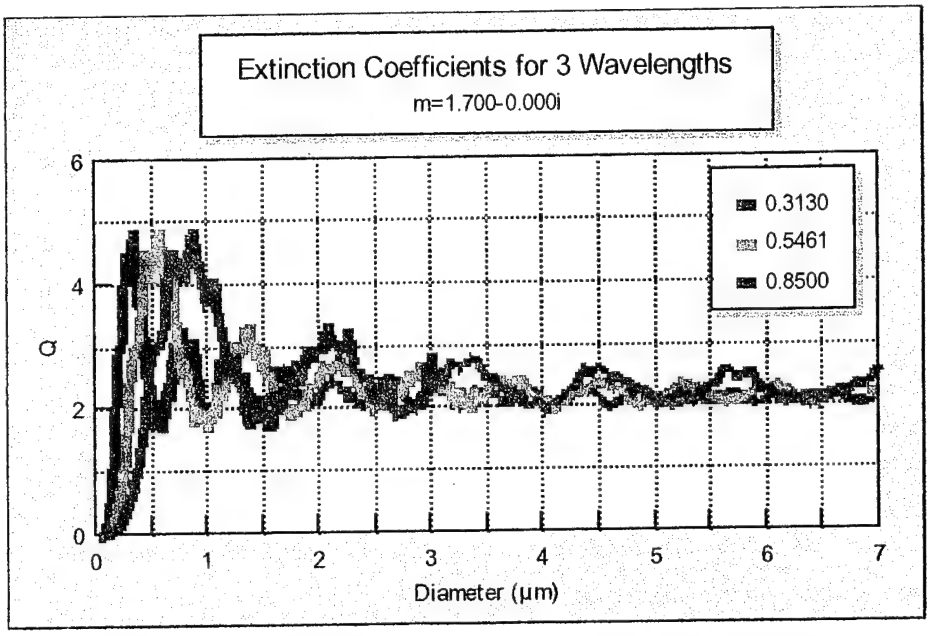

Figure 2. Extinction Coefficients for Three Wavelengths.

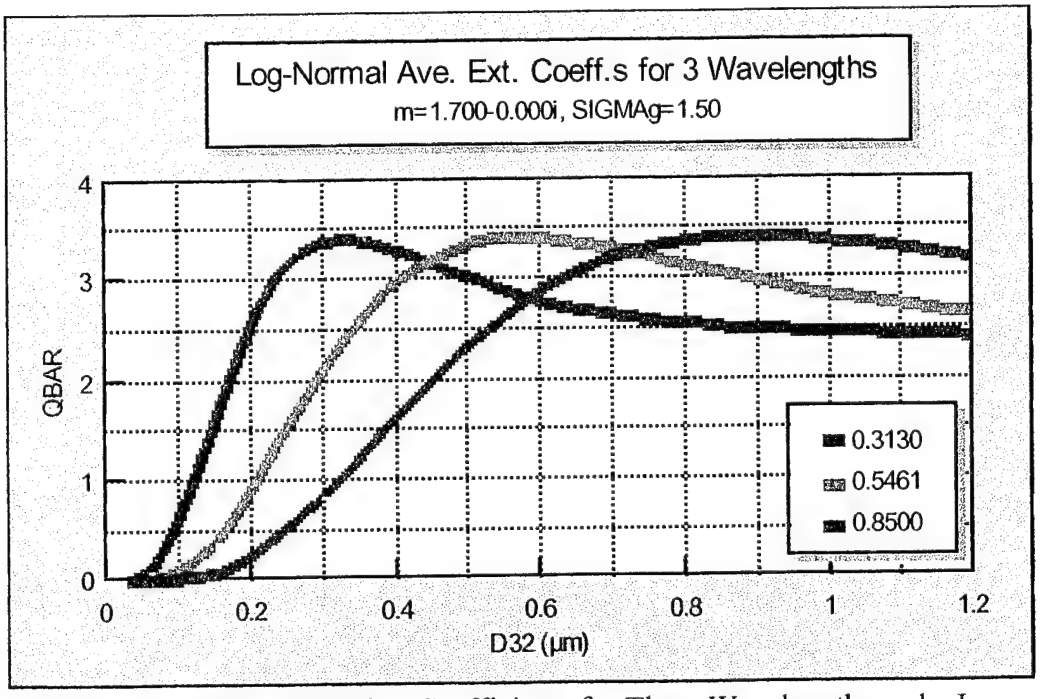

Figure 3. Average Extinction Coefficients for Three Wavelengths and a Log-Normal Distribution.

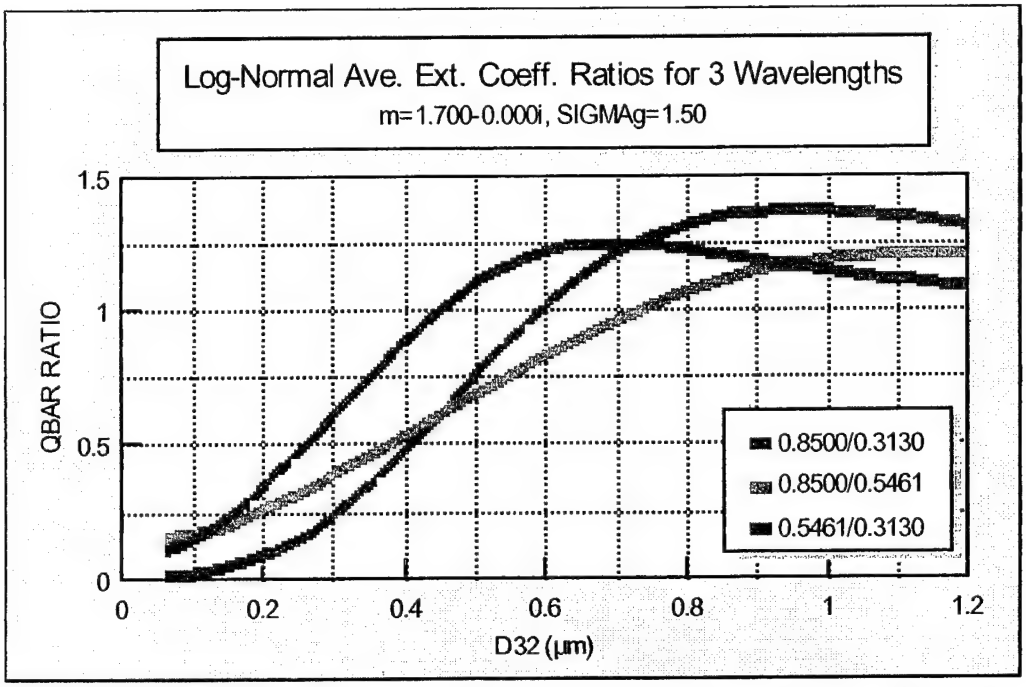

Figure 4. Average Extinction Coefficient Ratios for Three Wavelengths and a Log-Normal Distribution.

III. EQUIPMENT DESCRIPTION & SETUP

A. ROCKET MOTOR

For all of the test firings, a sub-scale motor was used as shown in Figure 5. The motor consists of a stainless steel cylindrical chamber with a 2" inside diameter, 0.625" wall thickness, and overall length of 9.25". The head of the chamber is closed off by a 1" thick end plate with rubber o-ring seal and secured by six bolts. The nozzle end of the chamber has a slightly larger inside diameter to allow the nozzle insert to slide in place, and is sealed by another end plate and six bolts. A simple converging-diverging nozzle insert is used. Gas leakage around the nozzle is prevented by the use of two o-rings fit into grooves around the exterior of the nozzle insert. A pressure transducer and pressure relief fitting are screwed into the chamber. Prior to motor firing, a hydraulic dead-weight tester is used to determine the calibration slope and zero for the pressure transducer. The pressure relief fitting consists of a steel elbow with a 1000 psia burst disk. The propellant is bonded to the head-end plate and inner chamber wall using Permatex High Temp RTV. The igniter consists of a 3/8" steel bolt, described below, that is screwed into the optimum

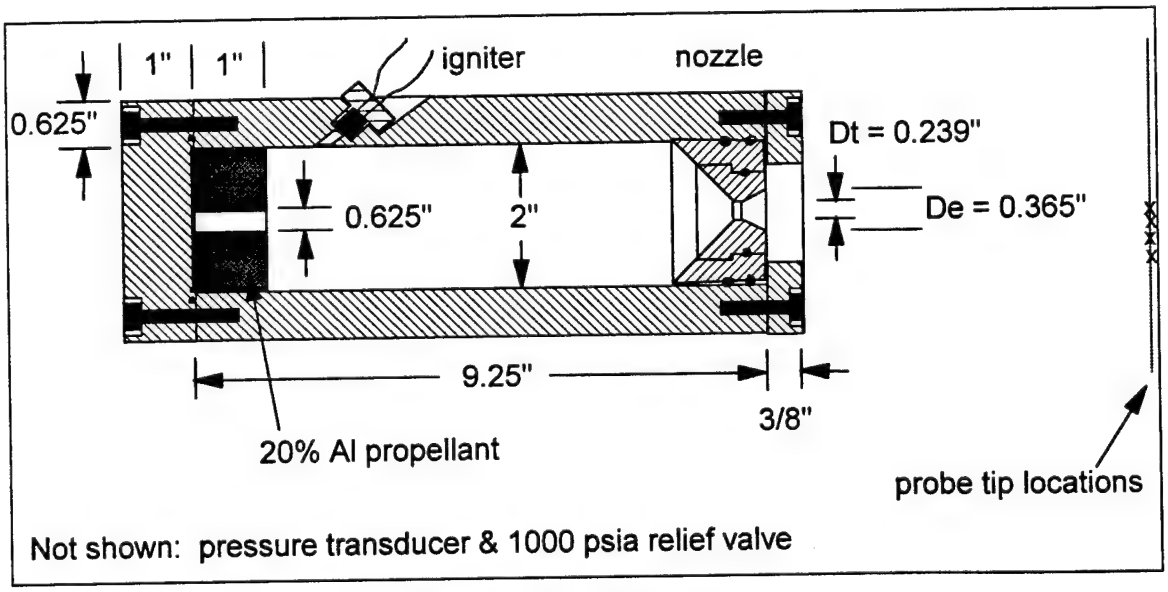

Figure 5. Sub-Scale Motor.

of four available holes angled toward the head of the chamber. The remaining holes are filled with standard bolts. All o-rings are lubricated with Dow High Vacuum Grease.

1. Propellants

Two different propellants provided by the Air Force Phillips Laboratory were used. A 1" thick and approximately 2" diameter propellant grain was cut from the stock using a large knife, then the desired cutouts were made using a three-piece steel cutting tool and a press. The tool could make 0.6" I.D., 1.4" O.D., 1.5" I.D. and 2" O.D. cutouts. The grain geometry was chosen to optimize the burning surface area A_b for a neutral burn with a chamber pressure of at least 250 psia lasting for about one second. RTV was used to bond each grain in the motor as well as to inhibit certain surfaces from burning.

For testing of the experimental setup, especially the three-wavelength apparatus, several firings were conducted using a propellant (AC-14) that was on hand. Its composition is shown in Table 1. It was undesirable for data analysis due to the silicon which caused oxides of silicon or aluminum together with mullite in the exhaust. To achieve the desired performance several grain configurations were tried. Initially, a single 1" thick end-burning grain (2" O.D.) was tried, then two 1" thick grains were tried, one end-burning (1.4" O.D.), the other radial- and end-burning (1.5" I.D., 2" O.D.). Finally, good performance was obtained using two 1" thick radial- and end- burning grains. The first had a 2" O.D. and a 1.5" I.D. (0.25" web). RTV was used to inhibit the downstream end and bond the grain to the chamber wall just downstream of the igniter hole. The second grain was cut from the center of the first. It had a 1.4" O.D. and a 0.6" I.D. (0.4" web). RTV was used to bond the upstream surface to the endplate and to inhibit the outer radial surface.

ID	AC-14
Composition: AP	67.15%
Al	12.0%
R45M	10.14%
Si	6.0%
Dioctyl Adipate	3.91%
IPDI	0.78%
Triphenyl Bismuth	0.02%
Density (lbm/in^3)	$\rho_p = 0.06$
Burning rate pressure coefficient	a = 0.0086
Burning rate pressure exponent	n = 0.566
Characteristic exhaust velocity (ft/s)	$c^* = 4957$

Table 1. Test Propellant AC-14 Specifications.

As previously mentioned aluminized propellants have been the subject of particle sizing for the past thirty years. Therefore, it was desired to obtain such a propellant since various parameters are better known (e.g., particle index of refraction) and this enables comparison to past research. The USAF Phillips Lab provided four propellants, all of which were class 1.3, conventional composites. The one selected for this thesis research was PS-1. Its composition (by mass %) and characteristics are listed in Table 2. Initially, a single 1" thick end-burning grain (2" O.D.) was tried; however, the required small nozzle throat diameter and propellant's high aluminum content resulted in clogging of the throat. A single perforated end- and radial-burning grain was then chosen and used for the remainder of the research. It was 1" thick with a 2" O.D. and a 0.625" I.D.

ID	PS1
Composition: AP (coarse)	50% 200μm
AP (fine)	20%
Al	20%
HTPB	10%
Density (lbm/in^3)	$\rho_p = 0.0667$
Burning rate pressure coefficient	a = 0.0328
Burning rate pressure exponent	n = 0.376
Characteristic exhaust velocity (ft/s)	$c^* = 5119$

Table 2. Operational Propellant PS-1 Specifications.

2. Igniter

Each pyrotechnic squib igniter was processed as follows: First, a hollow 3/8" steel bolt had two holes drilled in the bolt head to accomodate the lead wires. Two approximately 8" long copper lead wires were then cut and some insulation was stripped off both ends with an X-Acto knife. The wires were passed through the holes and then a small piece of nickel-chromium wire was soldered (using ruby flux and pure solder) to the ends leaving about a 1/16" gap. Next, the wire bridge was pulled inside the cavity in the bolt and the bolt head was epoxied on the outside to secure the wires. After the epoxy had dried the cavity was filled with $BKNO_3$ and a paper hole from a hole punch was glued on the end with Elmer's Glue. Continuity checks were performed at various times in the process to verify that the wires were not shorted by touching the inside of the bolt.

For firing the igniter, lead wires were connected to a 12 volt battery with battery charger and a firing button in the control room. When the firing circuit was completed by depressing the button, the heat dissipated in the nickel-chromium bridge wire flashed the $BKNO_3$. The burning matter burst through the paper hole and impacted the grain, thereby initiating propellant combustion.

3. Nozzle

A copper nozzle insert was selected to obtain reasonable chamber pressure. The following steady-state mass conservation equation was used:

$$p_c = \left[\left(\frac{A_b}{A_t} \right) \frac{\rho_p a c^* \eta_{c^*}}{g_c} \right]^{\frac{1}{1-n}} \tag{3.1}$$

where

p_c = chamber pressure
A_b = burning surface area
A_t = nozzle throat area
ρ_p = propellant density
a = burning rate pressure coefficient
c^* = characteristic exhaust velocity
η_{c^*} = characteristic exhaust velocity efficiency
g_c = gravitational constant (for English units)
n = burning rate pressure exponent

The MICROPEP computer program [Ref. 14] was run with the propellant ingredients to obtain ρ_p and c^*. See the output in Appendix A. Based upon previous results, the efficiency η_{c^*} was assumed to be 0.9. Then, the available nozzle throat areas were substituted to calculate p_c. Due to clogging of the throat from the high aluminum content, the largest A_t that would yield $p_c \geq 250$ psia was selected. The copper nozzles were converging-diverging and Table 3 shows the selection that was available.

For initial testing with propellant AC-14 several nozzles were used. The

d_t (in)	0.207	0.340	0.239	0.165	0.452	0.216	0.270	0.200	0.208	0.268	0.286
d_e (in)	0.378	0.440	0.365	0.230	0.662	0.395	0.808	0.368	0.425	0.500	0.322
$\varepsilon = A_e/A_t$	3.335	1.675	2.332	1.943	2.145	3.344	8.956	3.386	4.175	3.481	1.268
Con/Di (deg)	45/15	45/15	45/15	45/15	45/15	45/15	???	???	???	45/15	???

Table 3. Nozzle Selection Where d_t is the Nozzle Throat Diameter, d_e is the Nozzle Exit Diameter, ε is the Nozzle Area Ratio, and Con/Di are the Nozzle Converging and Diverging Half-Angles Respectively.

d_t = 0.165" nozzle was tried with the single end-burning grain and resulted in twice the expected p_c, probably due to clogging. Next, the first two-grain configuration was paired with the d_t = 0.239" nozzle and resulted in a progressive initial burn and a long low p_c tail-off. Finally, the second two-grain configuration was paired with the d_t = 0.268" nozzle with good results.

For the PS-1 firings, two nozzles were used. The d_t = 0.207" nozzle was tried with the single end-burning grain but clogging caused a highly progressive burn. For use with the single end- and radial-burning grain, the d_t = 0.239" nozzle was chosen and Figure 6 shows the expected ideal performance. The actual performance resulted in a higher chamber pressure of about 350 psia. Post-firing inspection of the nozzle revealed a fairly uniform layer of Al_2O_3 reducing d_t to about 0.15".

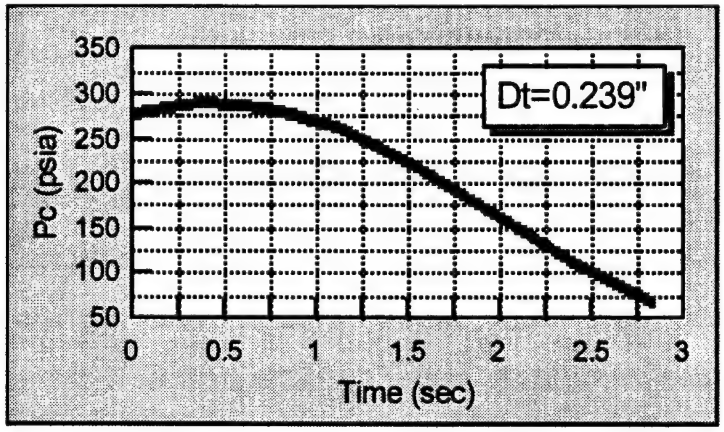

Figure 6. Expected Ideal Pressure-Time Trace for PS-1.

B. PROBE AND TUBES

A particle collection probe that consists of a narrow, hollow steel box with a conical tip for swallowing a portion of the plume exhaust was previously developed [Ref. 20]. The design of the probe was to swallow the normal shock, forming weaker, internal oblique shocks that would not break up the particles. It was positioned to avoid Mach disk locations. Windows on either side had been used with optical sizing techniques and a filter on the downstream end had been used to collect particles for scanning electron microscope (SEM) analysis. For the current uses, the windows were removed and steel

tubes added on the sides to enclose the PDPA beams and to vertically enclose the Hg-Xe beam described below. The insides of the tubes were spray-painted flat black. To protect from burnthrough, an additional steel plate was welded on the funnel side tube. To ensure that the PDPA lenses would not be coated by exhaust, circular plate glass was taped in the ends of the side tubes. A nitrogen line with a sonic choke was connected to the probe and provided an ejector flow around the probe tip where it exhausted into the probe body. The back pressure in the probe was regulated to provide and approximate isokinetic sampling condition. For some runs particles were wiped from the inside of the box for SEM analysis. RTV was put on parts of the front of the probe body for thermal protection. See the diagrams in Appendix B.

C. WHITE LIGHT SOURCE AND DIODES

An Oriel Model 66002 Hg-Xe arc lamp with a f/1 condensing lens and 200 W power supply was used as the light source. It was mounted below the lab table and a magnetically held mirror was positioned to reflect the beam up through a 1/2" diameter hole in the table. From the top of the table, tubing enclosed the beam up into the probe and above the probe to the diode box. Both tubes were spray-painted flat black inside. The lower tube had a 0.5" O.D. and 7/16" I.D. and a collar adapted it to the probe's lower vertical tube O.D. A larger upper tube (1" O.D., 7/8" I.D.) was used to cut down on internal reflection and was fit over the probe's upper vertical tube. The diode box contained an adjustable pinhole, two beamsplitters, three EG&G Model HUV-4000B diodes, each with a Melles Griot narrow band interference filter (0.01 μm bandwidth) to measure wavelengths 0.3130, 0.5461, or 0.8500 μm, neutral density filters, and an NPS-built preamplifier for the diodes. The pinhole and neutral density filters were adjusted to get as high an output voltage as possible but less than 10 volts (LABTECH Notebook limitation; the diodes saturated near 15 volts). The total length from the condensing lens to each diode was about 80". From the probe center to the diode pinhole was about 36". Therefore, since the pihole was open to about $d = 0.19$" the detector viewing half-angle was about 0.15°, easily satisfying the requirement of Equation (2.29).

For one run a light chopper was used between the arc lamp and mirror. Figure 7 (lower curve) shows the spectral irradiance from 0.200 to 0.900 μm of the light source and the bandpass filter locations.

D. PDPA SYSTEM

The Aerometrics Phase Doppler Particle Analyzer (PDPA) system consists of a laser transmitter, receiver, doppler signal analyzer (DSA), and computer digital signal processor (DSP) and software. A Lexel Model 95-4 argon ion laser, tuned to 0.5145 μm and operating at 2 W, with beam waist adjustor, polarization rotator, and steering mirrors provided the input beam to the transmitter. The transmitter uses a Bragg cell to split the incoming laser beam into two beams of equal intensity, a Zero order beam and a 40 MHz shifted First order beam, then bends the beams with prisms and mirrors and converges them with the exit lens. The beams converge until they cross, forming an ellipsoidal Gaussian volume, approximately 10" in front of the transmitter. When a particle passes through the crossing volume, light is scattered. For particles with $d > 0.5$ μm this is

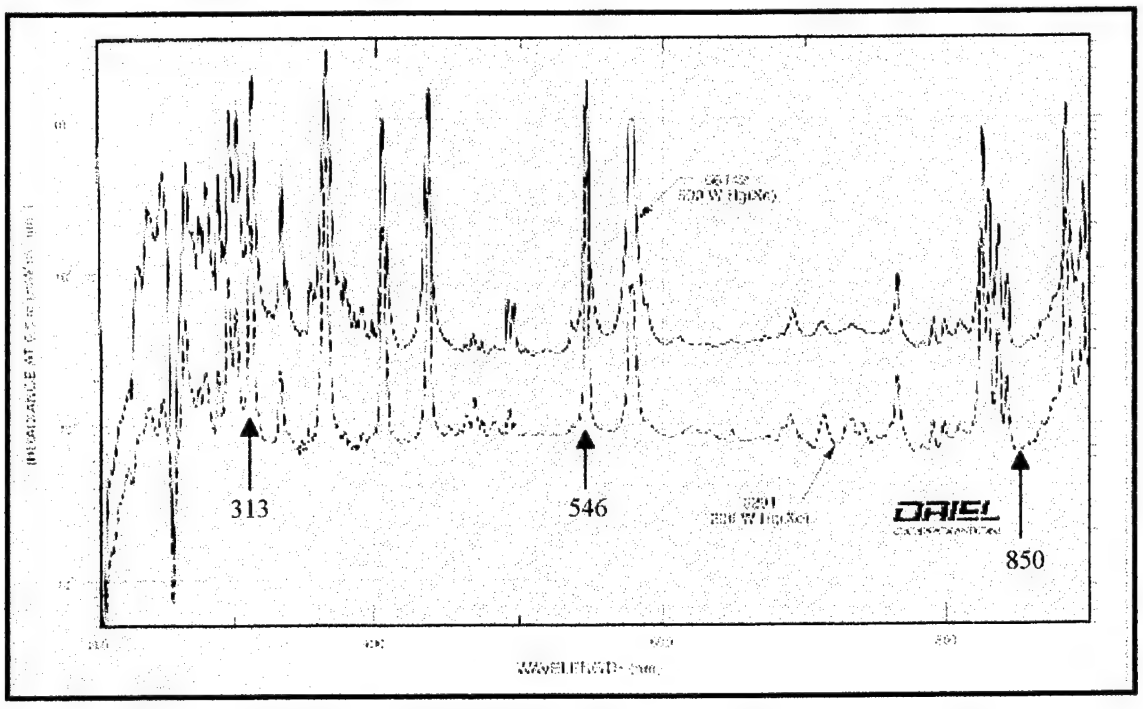

Figure 7. Spectrum of Oriel Hg-Xe light source. [Ref. 15, p. 1-41, fig. 8]

scattering in the Mie and geometric optics regimes of scattering. To simplify processing the system assumes only the geometric optics regime applies. The receiver, consisting essentially of optics and photo multiplier tubes, is positioned at a predetermined optimum angle to collect a portion of the scattered light. Aerometrics ran simulations, given estimated particle indices of refraction for different motor locations, to determine this optimum angle for a linear phase response over the range of particle diameters. They found that a scattering angle of 130° (backscatter or reflection) was best for through-the-chamber particle sizing and a scattering angle of 45° (forward scattering or refraction) was best for through-the-plume measurements as presented in this paper. The receiver was mounted on a support at a 45° angle and approximately 8" from the crossing volume. The horizontal tubes of the probe were designed to fit around the collars of the transmitter and receiver. [Ref. 16]

Data acquisition and processing was done with a personal computer (PC) and the DSA. The DSP was located in the PC and was used to quickly perform discrete and fast Fourier transforms on the data. The DSA performed several functions. It provided the input to the transmitter to create the two beams and conducted calibration and data processing. The software created the user interface through menus for setup, calibration, data acquisition, processing, display, and storage. The PDPA was externally triggered to take data through the LABTECH Notebook program run on a separate PC as described below. [Ref. 16]

The PDPA software rejects particles for various reasons. The most important ones for this paper are multiple particles and undersize particles. Only single particles can be accurately accounted for, therefore if the system detects multiple particles that sample is rejected. Particles with diametersas small as approximately 0.2 μm are detected but if less than 0.5 μm they are rejected by the system. No information is available for particles less than 0.2 μm since the scattered light intensity is too low to be detected. The PDPA has Probe Volume Correction (PVC) that allows for correcting the measured distribution for the smaller particles. However, at least 100 valid samples must be taken

Figure 8 shows the experimental setup for the PDPA and three- wavelength extinction measurements in the probe.

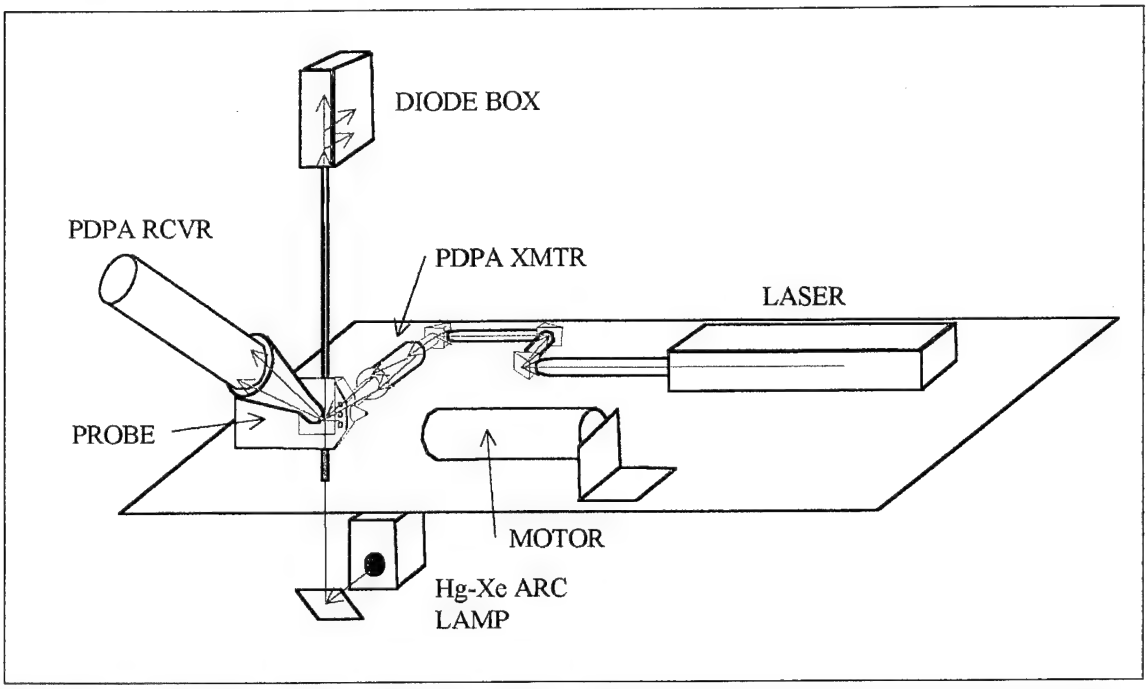

Figure 8. Equipment Setup for PDPA and Three-Wavelength Measurements (Deflector, Video Camera, and Supporting Hardware Not Shown).

E. DEFLECTOR

A pneumatically actuated, computer controlled steel deflector plate was positioned between the motor nozzle and probe. Its purpose was to protect the probe and only allow exhaust entry into the probe during steady burning (i.e., the plateau of the chamber pressure-time trace for a neutral burning grain). Some firings burned holes through the plate, requiring repair by welding and reinforcement.

F. DATA ACQUISITION SOFTWARE & HARDWARE

A 486DX/33 MHz PC controlled the experiment through a Windows™ application known as LABTECH Notebook. Icon blocks, representing analog and digital input or output devices, with connecting arrows were used in the software to visualize the control of equipment and the flow of data. See Figure 9. Each icon block could be

opened to set various parameters. When the data acquisition file was run the following events were executed:

1. The diode and pressure transducer outputs were recorded for the entire run (20 seconds),
2. The nitrogen ejector flow was turned on from 2 to 18 seconds,
3. An audio signal was sent to the videorecorder at 0.5 seconds as a time reference,
4. When the motor chamber pressure reached 100 psia a 1 second delay occurred, then the deflector was triggered to slide out of the way (for 0.7 seconds) and the PDPA was triggered to take data 0.25 seconds later, and
5. At the termination of the run the clock, chamber pressure, three diodes, and deflector position data were output to a separate file.

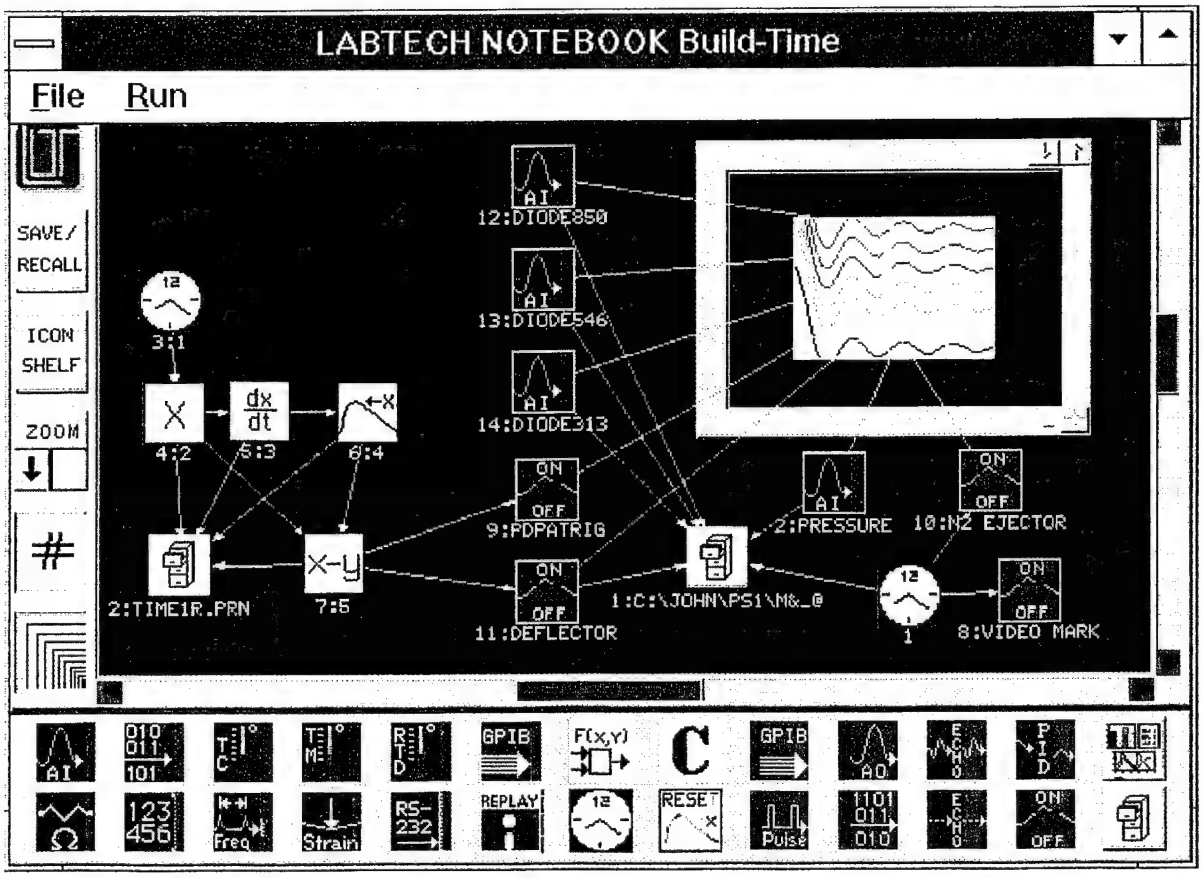

Figure 9. LABTECH Notebook Data Acquisition and Experiment Control Program for PDPA and Three-Wavelength Extinction Measurements.

Keithley MetraByte hardware provided the interfaces between the computer and the equipment. The 24-Bit Parallel Digital I/O Board (PIO-24) and the Analog & Digital I/O Board (DAS-16F) were internal to the computer. Externally, the PIO-24 was connected to a 24 Channel Relay Output Board (ERB-24). The DAS-16F connected to the Screw Terminal Accessory Board (STA-16).

G. MALVERN 2600

Ensemble particle-sizing was done using the Malvern 2600. This device consists of a laser transmitter and receiver and computer for control and data acquisition. A 9 mm diameter He-Ne laser beam with wavelength $\lambda = 0.633$ μm exits the transmitter and is scattered (Fraunhofer diffracted) by the particles based on their size. The scattered light then passes through a Fourier transform len and is focused on 32 semicircular detector rings to measure the intensity of light at different solid angles up to a scattering angle θ of 14°. Due to the physical limitations of positioning the Malvern, it was not possible to simultaneously conduct Malvern, PDPA, and three-wavelength extinction measurements. Therefore, the Malvern was used to take a sample through the plume at the same longitudinal position 6" downstream of the nozzle as the main PDPA measurements. It was triggered using a separate LABTECH Notebook program to take 50 sweeps of data in 0.4 seconds, starting 1 second after the chamber pressure reached 100 psia. [Ref. 17]

H. VIDEO CAMERA

A video camera was positioned above the setup and framed on the plume region. The signal was sent live into the control room where it was monitored and recorded on a Sony S-VHS VCR. Text annotation and a time reference were displayed on the screen, however the time signal was not synched with the LABTECH Notebook clock. Therefore, an approximate time hack was sent from the data acquisition program in the form of an audio signal that would spike the VU meter on the VCR. The display was used to measure the plume dimensions, determine probe tip position relative to the plume centerline, and safely observe the progress of the run. Although 1" separated holes in the

lab table were typically visible, parallax prevented their direct use in measuring motor nozzle to probe tip position.

IV. EXPERIMENTAL PROCEDURES

Preparation for each firing required several steps as discussed below. Since the igniters required extra time to fabricate, they were normally made in advance during non-firing days. Each propellant grain was cut, bonded to the motor case and allowed to cure overnight. On the day of the firing the probe and side tubes were assembled and coarsely aligned on their mount using pencil marks of the final previous position as a guide. The argon laser, with its water cooler and fan, and the PDPA were then energized to conduct fine alignment. Cigar smoke, deodorant spray, or humidifier water vapor were used in the probe to see the beam and test the PDPA. The white light source was also turned on and its beam checked using a white card at various spots. The crucial check was a clean, collimated beam exiting the top vertical tube of the probe. Next, the diode box was coarsely aligned and the extension tubes were put in place. The diode box was opened and the filters and beam splitters cleaned and secured. The incoming beam exiting the pinhole was positioned on the center of each diode. The cover was replaced and the diode outputs verified. The propellant surface was scraped to provide a fresh surface to aid in ignition. The motor was assembled without the igniter and mounted at the proper longitudinal, lateral, and vertical position in front of the probe tip. The video camera was turned on and adjusted. The probe N_2 ejector flow valve was activated to purge the line and then connected to the probe. The deflector was aligned and the activator air was turned on. All computers were booted and data acquisition software loaded. The videotape recorder, monitor, and screen annotator were turned on and set up. The white light beam was covered temporarily so "no light" diode readings could be taken. Several dry runs with the LABTECH Notebook program were performed and a manually actuated voltage to simulate the pressure transducer was input to fully check system performance and data acquisition. Old files were deleted to ensure adequate hard drive space for the 0.5 MB data file. Finally, protective shields and plastic covers secured

with duct tape were attached to protect the PDPA from exhaust products. The igniter was installed and battery/charger hooked up.

The firing sequence started by clearing the perimeter area of personnel. Next, the warning horn was sounded, VCR set to record, PDPA set to acquire data when externally triggered, and the LABTECH Notebook program started. The final event was a short countdown "3-2-1-FIRE" and the ignition button pressed and held until the firing was initiated or the program was terminated in the event of a "no-fire".

Initial post-firing procedures consisted of stopping PDPA data acquisition and saving the data, stopping the VCR, and securing the firing circuit. The laser, arc lamp, diodes, and video camera were turned off. The battery charger was unplugged and N_2/air valves closed for the ejector and deflector. If SEM samples were to be taken, then they were obtained by wiping from the inside of the back of the probe with a surgical gloved finger dipped in acetone. Lenses, mirrors, and other glass or optics were wiped with methanol or spray-cleaned with compressed air. All exposed areas were wiped with acetone to try to prevent corrosion from the exhaust. The probe and all tubes as well as the motor were disassembled and cleaned with water or acetone.

A. PHASE 1 FIRINGS

Prior to the operational propellant PS-1 firings, several test firings were conducted with AC-14 to check the setup and to make any necessary modifications. Measurements using the PDPA and original probe were made and drawings made of the required changes and additional hardware. Several months were required to get the probe modified (new hole cut and vertical tubes added) and the PDPA side tubes machined. A collimation tube with pinhole and lens holders was manufactured for use with the arc lamp. Additional probe tips (spares) were also made in case some were damaged during firings.

1. AC-14 10/24/94

This first firing was to check whether an end-burning grain and the $d_t = 0.165$" nozzle would yield the desired 250 psia without clogging. It also was an opportunity to

test the PDPA through the newly modified probe with side tubes. The probe tip was positioned 5.5" (24 d_e) from the nozzle and 1" (4 d_e) off of centerline. Unfortunately, the nozzle clogged with molten aluminum and silicon forcing the chamber pressure up to 600 psia. The data acquisition program, N2 ejector, deflector, and PDPA appeared to work as desired, although the trigger times needed adjustment.

2. AC-14 11/23/94

The second firing was an opportunity to try a different grain configuration and nozzle combination. Two grains, one end- and the other end- and radial-burning (described in Chapter III), were used with the d_t = 0.239" nozzle to ideally achieve 350 psia for about 1 second. However, a somewhat progressive burn resulted in a chamber pressure of 470 psia. Clogging was still a problem. The probe was positioned 5.5" (15 d_e) downstream and 1.5" (4 d_e) laterally. The PDPA did not acquire any meaningful data.

3. AC-14 12/8/94

This was the first run with the three-wavelength extinction apparatus in addition to the PDPA. A small diameter tube connected the top vertical tube of the probe to the diode box. The arc lamp was positioned on a stand next to the lab table. The collimation tube was attached to the condenser housing on one end and on the other end to a box containing a 45° mirror beneath the lower vertical tube of the probe. It was discovered that the neutral density filters and beamsplitters were blocking UV light (0.365 or 0.313 μm), so the UV filter was moved to the lowest diode in the box and the neutral density filter at the box entrance was removed. This also required changing neutral density filters in front of the other diodes until suitable output levels were attained. The other two-grain configuration for AC-14 described in Chapter III was used with the d_t = 0.268" nozzle to ideally achieve 300 psia for 1 second. The actual pressure peaked at 420 psia and was regressive burning for approximately one second. Since this grain and nozzle combination worked quite well it was used for all subsequent runs with AC-14. The diode outputs initially started to drop as expected, then saturated, then decayed to a new

full light value. This was interpreted as a vibration or shock problem resulting from having the lamp, collimator, and mirror too close to the motor. The N_2 ejector line had been damaged on previous runs and was burned off this time.

4. AC-14 1/18/95

For the fourth test firing several changes were made. A hole was drilled in the table and the white light source was moved below the table. An adjustable mirror on a post with a magnetic mount was added below the table and replaced the mirror in the box. It was also determined that a more intense and clean beam resulted without the secondary collimator, so it was no longer used. The light was collimated instead simply by the lamp housing lens and the 80" distance from the lamp to the diodes. The probe had a new N_2 ejector connector hole drilled on the opposite side for better protection. The pressure-time trace contained a 1 second neutral burn at 400 psia and the diodes responded properly although at a questionable rate. It was noted that the diode outputs dropped during N_2 ejector activation, probably due to circulation of stray particles. The vibration problem appeared to be solved. A hole was burned in the side funnel which connected the probe body to the PDPA detector.

5. AC-14 2/8/95

The side funnel was repaired and had a protective plate added in front. The diode response question was handled in several ways. Unnecessary amplifiers that had a 1 Hz filter were disconnected. The diode outputs were then increased by adjusting trim pots and swapping out neutral density filters. The sampling rate for the diodes was increased to 300 Hz (this also applied to the pressure transducer and deflector trigger). Finally, a light chopper was used to produce a 15 Hz square wave and the diodes had no difficulty measuring the alternating light conditions. It was also considered that a sluggish deflector could have caused the appearance of slow diode response. Therefore, the video replay was used to verify that the deflector was operating as commanded as accurately as could be measured. This was the final AC-14 firing because everything seemed to work properly. The acquisition run time was decreased from 30 to 20 seconds. The deflector

retraction interval was increased from 0.65 seconds to 1 second. The probe tip was located 5.5" (11 d_e) from the nozzle and 1" (5 d_e) off centerline. The N_2 ejector flow was regulated at 300 psia, but may have been too high (non-isokinetic flow) as evidenced by the diode outputs dropping prior to the deflector retracting. In addition, good transmittance data was obtained although the UV diode nearly reached $T = 0$. This was probably due to too large a regulated N_2 pressure. The pressure-time trace showed an average of 350 psia for about 1 second. Good PDPA data was obtained (97 valid particles with a d_{32} = 10.3 μm).

B. PHASE 2 FIRINGS

Since the AC-14 firings had enabled fixing most of the experimental problems, the operational firings with PS-1 were able to proceed at a much faster pace. The new propellant had good burning characteristics, ignited easily, and did not produce the erratic "puffing" of exhaust that was typically observed with other propellants. It also was easy to cut and scrape. However, the high aluminum content of the propellant produced a very difficult to remove Al_2O_3 layer in the nozzle.

1. PS-1 2/23/95

As with AC-14 an end-burning grain was initially tried for simplicity and assurance of neutral burning. The d_t = 0.207" nozzle was used and ideally should have resulted in a chamber pressure of 224 psia for 4 seconds. However, nozzle clogging was a major problem and a highly progressive burn resulted with a peak chamber pressure of 430 psia. The probe, PDPA, and three-wavelength apparatus were not used since this first run was for plume visualization and measurement. The clogging problem caused the plume to be irregular, so this run was not as useful as desired.

2. PS-1 2/25/95

A new calibration curve was generated for the pressure transducer prior to this run. A single perforated grain and the larger d_t = 0.239" nozzle were selected and used for the rest of the work. Ideally an approximately neutral burn near 300 psia for 1.5

seconds would occur. The deflector and PDPA triggering were changed to the intervals 0.25 - 1.25 and 0.45 - 1.25 seconds after reaching 100 psia respectively. The N_2 ejector regulated pressure was decreased to 100 psia. The motor was positioned for a nozzle-to-tip distance of 6" (16 d_e) and a lateral offset of 1.2" (3 d_e). The diode box pinhole was opened slightly creating a beam with a diameter of about 0.29". The narrow top tube from the probe to the diode box was replaced with a much larger 1" O.D. tube to cut down on internal reflection, improving the beam. The actual chamber pressure peaked at 400 psia. The PDPA did not measure any particles. The transmittances looked good, however they dropped to a very low value. Also, because the transmittances started dropping early it was felt that the N_2 pressure was again too high. From the video replay it appeared that the tip was located in the smoke periphery of the plume as desired. The plume width was estimated to be 3" with the highly visible portion about 1.5" wide.

3. PS-1 2/27/95

This run was to be on centerline. Since only large particles ($d > 0.5$ μm) were anticipated, only the PDPA was used. Concern for being too close and melting the tip drove the nozzle-to-tip distance up to 12" (33 d_e). To reduce the tip's exposure time to the hot plume the deflector trigger interval was shortened to 0.25 - 0.95 seconds after 100 psia chamber pressure was reached. The actual run had an essentially neutral burn at a chamber pressure of about 300 psia for 2 seconds. Unfortunately, the PDPA only measured 8 valid particles with a $d_{32} = 12.0$. It was decided that the three-wavelength measurements should always be taken to aid in evaluating what the PDPA measured. The nozzle throat diameter was reduced by the Al_2O_3 , and was measured after the run to be 0.15". This was typical of all the subsequent runs.

4. PS-1 3/1/95

From the two previous runs it appeared that the deflector and PDPA were being triggered early, so the intervals were again changed to 1 - 1.7 and 1.25 - 1.7 seconds after 100 psia respectively. The nozzle-to-tip distance was significantly reduced to 4" (11 d_e)

and this run was on centerline. No PDPA data was collected, possibly due to a computer problem after an automatic laser shutdown occurred after an overheat condition with the water cooler. The probe tip melted, probably 0.3 seconds after deflector retraction. Particles were collected for SEM analysis.

5. PS-1 3/2/95

The nozzle-to-tip distance was set to 6" (16 d_e) and 0.2" (0.5 d_e) laterally. The chamber pressure peaked near 380 psia had an essentially neutral burn. Transmittance data from this and the previous run showed that the ejector flow was still too high. Good PDPA data was acquired with 44 valid particles. Particles were collected again for SEM analysis. The tip melted, probably 0.1 seconds after deflector retraction.

6. PS-1 3/3/95

For this run the nozzle-to-tip distance was set to 6" (16 d_e) and 0.4" (0.5 d_e) laterally. The ejector flow pressure was reduced to 35 psia. An essentially neutral burn for 1.5 seconds was achieved with a peak pressure of 360 psia. The PDPA data appeared to be correct. However, it had to be copied by hand and then reconstructed due to a computer hard drive problem. Only four valid particles were measured with a d_{32} = 2.3 μm. Transmittance data still suggested that the ejector flow rate was too high.

7. PS-1 3/4/95

This run had a nozzle to tip distance of 6" (16 d_e) and was offset 0.6" (1.6 d_e) laterally. The ejector flow pressure was reduced to 25 psia. Due to rainy weather the motor took a while to light-off, but did achieve a neutral burn for two seconds near 375 psia. The PDPA measured only one valid particle at 6.4 μm, and the transmittance data looked good.

8. PS-1 3/5/95

In order to conduct a background radiation check and try an open-air, three-wavelength measurement, the probe with side and vertical tubes as well as the PDPA were not used. The motor was set up for a 6" plume length and a 0.75" offset from the

light beam emanating from the lab table. The neutral density filters and diode box pinhole had to be adjusted to prevent the diodes from saturating with the increased radiance. During the video replay a faint glow of the beam was visible where it came out of the table prior to ignition. Once the motor fired the beam was very visible as it was scattered by the particles in the plume. The plume appeared to be approximately 3" across at the location of the beam. The surprising result was plume emission at the UV wavelength $\lambda = 0.313$ μm, and potentially at the other wavelengths.

9. PS-1 3/6/95

Due to the results of the previous run a light chopper was added to the setup between the light source and mirror and run at a speed to produce an approximately 40 Hz square wave of alternating light and darkness. This frequency was selected because with the sampling rate of 300 Hz it was the highest frequency that would provide two to three sample points near the top and bottom, corresponding to light and no light, of the wave. The motor was positioned 6" (16 d_e) from the probe tip on centerline. The burn was fairly regressive with a peak of 500 psia. The PDPA had no valid particles of 192 attempts, however the tip melted at some point during the run. Transmittance data indicated that, inside the probe plume, emission was not a problem since throughout the run accurate "no light" samples were recorded at the bottom of the square wave.

10. PS-1 3/7/95

The final firing used only the Malvern particle sizer. The Malvern was set up in a separate test cell with a 100 mm Fourier transform lens, providing a vignetting distance of approximately 5" in front of the receiver lens. A laser bandpass filter was used to eliminate background radiation. The motor was mounted for a nozzle-to-beam distance of 6" with the plume centerline 2.5" from the receiver lens. A separate LABTECH Notebook program was used to trigger the Malvern 1 second after 100 psia chamber pressure. The Malvern was initially aligned and adjusted for as low a background as possible. Then it was set in a program mode, awaiting external trigger to take 50 sweeps

in 0.4 seconds, followed by a 10 second delay, then another 50 sweep sample in 0.4 seconds. This latter sample was to check the condition of the windows under post-firing conditions. The video camera was also set up looking down on the plume. The motor did not have much of a neutral burn and reached a peak of about 475 psia. The Malvern measurement was successful and occurred near the peak pressure. Post-firing inspection of the receiver window showed that it was partially obscured by some exhaust particle residue. The video replay provided an excellent opportunity to measure the plume dimensions that were lost on the first motor firing with PS-1. The highly visible portion of the plume appeared to be 12" long and 1.5" wide with the widest point at the 6" longitudinal position. The outer smoky portion of the plume grew from about the 3" aft position to a maximum diameter of about 4" near the 6" aft position, and maintained this width to the edge of the field of view.

V. RESULTS & DISCUSSION

This chapter examines the results obtained with the Malvern, PDPA, and the three-wavelength apparatus. The discussion refers to the PS-1 firings on 2/25/95 and later. Calculations are presented to correlate the data by different means. Table 4 presents the PS-1 firings that were used for data reduction (i.e., the first firing has not been included). The d_t = 0.239" nozzle which was used resulted in an average chamber pressure (P_c) between 290 and 480 psia. This yielded underexpanded nozzle flow (exit pressure between 30 and 40 psia as verified with the MICROPEP equilibrium, adiabatic combustion/performance code run in the off-design mode for the appropriate expansion ratio).

Firing	Position†	PDPA	3-λ Ext.	Malvern	SEM	Ave. P_c (psia)	Comments
2/25/95	6"/1.2"	Yes*	Yes	No	No	380	
2/27/95	12"/0.2"	Yes	No	No	No	290	
3/1/95	4"/0"	No	Yes	No	Yes	375	Melted tip
3/2/95	6"/0.2"	Yes	Yes	No	Yes	360	Melted tip
3/3/95	6"/0.4"	Yes	Yes	No	No	325	
3/4/95	6"/0.6"	Yes	Yes	No	No	370	
3/5/95	6"/0.75"	No	Yes	No	No	400	Bare light
3/6/95	6"/0"	Yes*	Yes	No	No	480	Light chopper, melted tip
3/7/95	6"/NA	No	No	Yes	No	470	

Table 4. Summary of PS-1 Firings Used for Data Reduction. (* - An attempt was made but there were no valid particles. † - Axial location/radial displacement)

A. MOTOR

As discussed in the previous chapter the propellant always burned in a smooth fashion. Periodic puffing of the exhaust from shedding of Al_2O_3 slag was not observed. Formerly used propellants have shown a propensity for this shedding phenomenon and

with such a high aluminum content in PS-1 it was anticipated. Chamber pressures varied between 250 and 500 psia compared to the near 300 psia calculated for ideal conditions, due primarily to a reduction in throat area from Al_2O_3 deposits.

B. EXPECTED RESULTS

Previous experimentation had demonstrated the individual usefulness and limitations of the PDPA, the Malvern, and the multiple-wavelength extinction techniques for the solid rocket motor environment. The Malvern takes an across-the-plume measurement of "large" particles with $d > 0.5$ μm and provides number and volume distributions assuming there are no particles smaller than 0.5 μm. The PDPA counts individual particles with $d > 0.5$ μm passing through its probe volume and provides number and velocity distributions as well as representative mean diameters. It has been demonstrated to accurately measure the distribution of particles with $d > 0.5$ μm suspended in liquid. Multiple-wavelength extinction measurements have also been used before at the laboratory. A Mie code and an assumed distribution shape (e.g., log-normal) permitted the particle index of refraction and distribution parameters for "small" particles in the plume edges to be found. Since past work had found the larger particles only toward the center of the plume and the smaller particles throughout the plume, the goal of this investigation was to use the PDPA to obtain "large" particle distributions at various radial positions across the plume and to use the extinction technique at the plume edge to get distribution information for the "small" particles which then could be applied across the whole plume. The Malvern was to be used to provide a check on the combined radial PDPA measurements. In order to accomplish this objective experiments were conducted using the probe at radial positions of 0", 0.2", 0.4", 0.6", 0.75", and 1.2" from the plume centerline and a final measurement was made across the plume.

To investigate the potential for taking the obtained log-normal distribution, found for the small particles using the extinction technique, and curve-fitting it to a PDPA distribution, a spreadsheet was created in LOTUS® 1-2-3® Release 4 for Windows™.

The PDPA distribution was manually entered for all the possible bin diameters and bins for additional diameters smaller than 0.5 μm were inserted for use with the log-normal distribution. The equation for the cumulative log-normal distribution, Equation (2.26), was used to determine the number of particles in each individual bin to create a number distribution in histogram form for comparison to that of the PDPA. An overlapping portion of the two distributions for diameters greater than 0.5 μm was used for the curve-fit. A Sum of the Squared Deviations (SSD) approach was used to obtain a single number to evaluate the curve-fit. The SOLVER routine in 1-2-3 was used to adjust d_{gn}, σ_g, and N to minimize the SSD. Unfortunately, even with constraints the routine could not accomplish this. It could, however, work with a single parameter if the other two were fixed. By manually adjusting the parameters the problem was readily apparent. Many log-normal distributions can provide an equally good fit. Thus, curve-fitting will not result in a unique solution.

The Mie code FORTRAN program at NPS, obtained from Cashdollar [Ref. 12], was formerly only available on the main-frame computer. Therefore, to speed up the data reduction and analysis, it was copied and modified for use on a personal computer with Microsoft MS-Fortran 4.1. To simulate experimental conditions in the 1-2-3 spreadsheet and examine expected transmittance values for different distributions and at different wavelengths "miescat3.exe" (see Appendix C) was used and a macro was written for 1-2-3 to be able to properly import the output file (see Appendix D). What was more important was also to be able to examine the $\ln T$ or $\bar{Q}$ ratios as the mass of "small" particles was varied with respect to the mass of the "large" particles. Finally, for data reduction (i.e., finding the index of refraction m, d_{32}, and σ_g that best fits the experimentally derived transmittances) the program "miescat6.exe" was developed (see Appendix E).

The most optimistic result desired was to be able to take the end-product, experimentally-derived distributions for various radial positions across the plume and

conduct a mass calculation for comparison to the calculated mass that should be present from burning the propellant.

C. MALVERN

The Malvern data were typical of past observations with propellants of various composition. Beam steering occurred as evidenced by the increased intensities on the first six detector rings. The voltages on these rings were deleted before the size distribution was calculated. Elimination if these inner six rings does not affect the distribution when all the particles have diameters less than the expected value of approximately 30 μm. In agreement with previous data obtained with the subscale motor [Ref. 18], the Malvern measured ~25% of the volume in particles with $d < 2.0$ μm, the remaining ~75% of the volume in particles with $d = 4 - 5$ μm, and a $d_{max} \sim 6$ μm. An obscuration of 86% (therefore $T = 0.14$) was recorded, with beam-steering present, and a $d_{32} = 2.59$ μm was determined.

In order to conduct a check on the above value of T, Dobbins' formula (Equation 2.30) was used. First, a stagnation enthalpy energy balance equation was used to estimate the ratio of the mass flow rates of air to propellant gas in the plume at the measurement location for use in calculating the mass concentration of particles.

$$\dot{m}_{p_{gas}} C_{p_{gas}} T_{t_{gas}} + \dot{m}_{air} C_{p_{air}} T_{t_{air}} = (\dot{m}_{p_{gas}} + \dot{m}_{air}) C_{p_{mix}} T_{t_{mix}} \tag{5.1}$$

where

$\dot{m}_{p_{gas}}$ = mass flow rate of propellant gas
$C_{p_{gas}}$ = specific heat for propellant gas = 1431 J/kg-K from MICROPEP
$T_{t_{gas}}$ = stagnation temperature of the propellant gas = 3584 K from MICROPEP
$\dot{m}_{air}$ = mass flow rate of entrained air
$C_{p_{air}}$ = specific heat for entrained atmospheric air = 1004 J/kg-K
$T_{t_{air}}$ = stagnation temperature of entrained air = 520 K
$C_{p_{mix}}$ = specific heat of the mixture of gases = 1217 J/kg-K from average of gas and air
$T_{t_{mix}}$ = stagnation temperature of the mixture of gases ~1500 K [Ref. 19 at 16 d_e]

Dividing by the mass flow rate of propellant gas, the ratio of the mass flow rates was calculated. The mass flow rate of entrained air was approximately 2.5 times that of the propellant gas. Therefore, the mass flow rate of the mixture of gases was 3.5 times the mass flow rate of the propellant gas alone. The equation used for C_m was

$$C_m = \frac{\dot{m}_{p_{Al_2O_3}}}{\dot{V}_{mix}} = \frac{\dot{m}_{p_{Al_2O_3}} \rho_{mix}}{\dot{m}_{mix}} = \frac{\dot{m}_{p_{Al_2O_3}} p_{mix}}{\dot{m}_{mix} R_{mix} T_{mix}} \tag{5.2}$$

where

$\dot{V}_{mix}$= volume flow rate of the mixture of gases
ρ_{mix}= density of the mixture of gases
p_{mix}= pressure of the mixture of gases ~ 14.7 psia
R_{mix}= gas constant for the mixture of gases ~ 54 ft-lbf/lbm-°R
T_{mix}= temperature of the mixture of gases ~ 1500 K

First, the mass flow rate of the propellant had to be calculated using

$$\dot{m}_p = \rho_p A_b a p_c^n \tag{5.3}$$

where

$\dot{m}_p$ = mass flow rate of the propellant
ρ_p = propellant density = 0.06665 lbm/in³ from MICROPEP
A_b = propellant burning surface area = 4.8 in² average during steady burn
a = propellant burning rate pressure coefficient
p_c = chamber pressure = 400 psia
n = propellant burning rate pressure exponent

Next, the mass flow rate of Al_2O_3 was found by using the mass percentage of aluminum in the propellant (20%) times the ratio (1.89) of the molecular weights of Al_2O_3 (101.96 g/mol) to aluminum (2 x 26.98 g/mol) times the mass flow rate of the propellant found using Equation (5.3). Finally all values were plugged into Equation (5.2) to find C_m= 1.4 x 10^{-6} lbm/in³. Using Equation (2.30) with L = 3", $\bar{Q}$ = 2, $\rho = \rho_{Al2O3}$ = 0.138 lbm/in³ at 1500 K, and d_{32} = 2.59 μm a transmittance of T = 0.40 was calculated. This is much higher than the Malvern measured value of 0.14, most likely due to beam steering as discussed above. Beam steering is the refraction of the beam due to the thermal gradient

in the path of the beam. This causes the central detector, which measures the obscuration, to receive less intensity than it should and the innermost detector rings to receive too large an intensity.

Another calculation was performed to compare the mass in the observed modes for the calculated d_{32} of 2.59 μm. For the Malvern volume distribution two modes were apparent, near 1 and 4.5 μm. Therefore, it was assumed that all the particles were either 1 or 4.5 μm and the number ratio of 1 to 4.5 μm particles was found to be 24.3 using:

$$\frac{N_1}{N_{4.5}} = \frac{d_{32}(4.5)^2 - (4.5)^3}{(1)^3 - d_{32}(1)^2} \tag{5.4}$$

where N_1 is the number of 1 μm particles and $N_{4.5}$ is the number of 4.5 μm particles. Then, the mass percent of the 1 μm particles to the total mass of the particles was calculated as 21.1% using

$$\frac{V_1}{V_{total}} = \frac{\frac{N_1}{N_{4.5}}(1)^3}{\frac{N_1}{N_{4.5}}(1)^3 + (4.5)^3} \tag{5.5}$$

where V_1 is the volume of 1 μm particles and V_{total} is the volume of all the particles. Thus, the Malvern data implied that most of the mass was contained in particles with diameters greater than 1 μm. This is evident in Figure 10 of Appendix G.

D. PDPA

Six attempts were made to obtain measurements at various radial positions in the plume with the PDPA, from the centerline out to 1.2" (3 d_e). Both centerline firings resulted in no valid particles. On both of these runs as well as the 0.2" offset run the probe tip was melted. Therefore, flow deflection and/or a strong detached normal shock could have caused the lack of "large" particles in the probe by breaking them up into "small" particles.

The Malvern number and volume distributions were compared to an equivalent across-the-plume distribution formed by scaling the 0.2", 0.4", and 0.6" offset PDPA distributions. This scaling was done by assuming the plume was axisymmetric and could be divided up into concentric zones. Within each zone the distribution was assumed to be constant. Since there were three PDPA distributions that could be used three zones were formed with the constraint that each zone could contain only one PDPA distribution. This forced the inner zone to be constrained to an outside radius of 0.2 - 0.4". Similarly, the middle zone extended from the outside of the inner zone to 0.4 - 0.6" and the outer zone extended from the outside of the middle zone to 0.6 - 0.75". Each distribution was then multiplied by twice the difference between its zone's inside and outside radii. This was the scale factor. Next, the scaled distributions were combined and the total number of particles found. This total was then divided into each number value and multiplied by 100 to obtain number % at a given diameter. Finally, the number %'s were added together according to the bin diameters used by the Malvern and plotted with the Malvern distribution. An additional step was required for the volume distribution. Each scaled number was multiplied by d^3. Then when combined, the total volume of particles was found rather than number. The PDPA and Malvern plots of the number and volume distributions (see Figures 10 - 13 in Appendix G) agreed that there was a mode at < 1 μm and another mode between 4 and 5 μm. The PDPA volume distribution highlights individual larger particles that it measured, whereas individual particles are essentially lost by the Malvern as it looks at an ensemble of particles.

The PDPA distributions also showed that there were almost no "large" particles ($d > 0.5$ μm) outside of 0.6" off the centerline. This was in agreement with the visual appearance of the plume. The brighter plume core area appeared to have approximately a 1" diameter.

There are several ways to improve the future performance of the PDPA when used in the plume environment. First and foremost, if the probe tip were cooled or made of a more thermally resistant material the tip erosion problem could be minimized. A shorter

time for tip exposure would also help in this regard. The ejector flow needs to be optimized to prevent sucking in too many of the small particles since this biases the data toward smaller particles. It would be very difficult to obtain isokinetic sampling because of the required short explosive time. The probe needs to be redesigned with a smaller frontal area, probably circular, and with a diameter no larger than the present maximum tip diameter. This would cut down on the plume obstruction and remove some of the excess internal volume that presently causes recirculation within the probe. If fiber optics were used, the large side tubes could also be removed, further improving the plume obstruction problem. With subscale motors it may also be possible to not use the probe, allowing the PDPA to traverse the plume cross-section.

E. THREE-WAVELENGTH EXTINCTION

Transmittances were calculated for seven firings and used to obtain "best fit" values of index of refraction m, σ_g, and d_{32} for a log-normal distribution. The following formula was used:

$$T = \frac{V_p - V_0}{V_f - V_0} \tag{5.6}$$

where V_p is the diode output in volts for particle obscured light, V_0 is the diode output for no light, and V_f is the diode output for unobstructed full light. The no-light reading was made prior to firing by covering the hole in the bottom of the lab table. The full light value was found by taking an average of the first two seconds of the run (i.e., before ejector gas activation which typically reduced the diode reading slightly). The particle obstructed reading was taken over a flat minimum during steady-state burning.

Once the three transmittances were calculated for a firing they were inserted into the data input file "miescat6.dat" and iteration intervals were chosen for m and σ_g. The data reduction file, "miescat6.exe", was run and provided the best d_{32} for each combination of m and σ_g as well as a calculation of the degree-of-fit. This value was the Sum of the Squared Deviations (SSD) between $\ln T$ ratios and $\bar{Q}$ ratios. The closer SSD

approached zero the better the fit. Table 5 presents all of this information. The SSD values are presented as integers rather than the eight digits to the right of the decimal that they really were (i.e., 237 is really 237E-08). The 3/5/95 firing was different from the others because the probe was not used and the plume was definitely emitting at 0.313 μm. Therefore, a transmittance value was not calculated at this wavelength and a fit could not be obtained.

It was discovered that the process used to iterate toward the "best-fit" values was convergent for σ_g and d_{32}, but not for m. Therefore, since a reasonable value for m of Al_2O_3 in the plume is 1.70 - 0i, this value was used as a starting point to find a reasonable

Firing	Position	T_{313}	T_{546}	T_{850}	m	σ_g	d_{32}	SSD
2/25/95	6" / 1.2"	0.0557	0.0533	0.0958	1.70-0i	1.82	0.6	237
3/1/95	4" / 0"	0.2891	0.3304	0.4905	1.70-0i	1.7	0.44	1,708
3/2/95	6" / 0.2"	0.4957	0.5054	0.5666	1.70-0i	2.1	0.69	925
3/3/95	6" / 0.4"	0.3026	0.425	0.5567	1.70-0i	3.24	0.36	292
3/4/95	6" / 0.6"	0.2518	0.3315	0.4316	1.70-0i	3.38	0.58	253
3/5/95	6" / 0.75"	N/A	0.794	0.7184	N/A	N/A	N/A	N/A
3/6/95	6" / 0"	0.1711	0.2268	0.3007	1.70-0i	3.9	0.84	207

Table 5. Three-Wavelength Extinction Results.

value for σ_g and d_{32}. Then, if a better fit was desired, m had to be varied over its entire possible range in 0.01 increments as σ_g was stepped in its smallest increment of 0.01 about the reasonable value and the minimum SSD set chosen. This entire somewhat lengthy process was not done, however some excellent fits were found. For the 2/25/95 firing m = 1.79 - 0i, σ_g = 1.84, d_{32} = 0.55 resulted in an SSD = 1E-08. For the 3/4/95 firing m = 1.85 - 0i, σ_g = 3.38, d_{32} = 0.50 resulted in an SSD = 2E-08. The large values of σ_g and d_{32} relative to the 0.5 μm particles is really indicative of a significant amount of the mass in "large" particles. It should be noted that only two independent ratios were available using three wavelengths. Kim et al. [Ref. 20] used six wavelengths for five

independent ratios and determined a $\sigma_g \sim 1.50$ and $d_{32} \sim 0.150$ μm in the edge of the plume. Thus, if further work is to be done, it should use as many wavelengths as possible with a large difference between λ_{min} and λ_{max}.

An uncertainty analysis was conducted on the transmittances, then applied to a single transmittance and propagated through the fit process to determine how much the distribution parameters changed. Using Holman's [Ref. 21] approach the transmittance uncertainty was found with

$$w_T = \sqrt{\left(\frac{1}{V_f - V_0} w_{V_p}\right)^2 + \left(\frac{V_p - V_f}{[V_f - V_0]^2} w_{V_0}\right)^2 + \left(\frac{V_0 - V_p}{[V_f - V_0]^2} w_{V_f}\right)^2} \tag{5.7}$$

where w_T, w_{Vp}, w_{V0}, and w_{Vf} are the uncertainties in the transmittance, particle obscured diode output, no-light diode output, and full-light diode output, respectively. Using the values from the 3/4/95 data set w_{Vp}, w_{V0}, and w_{Vf} were set equal to 0.0397, the 1 σ deviation on the 546 diode between 0 and 2 seconds elapsed time. This resulted in a transmittance uncertainty of 0.008974. This was added to T_{546} to create a perturbed set, then the fit process was conducted using $m = 1.70 - 0i$. This produced a $\sigma_g = 5.85$, $d_{32} = 0.71$, and an SSD = 8E-08. If this is compared to the original fit in Table 5 it is obvious that these values correspond to two unique distributions. Therefore, the multiple wavelength extinction technique is highly sensitive to any experimental uncertainties.

The 3/5/95 bare-light data (no probe) were used to compare the mass of small particles to large particles. Since the light beam was 0.75" from the centerline of the plume and appeared in the video replay to be in the smoky portion of the exhaust, it was assumed to be in the small-particle region. Equation (2.30) was used to determine C_m. The plume was estimated to be 3" in diameter, so L was calculated to be 2.60". The distribution parameters found using the fit routine with the 2/25/95 data taken in the plume edge were used with the Mie code to find $\bar{Q}$. However, the transmittance values were not used because the high probe purge rate resulted in a high concentration of small particles in the probe (note low values of T). Using the 3/5/95 T_{850} value, a C_m of 1.2E-07

lbm/in³ was calculated. When compared to the total C_m of 1.4E-06, calculated above, this showed that the small particles accounted for only 8% of the total mass. Similarly, using the 3/5/95 T_{546} value a C_m of 6.4E-08 lbm/in³ was calculated which corresponds to a small particle mass of only 4% of the total. When the mass distribution is plotted for the small particles (see Figure 18 in Appendix G) notice that only 30% of the "small particle" mass is in particles with diameter less than 0.5 μm. Therefore, the mass % of particles with $d < 0.5$ μm is less than 3%. Thus, accurate measurement of the size distribution in the plume should be possible using only the PDPA. This greatly simplifies the diagnostics required to make the needed plume particle size measurements.

F. SEM ANALYSIS

Several samples of the particles coating the inside rear of the probe were taken for analysis under a scanning electron microscope (SEM). First, the particles were sedimented in a beaker with acetone to try to remove any other matter. Next, they were scraped from the bottom and sprinkled on carbon painted mounts. Finally, the mounts were placed in a vacuum container where carbon fibers were vaporized to carbon coat the samples. This was to help with the sample charging problem. The samples were examined qualitatively under the SEM for an idea of the general size distribution. See the photographs in Figure 19 of Appendix G. It was noted that there were many 1 to 2 and 4 to 6 μm particles and few smaller or larger particles. This is consistent with the measured distribution, using the Malvern and the PDPA , as well as the various mass calculations.

VI. CONCLUSIONS

The PDPA and Malvern distributions agreed in the observed modes near 1 and 4.5 μm. SEM pictures of collected particles were in good qualitative agreement with the Malvern Sauter mean diameter d_{32} = 2.59 μm. Data analysis indicates that less than 3% of the total mass of the particles was contained in particles with diameter $d < 0.5$ μm. This means that the PDPA, which can typically measure particles down to a minimum diameter of 0.5 μm with a dynamic range (d_{max}:d_{min}) of 50:1, can be used by itself to determine the particle size distribution. Although multiple-wavelength measurements were not required, they were found to be very sensitive to inaccuracies in the measured transmittances. The modified particle collection probe allowed simultaneous PDPA and multiple-wavelength measurements. However, the design should be improved in several ways. The frontal area of the probe should be reduced to lessen plume obstruction. One option is to use a small cylindrical cross-section and use fiber optics with the PDPA, thereby removing the large side tubes which also obstruct the plume. In addition, the tip exposure time should be reduced or a more thermally resistant material chosen for the tip. Further studies should be conducted to check shock formation in and around the tip. A "rake" of PDPA miniature fiber optic probes may be a reasonable design to investigate for taking simultaneous radial measurements. Traversing such a rake across the plume is another option.

APPENDIX A. MICROPEP OUTPUT

The following pages contain a printout from the equilibrium, adiabatic combustion/performance code MICROPEP. This particular run was for propellant PS-1 with a chamber pressure of 400 psia and a nozzle area ratio of 2.33 operating off-design for an ambient sea level pressure of 14.7 psia. The area ratio pertains to the $d_t = 0.239$" nozzle used for most of the experiments with PS-1. Note that the exit pressure is about 40 psia, indicating underexpanded flow.

```
Feb. 1994  - Modified by A. McAtee
Naval Postgraduate School, Monterey, CA
                    **** NEWPEP ****
* PS-1 Ae/At=2.33   *
INGREDIENT                      MASS      HF        DENSITY      COMPOSITION
                                (gm)   (kcal/kg)  (kg/m**3)
AMMONIUM PERCHLORATE (AP)       70.00    -602.0   1948.6650     1CL  4H   1N   4O
ALUMINUM (PURE CRYSTALINE)      20.00       .0    2701.5590     1AL
HTPB (SINCLAIR)                 10.00      13.0    918.9728   103H  73C   1O

VOLUME PERCENT OF INGREDIENTS (IN ORDER)

   66.2684    13.6572    20.0744

THE PROPELLANT DENSITY IS  .06665 LB/CU-IN OR  1.8448 GM/CC

THE EQUIVALENCE RATIO IS   1.3260

NUMBER OF GRAM ATOMS OF EACH ELEMENT PRESENT IN INGREDIENTS

   3.416525 H      .732471 C      .595760 N     2.393073 O
    .741290 AL     .595760 CL

**************************CHAMBER RESULTS FOLLOW*****************************

TEMP          PRESSURE            ENTHALPY   ENTROPY   CP/CV  SGAMMA    Pi/ni
(K)        (MPa/ATM/PSI)          (kJ/kg)   (kJ/kg-K)                 (MPa/kmol)
3584.7   2.758/ 27.22/ 400.00  -1757.6980     9.398   1.1620  1.1212   84385.270

DAMPED AND UNDAMPED SPEED OF SOUND=  848.508 AND 1063.794 m/sec

SPECIFIC HEAT (MOLAR) OF GAS AND TOTAL=39670.840  54036.950 J/kmol-K
NUMBER MOLS GAS AND CONDENSED=   3.2682    .3392

(*=liquid,&=solid)
   .84621 H2          .68459 CO          .48272 H2O          .45869 HCl
   .33919 Al2O3*      .29499 N2          .22731 H            .08121 Cl
   .06428 HO          .04771 CO2         .03125 AlCl         .01142 AlOCl
 9.90E-03 O        5.82E-03 AlCl2     5.60E-03 NO        4.92E-03 AlHO2
 3.22E-03 AlO      2.99E-03 AlHO      2.21E-03 O2        1.46E-03 Al
 5.45E-04 Al2O     3.80E-04 AlCl3     1.56E-04 AlH       1.12E-04 Cl2
 8.25E-05 OCl      7.47E-05 Al2O2     6.17E-05 N         5.99E-05 CHO
 4.18E-05 AlO2     4.07E-05 HOCl      2.93E-05 COCl      1.82E-05 NH
 1.81E-05 NH3      1.81E-05 HO2       1.75E-05 NH2       8.93E-06 CNH
 7.17E-06 NHO      4.92E-06 AlHO      2.68E-06 CH2O      1.00E-06 CNO

THE MOLECULAR WEIGHT OF THE MIXTURE IS   27.721 gm/mole
THE GAS CONSTANT IS   299.93 J/kg-K

TOTAL HEAT CONTENT (298 REF)   =    6284.328 kJ/kg
SENSIBLE HEAT CONTENT (298 REF)=    5721.090 kJ/kg

**************************EXHAUST RESULTS FOLLOW*****************************

TEMP          PRESSURE            ENTHALPY   ENTROPY   CP/CV  SGAMMA    Pi/ni
(K)        (MPa/ATM/PSI)          (kJ/kg)   (kJ/kg-K)                 (MPa/kmol)
2917.2    .276/  2.72/  40.02  -3746.0840     9.398   1.1556  1.1201    8780.586

DAMPED AND UNDAMPED SPEED OF SOUND=  732.222 AND  938.454 m/sec
```

```
SPECIFIC HEAT (MOLAR) OF GAS AND TOTAL=39437.610  55329.410 J/kmol-K
NUMBER MOLS GAS AND CONDENSED=   3.1425    .3642

(*=liquid,&=solid)
   .88420 H2          .67999 CO          .53227 HCl          .48500 H2O
   .36417 Al2O3*      .29725 N2          .12299 H            .05240 CO2
 5.05E-02 Cl        2.15E-02 HO        6.85E-03 AlCl       3.03E-03 AlOCl
 1.82E-03 O         1.27E-03 AlCl2     1.20E-03 NO         8.34E-04 AlHO2
 4.60E-04 AlHO      4.01E-04 O2        2.01E-04 AlO        1.33E-04 AlCl3
 9.42E-05 Al        3.24E-05 Cl2       1.53E-05 Al2O       8.73E-06 OCl
 6.01E-06 CHO       5.81E-06 AlH       5.79E-06 HOCl       4.70E-06 N
 3.41E-06 COCl      2.96E-06 NH3       1.86E-06 Al2O2      1.42E-06 NH2
 1.15E-06 AlO2      1.09E-06 HO2       1.03E-06 NH         1.00E-06 CNO

THE MOLECULAR WEIGHT OF THE MIXTURE IS   28.517 gm/mole
THE GAS CONSTANT IS   291.56 J/kg-K

TOTAL HEAT CONTENT (298 REF)   =    4788.339 kJ/kg
SENSIBLE HEAT CONTENT (298 REF)=    4456.853 kJ/kg

********************************************************************************

An exact method for determining throat conditions was used
The frozen & shifting STATE gammas for the throat are:  1.1600  1.1199
GAMMA NU shown below is the gamma for the chamber to throat PROCESS.

**********PERFORMANCE:  FROZEN ON FIRST LINE, SHIFTING ON SECOND LINE,*********
**************SHIFTING TO THROAT/FROZEN AFTERWARDS ON THIRD LINE**************

SPECIFIC GAMMA  T*     P*    C*     ISP*    Pe    D-ISP    A*/m    Te     Cf
IMPULSE   NU                                  (gm-s/  (cm**2/
 (sec)          (K)   (MPa) (m/s)  (sec)  (MPa)    cm**3)   kg/s)  (K)
 222.8  1.1630 3314. 1.577 1539.2          .276 10192.710  5.5805 2590. 1.2718
 226.8  1.1202 3416. 1.601 1560.4 195.8    .297 10238.540  5.6571 2937. 1.2602
 224.9  1.1202 3416. 1.601 1560.4 195.8    .297 10140.370  5.6571 2702. 1.2482

FROZEN & SHIFTING KINETIC ENERGY OF EXHAUST  674708.  781129.  m**2/s**2
```

APPENDIX B. PROBE DRAWINGS

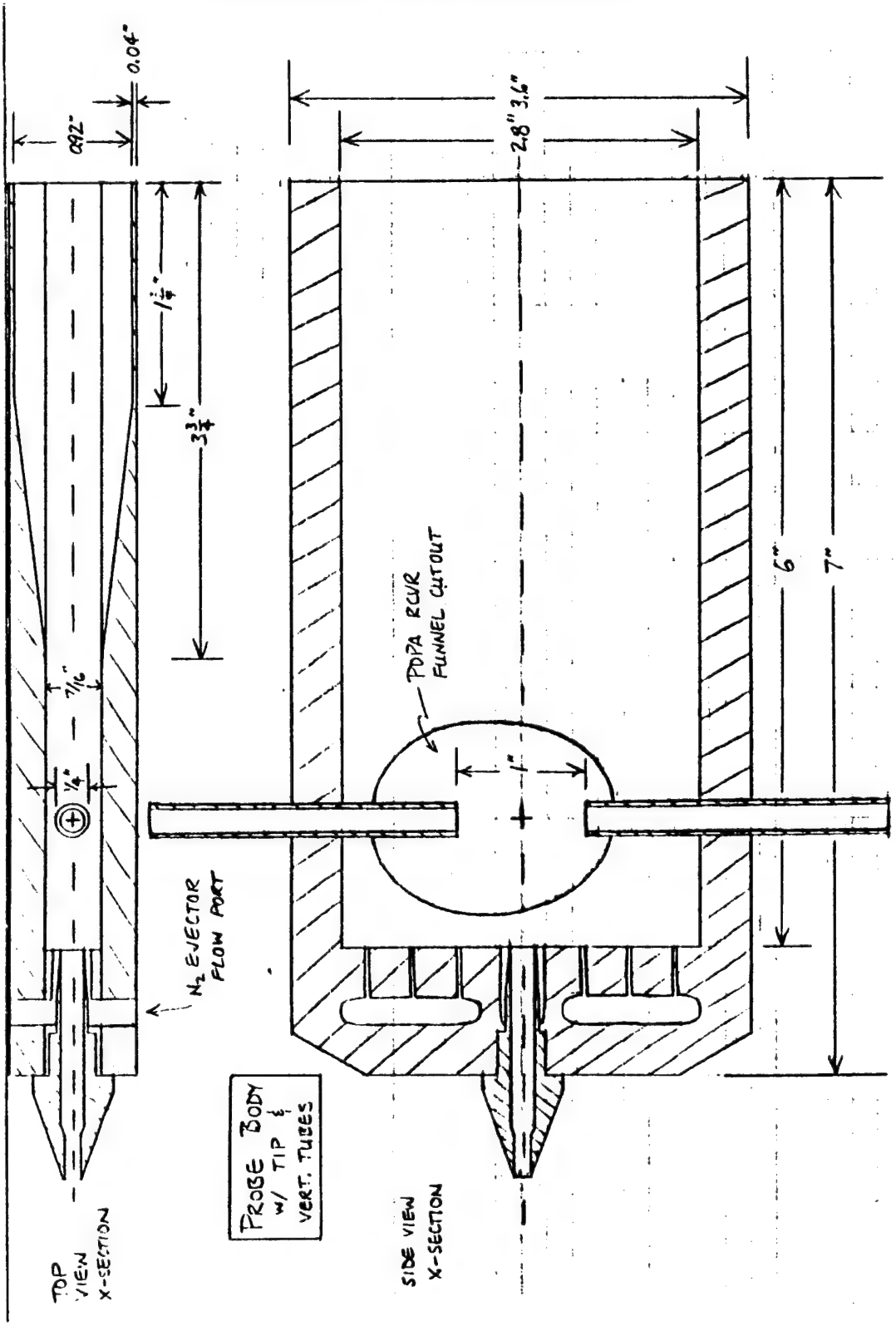

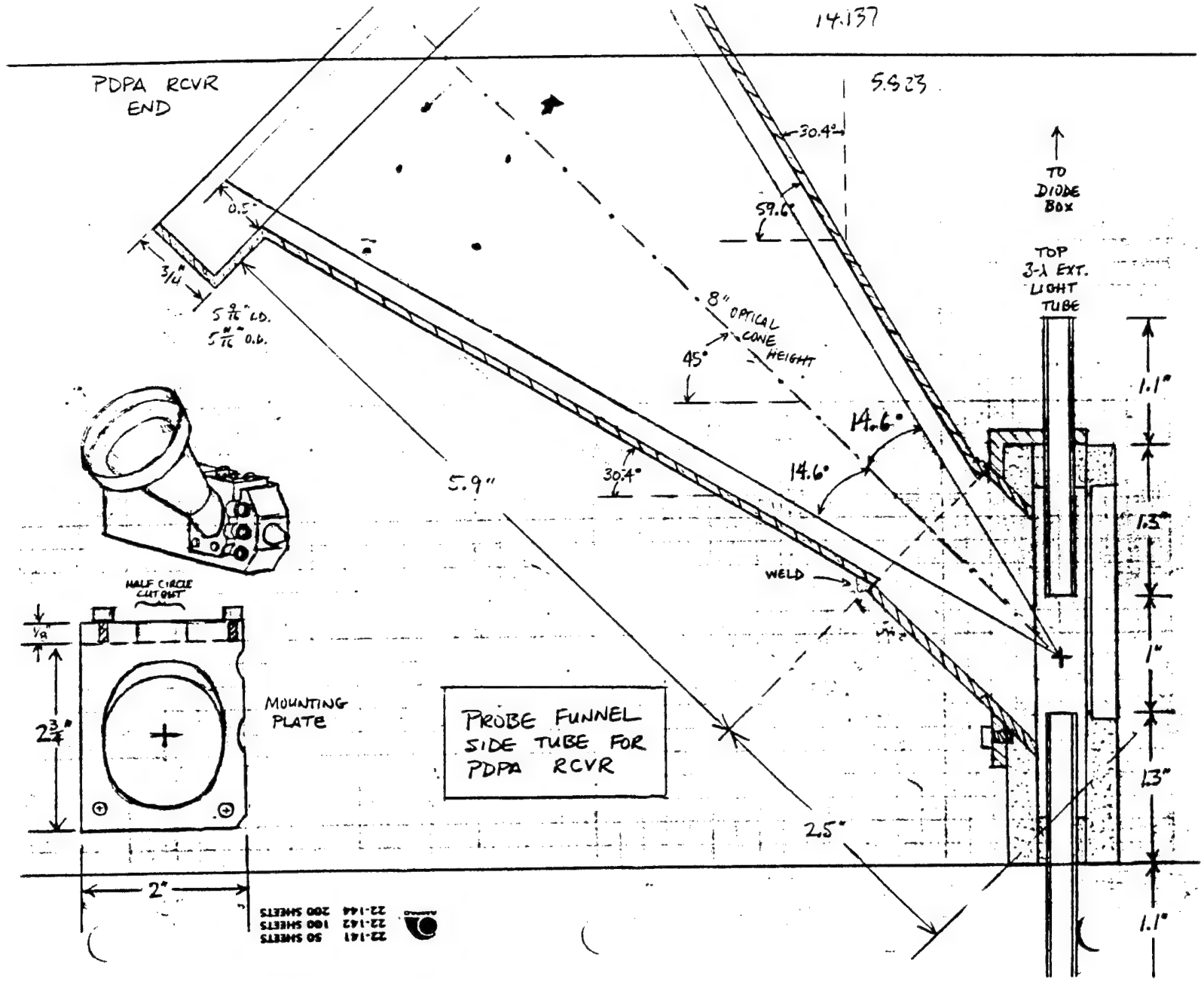
14.137
5.523
PDPA RCVR END
30.4°
TO DIODE BOX
59.6°
0.5"
3/4"
5 9/16" I.D.
5 11/16" O.D.
TOP 3-λ EXT. LIGHT TUBE
8" OPTICAL CONE HEIGHT
45°
1.1"
14.6°
14.6°
5.9"
30.4°
1.3"
WELD
HALF CIRCLE CUT OUT
1/8
1"
2 3/4"
MOUNTING PLATE
PROBE FUNNEL SIDE TUBE FOR PDPA RCVR
1.3"
2.5"
2"
1.1"
22-141 50 SHEETS
22-142 100 SHEETS
22-144 200 SHEETS

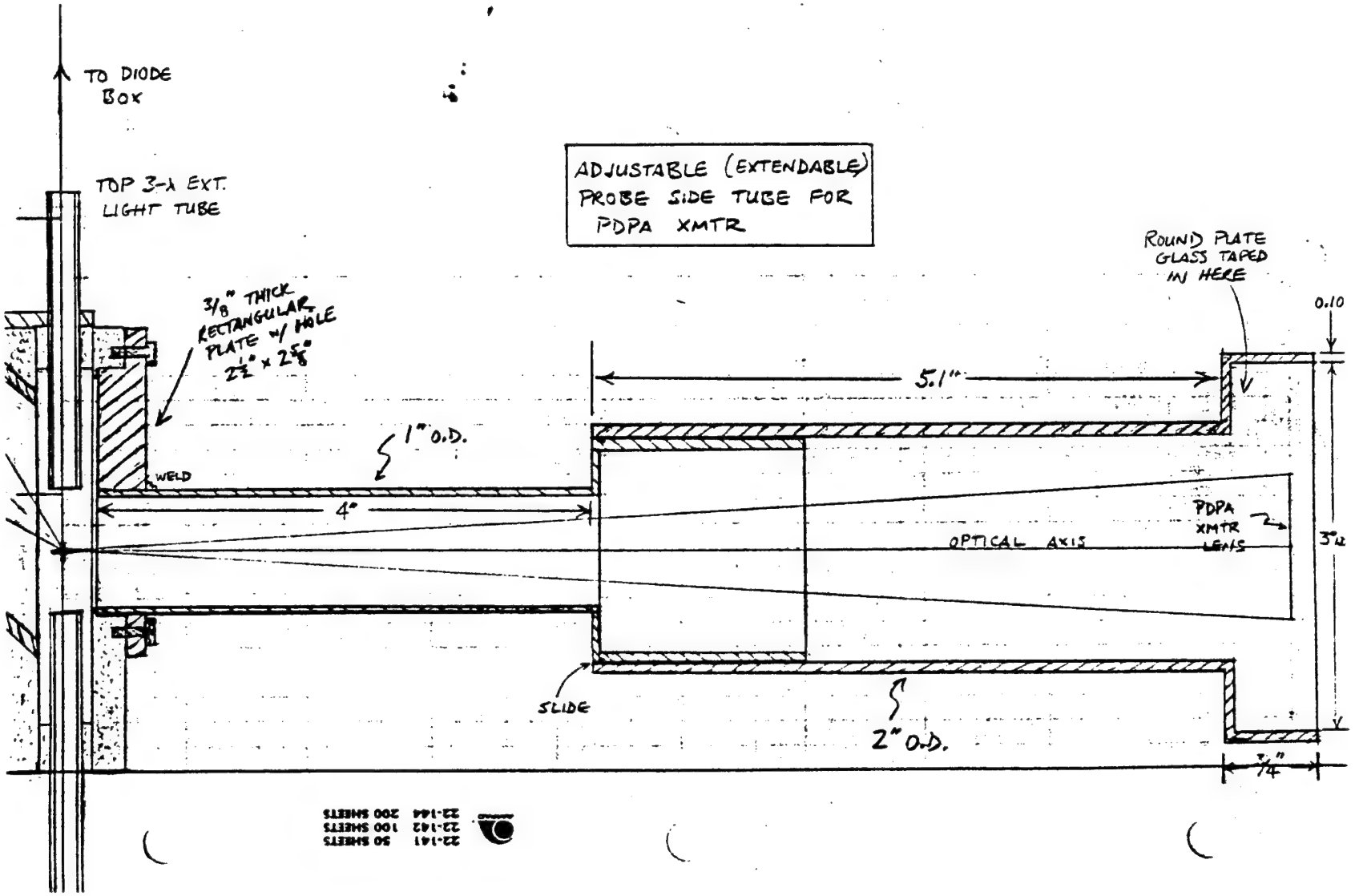
TO DIODE BOX
TOP 3-λ EXT. LIGHT TUBE
ADJUSTABLE (EXTENDABLE) PROBE SIDE TUBE FOR PDPA XMTR
3/8" THICK RECTANGULAR PLATE w/ HOLE 2 1/2" x 2 5/8"
ROUND PLATE GLASS TAPED IN HERE
0.10
5.1"
1" O.D.
WELD
4"
PDPA XMTR LENS
OPTICAL AXIS
3 1/2"
SLIDE
2" O.D.
3/4"

Manser/Netzer
10-26-94

TIP – PLUME PROBE

MAT'L: STAINLESS STEEL

SCALE: 2:1

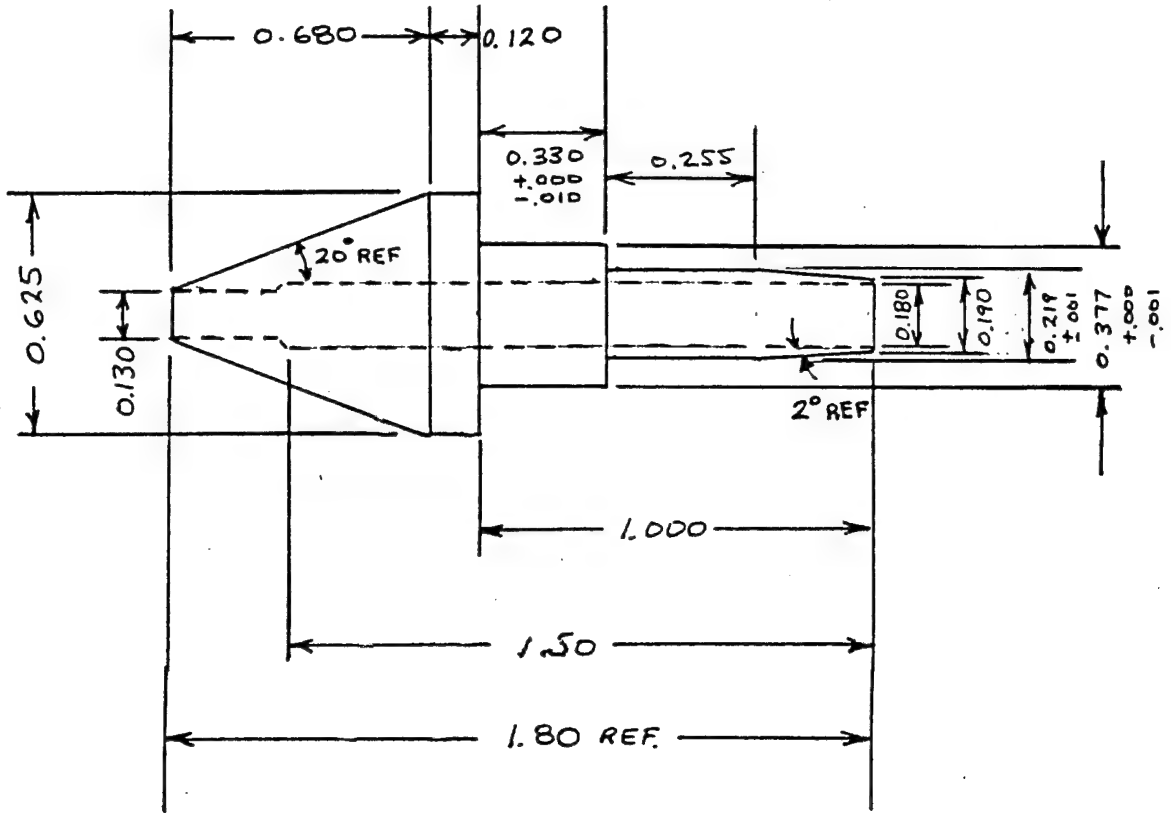

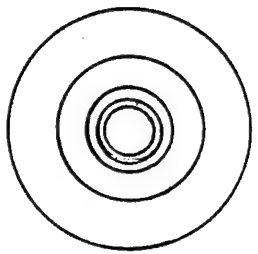

APPENDIX C. MIE CODE "MIESCAT3.FOR"

On the following pages is the Fortran program to calculate extinction coefficients Q, average extinction coefficients $\bar{Q}$, and ratios of average extinction coefficients for the inputs given in "miescat3.dat". The original program was run on the main-frame computer at NPS. Since the Combustion Research Lab (CRL) did not have a network connection to the main-frame the program was copied and modified to run on an IBM compatible PC using the Microsoft® MS® Fortran 4.1 compiler at the CRL.

The data block in the original program followed the end subroutine. Since the source code had to be compiled and linked prior to execution, it was inconvenient to have to repeat these steps each time the inputs were changed. Therefore, the data block was removed and put in the separate file "miescat3.dat" and the read statements modified in the source code.

```
C
C
C                BY KENNETH CASHDOLLAR,  1976
C                REVISED BY THOMAS WELDON, JULY, 1977
C                BASED ON PROGRAM MICOEF BY C D LITTON AND Z J FINK
C                REVISED BY LT JOHN MANSER, USN 1994-1995 (UPDATED FOR
C                   MS-FORTRAN 4.1,DATA BLOCK WITH WAVES PUT INTO
C                   EXTERNAL FILE)
C
C
C    "MIESCAT3.EXE" CALCULATES EXTINCTION COEFFICIENTS AND RATIOS FOR
C    LIGHT TRANSMISSION THROUGH DUST PARTICLES WITH COMPLEX REFRACTIVE
C    INDEX AND A LOG-NORMAL SIZE DISTRIBUTION
C
C
C
C
C**********  "MIESCAT3.DAT" INPUT DATA FILE FORMAT  ******************
C
C
C         VARIABLE NAMES AS IN PROGRAM
C
C     ROW 1.....WAV(1),WAV(2),WAV(3)
C     ROW 2.....NDATA
C     ROW 3.....RDUST,RMED
C     ROW 4.....L2,L3,DS,DELDS
C     ROW 5.....ND,SIGMA,SD32,SDL32
C
C        FORMATS AND VARIABLE DESCRIPTION
C
C     ROW 1....F6.4 (WAVELENGTH 1),2X,F6.4 (WAVELENGTH 2),2X,
C                F6.4 (WAVELENGTH 3)
C     ROW 2....I3 (DATA SET IDENTIFIER, IF EQUAL TO 999 SUBSEQUENT
C                DATA IS NOT PROCESSED).
C     ROW 3....2F6.3 (COMPLEX REFRACTIVE INDEX OF DUST PARTICLES),
C                2X,F6.3 (REFRACTIVE INDEX OF THE MEDIUM).
C     ROW 4....I3 (L2, THE NUMBER OF INCREMENTS TAKEN AT A SET DELTA
C                )(THE  NUMBER OF TIMES DELTA IS DOUBLED, L3),F6.3
C                (STAR DIAMETER),F6.3(INITIAL VALUE OF DELTA).
C     ROW 5....I3(NUMBER OF INCREMENTS TAKEN FOR LOG-NORM),F4.1(SIGM
C                F5.2(STARTING DIAMETER),F5.2(DELTA).
C
C
C
C***********************************************************************
C
C
C
C
      COMPLEX R,RDUST,DI,DELDI,RX,RINDX,DIS,DELIS
      COMPLEX COEFR,DPR(1000),XJR(1000),DJR(1000),PR(1000)
      DIMENSION XY(1000),WAV(3)
      DIMENSION DP(1000),XK(1000),XJ(1000),DJ(1000),P(1000)
      DIMENSION RAT1(100),RAT2(100),RAT3(100)
      DIMENSION PLOTDY(100)
      COMPLEX A(1000),B(1000),C(1000)
      COMPLEX ALPH,XH(1000),DH(1000),E(1000),DE(1000)
      COMMON/ADQ/DQ(500,2)
      COMMON ALLQ(100,4,3)
      COMMON/KPLT/RINDX(3),WAVL(3)
```

```
      COMMON DIAM32(100)
C
C
C
C
      IPEN = 4
C      CALL SHERPA('FILENAME','M',IPEN)
C
      OPEN (UNIT=1, FILE='MIESCAT3.DAT')
      READ (1,103)WAV(1),WAV(2),WAV(3)
  103 FORMAT(F6.4,2X,F6.4,2X,F6.4)
      DO 8 NDATA=1,10
      READ (1,105)NDAT
  105 FORMAT(I3)
      IF(NDAT.EQ.999) GO TO 9
C
C
C     RDUST IS COMPLEX REFRACTIVE INDEX OF DUST PARTICLES, WITH MINUS
C     RMED IS REAL REFRACTIVE INDEX OF MEDIUM
      READ (1,32)RDUST,RMED
   32 FORMAT(2F6.3,2X,F6.3)
C     RX IS RELATIVE REFRACTIVE INDEX,     (N-IK)/M
      RX=RDUST/RMED
C     IMAGINARY PART OF R CHANGED TO POSITIVE TO CONFORM TO EXPANSION
C     FORMULA IN PROGRAM
      R=CONJG(RX)
      RINDX(1)=RX
      RINDX(2)=RX
      RINDX(3)=RX
C
C     L2*L3 = NUMBER OF SIZE INCREMENTS
C     INITIAL DIAMETER IS DS, INITIAL VALUE OF DELTA IS DELDS
C
      READ (1,34)L2,L3,DS,DELDS
   34 FORMAT(2I3,2F6.3)
C
C     INITIAL VALUE OF COMPLEX DIAMETER IS DIS
      DIS=CMPLX(0.0,DS)
      DELIS=CMPLX(0.0,DELDS)
C
      READ (1,12)ND,SIGMA,SD32,SDL32
   12 FORMAT(I3,F5.2,2F5.2)
C     WAVE IS WAVELENGTH OF LIGHT IN MICRONS
C      WAV(1)=0.3650
C      WAV(2)=0.5461
C      WAV(3)=0.8520
C     INITIAL VALUES FOR ARRAY
      DO 51 K=1,3
      DO 52 J=1,2
      ALLQ(1,J,K)=0.0
      ALLQ(1,J+2,K)=0.0
      DO 53 I= 2,100
      ALLQ(I,J,K)=100.0
      ALLQ(I,J+2,K)=1.0
   53 CONTINUE
   52 CONTINUE
   51 CONTINUE
      DO 54 I=1,100
      DIAM32(I)=0.0
      RAT1(I)=0.0
```

```
      RAT2(I)=0.0
      RAT3(I)=0.0
      PLOTDY(I)=0.0
   54 CONTINUE
      DO 4 NI=1,3
C
      PRINT 106,NDATA
  106 FORMAT(/' DATA SET NUMBER',I3)
      PRINT 35
   35 FORMAT(' MIE COEFFICIENTS FOR MONODISPERSE DUST PARTICLES')
C
      PRINT 41,RDUST,RMED,RX
   41 FORMAT(' RDUST=',2F7.4,/' RMED=',F7.4,/' REL. REF. INDEX=',2F7.4)
      PRINT 104,R
  104 FORMAT(' R=',2F7.4)
      WAVE=WAV(NI)
      PRINT 30,WAVE
   30 FORMAT(' WAVELENGTH =', F7.4,2X,'MICRONS'/)
      PRINT 25
   25 FORMAT(6X,'A',12X,'D',13X,'QABS',11X,'QEXT'/)
      WAVL(NI)=WAVE*10000.0
C
C
C     INITIAL VALUES SET
C
C     MAX VALUE FOR D IS (1000*WAVE)/(1.3*PI*RMED) = 244*WAVE/RMED
C     D IS REAL DIAMETER IN MICRONS,DELD IS INCREMENT
C     DI=I*D IS COMPLEX DIAMETER, DELDI IS INCREMENT
C     X IS REAL SIZE PARAMETER  X= PI*DIAMETER*RMED/WAVELENGTH
C     ALPH IS COMPLEX SIZE PARAMETER, ALPH=I*X
      D=DS
      DELD=DELDS
      DI=DIS
      DELDI=DELIS
C
C
C
      M=1
      DO 3 J=1,L3
      DO 2 I=1,L2
      X=3.14159*D/WAVE*RMED
      ALPH=3.14159*DI/WAVE*RMED
      XJ(1)= SIN(X)/X
      XJ(2)= SIN(X)/(X**2)- COS(X)/X
      XJR(1)=CSIN(R*X)/(R*X)
      XJR(2)=CSIN(R*X)/((R*X)**2)-CCOS(R*X)/(R*X)
      XH(1)=CEXP(ALPH)/ALPH
      XH(2)=((-CEXP(ALPH))/X)-((0.,1.)*CEXP(ALPH)/(X**2))
      DJ(1)= COS(X)/X- SIN(X)/(X**2)
      DJR(1)=CCOS(R*X)/(R*X)-CSIN(R*X)/((R*X)**2)
      DH(1)=CEXP(ALPH)/X+((0.,1.)*CEXP(ALPH)/(X**2))
      QEXT=0.0
      QSCA=0.0
C
C     L1 = ITERATIONS FOR SPHERICAL FUNCTIONS,  L1=1.3*X
      L1=1.3*X
      IF(L1.LE.10)  L1=10
      DO 1 L=1,L1
      CO=(FLOAT(L))/(2*L+1)
      COE=(FLOAT(L+1))/(2*L+1)
```

```
      COEF=(FLOAT(2*L+1))/X
      COEFR=(FLOAT(2*L+1))/(R*X)
      XJ(L+2)=COEF*XJ(L+1)-XJ(L)
      XJR(L+2)=COEFR*XJR(L+1)-XJR(L)
      XH(L+2)=COEF*XH(L+1)-XH(L)
      DJ(L+1)=CO*XJ(L)-COE*XJ(L+2)
      DJR(L+1)=CO*XJR(L)-COE*XJR(L+2)
      DH(L+1)=CO*XH(L)-COE*XH(L+2)
      P(L)=X*XJ(L+1)
      PR(L)=(R*X)*XJR(L+1)
      DP(L)=XJ(L+1)+X*DJ(L+1)
      DPR(L)=XJR(L+1)+(R*X)*DJR(L+1)
      E(L)=X*XH(L+1)
      DE(L)=XH(L+1)+X*DH(L+1)
      A(L)=((DPR(L)*P(L))-(R*PR(L)*DP(L)))/((DPR(L)*E(L))-(R*PR(L)*DE(L
     1)))
      B(L)=((R*DPR(L)*P(L))-(PR(L)*DP(L)))/((R*DPR(L)*E(L))-(PR(L)*DE(L
     1)))
      C(L)=A(L)+B(L)
      GAMMA=CABS(A(L))
      BETA=CABS(B(L))
      XK(L)=(FLOAT(2*L+1))*(2./(X**2))*((GAMMA**2)+(BETA**2))
      XY(L)=(FLOAT(2*L+1))*(2./(X**2))*(REAL(C(L)))
      QEXT=QEXT+XY(L)
      QSCA=QSCA+XK(L)
    1 CONTINUE
      QABS=QEXT-QSCA
      DQ(M,1)=D
      DQ(M,2)=QEXT
      PRINT 22,X,DQ(M,1),QABS,DQ(M,2)
   22 FORMAT(1X,F8.3,6X,F7.3,9X,F6.3,9X,F6.3)
C
C     D AND QEXT FOR MONODISPERSE PUT INTO PLOTTING ARRAY
C     EVERY FOURTH POINT CALCULATED IS PUT INTO ARRAY- ALLQ
C
      XM=M
      AREL=XM/4.0
      MINT=M/4
      XMINT=MINT
      IF (AREL.NE.XMINT) GO TO 60
      IF (D.GT.1.20) GO TO 60
C     NUMBER OF POINTS FOR PLOTS 1 AND 3 IS NPTS1
      NPTS1=MINT
      ALLQ(MINT+1,1,NI)=D
      ALLQ(MINT+1,3,NI)=QEXT
      ALLQ(MINT+1,1,NI)=D
      ALLQ(MINT+1,3,NI)=QEXT
   60 CONTINUE
C     INCREMENT SIZE PARAMETERS        D=DIAMETER
      D=D+DELD
      DI=DI+DELDI
      M=M+1
    2 CONTINUE
C      PRINT 36
   36 FORMAT (1H )
      DELD=2.0*DELD
      DELDI=2.0*DELDI
    3 CONTINUE
      PRINT 106,NDATA
      PRINT 235
```

```
  235 FORMAT(' MIE COEFFICIENTS FOR LOG-NORMAL DUST DISTRIBUTION')
      PRINT 236,SIGMA
  236 FORMAT (' SIGMA=',F4.2)
      PRINT 237,RX
  237 FORMAT(' RELATIVE REFRACTIVE INDEX=',2F7.4)
      PRINT 30,WAVE
      CALL QAVG(M,NI,SIGMA,NPTS2,SD32,SDL32,ND)
      K1=ND+1
      DO 499 N=1,K1
      PLOTDY(N)=ALLQ(N,4,NI)
  499 CONTINUE
C      IF(NI.EQ.2) GO TO 502
C      IF(NI.EQ.3) GO TO 503
C  501 CALL PLOTD(DIAM32,PLOTDY,41,.FALSE.,'LINLIN','NOLEGEND',
C     +           ' ','Diameter, microns','Extinction Coefficient')
C      GO TO 4
C  502 CALL PLOTD(DIAM32,PLOTDY,41,.FALSE.,'LINLIN','NOLEGEND',
C     +           ' ','Diameter, microns','Extinction Coefficient')
C      GO TO 4
C  503 CALL PLOTD(DIAM32,PLOTDY,41,.TRUE. ,'LINLIN','NOLEGEND',
C     +           ' ','Diameter, microns','Extinction Coefficient')
    4 CONTINUE
      PRINT 106,NDATA
    7 CONTINUE
      PRINT 500
  500 FORMAT(' QBAR RATIOS FOR 3 WAVELENGTHS')
      PRINT 236,SIGMA
      PRINT 237,RX
      PRINT 510,WAV(3),WAV(1),WAV(3),WAV(2),WAV(2),WAV(1)
  510 FORMAT(/2X,' D32 ',3(5X,'QBAR(',F6.4,')/QBAR(',F6.4,')')/)
      K=ND+1
      DO 600 N=2,K
      RAT1(N)=ALLQ(N,4,3)/ALLQ(N,4,1)
      RAT2(N)=ALLQ(N,4,3)/ALLQ(N,4,2)
      RAT3(N)=ALLQ(N,4,2)/ALLQ(N,4,1)
      PRINT 650,DIAM32(N),RAT1(N),RAT2(N),RAT3(N)
  600 CONTINUE
  650 FORMAT(1X,F6.3,13X,F7.4,23X,F7.4,23X,F7.4)
      PRINT 350,NDATA
  350 FORMAT (/'************************* END OF DATA SET NUMBER',I3/)
C      CALL PLOTD(DIAM32(2),RAT1(2),40,.FALSE.,'LINLIN','NOLEGEND',
C     +           ' ','Diameter, microns','Extinction Coefficient')
C      CALL PLOTD(DIAM32(2),RAT2(2),40,.FALSE.,'LINLIN','NOLEGEND',
C     +           ' ','Diameter, microns','Extinction Coefficient')
C      CALL PLOTD(DIAM32(2),RAT3(2),40,.TRUE. ,'LINLIN','NOLEGEND',
C     +           ' ','Diameter, microns','Extinction Coefficient')
    8 CONTINUE
    9 CONTINUE
C      CALL DONEPL
      END
C     ---------------------------------------------------------------
      SUBROUTINE QAVG(M,NI,SIGMA,NPTS2,SD32,SDL32,ND)
C
C                BY KENNETH CASHDOLLAR, 1976
C
C     QAVG CALCULATES D32 AND QBAR FOR A GIVEN QEXT VS D AND
C     A GIVEN LOG-NORMAL SIZE DISTRIBUTION
C
C
C     INPUT DATA = ND,SIGMA,D32,DEL32
```

```
C
C
      COMMON ALLQ(100,4,3)
      COMMON/ADQ/DQ(500,2)
      COMMON DIAM32(100)
C     DQ(I,1)=D,  DQ(I,2)=QEXT
C     NI=WAVELENGTH OR REFRACTIVE INDEX CHANGE
C     ND IS NUMBER OF D32,QBAR CALCULATIONS
C     SIGMA IS THE GEOMETRIC STANDARD DEVIATION
C     D32 IS THE SURFACE WEIGHTED MEAN DIAMETER
C     DEL32 IS INCREMENT FOR D32
C     DIST IS SURFACE WEIGHTED LOG-NORMAL SIZE DISTRIBUTION
C     M IS THE MAXIMUM NUMBER OF POINTS IN Q-ARRAY FOR MONODISPERSE
C
      PRINT 240
  240 FORMAT(3X,'D32',8X,'DMIN',7X,'DMAX',5X,'NMBR',6X,'D10X',7X,'D32X'
     1,7X,'QBAR'/)
C
      D32=SD32
      DEL32=SDL32
C
C     NUMBER OF POINTS FOR PLOTS 2 AND 4 IS NPTS2
      NPTS2=ND+1
      DO 17 NN=1,ND
      DMIN=D32/SIGMA**3.
      DMAX=D32*SIGMA**2.5
      AS=ALOG(SIGMA)**2.
      DG=EXP(ALOG(D32)-2.5*AS)
      QSUM=0.0
      DSUM=0.0
      XSUM=0.0
      DHOLD=0.0
      DNSUM=0.0
      XNSUM=0.0
      NMBR=0
      MM=M-2
      DO 13  N=1,MM
      IF (DQ(N,1).LT.DMIN) GO TO 13
      IF (DQ(N,1).GT.DMAX) GO TO 15
      IF (NMBR.GT.0) GO TO 242
      DMINZ=DQ(N,1)
  242 CONTINUE
      DD=DQ(N+1,1)-DQ(N,1)
      AA=(ALOG(DQ(N+1,1)/DG))**2/(2.0*AS)
      DIST=EXP(-AA)*DQ(N+1,1)/SQRT(6.2832*AS)
      QSUM=QSUM+(DIST*DQ(N+1,2)+DHOLD*DQ(N,2))*DD/2.0
      DSUM=DSUM+(DIST*DQ(N+1,1)+DHOLD*DQ(N,1))*DD/2.0
      XSUM=XSUM+(DIST+DHOLD)*DD/2.0
      XNSUM=XNSUM+(DIST/DQ(N+1,1)**2+DHOLD/DQ(N,1)**2)/2.0*DD
      DNSUM=DNSUM+(DIST/DQ(N+1,1)+DHOLD/DQ(N,1))/2.0*DD
      XHOLD=DQ(N+1,1)
      DHOLD=DIST
      NMBR=NMBR+1
   13 CONTINUE
   15 CONTINUE
      QBAR=QSUM/XSUM
      D32X=DSUM/XSUM
      D10X=DNSUM/XNSUM
      ALLQ(NN+1,2,NI)=D32X
      ALLQ(NN+1,4,NI)=QBAR
```

```
      DIAM32(NN+1)=D32
      PRINT 241,D32,DMINZ,XHOLD,NMBR,D10X,D32X,QBAR
  241 FORMAT(1X,3(F6.3,5X),I3,5X,2(F6.3,5X),F7.4,5X)
      D32=D32+DEL32
   17 CONTINUE
      RETURN
      END
```

APPENDIX D. MACRO FOR LOTUS 1-2-3 RELEASE 4

On the following pages is a macro for Lotus® 1-2-3® Release 4 for Windows™. When the output data file from "miescat3.exe" was imported into a 1-2-3 spreadsheet all the data would enter as a single column due to text blocks between sets of data. Therefore, data parsing was necessary to split the data and enter it into the appropriate number of columns. Since this operation needed to be performed every time the "miescat3.exe" data was to be used it was advantageous to create a macro to automate this task. The macro was recorded as the data parsing was done manually for one entire file, then the macro was edited until it was streamlined and all the bugs were fixed. It is included here specifically for those who must also work with the "miescat3.exe" output.

It has been subsequently discovered that by using the File Open, [miescat3.exe output filename], Combine, Formatted Text combination that the data will be imported properly. However, all of the text blocks including data labels will be missing. Therefore, the use of this macro may be the best option.

This file contains the macro to properly format the data output from "miescat3.exe"

```
{PARSE A:A10;A:A10;"*****L************L************L>>>***********L>>>"}          Data Set #1 Wave(1) labels
{SELECT A:A11..A:IV11;A:A11}
{DELETE-ROWS}
{SELECT A:A10..A:D10;A:A10}
{STYLE-ALIGN-HORIZONTAL "RIGHT"}
{PARSE A:A12..A:A241;A:A12;"***V>>>>********V>>>>**********V>>>>*********V>>>>"}          data
{SELECT A:A242..A:IV242;A:A242}
{DELETE-ROWS}
{PARSE A:A249;A:A249;"**L>>********L>>>*******L>>>*****L>>>******L>>>*******L>>>*******L>>>"}          labels
{SELECT A:A250..A:IV250;A:A250}
{DELETE-ROWS}
{SELECT A:A249..A:G249;A:A249}
{STYLE-ALIGN-HORIZONTAL "RIGHT"}
{PARSE A:A251..A:A290;A:A251;"*V>>>>******V>>>>******V>>>>*******V******V>>>>******V>>>>******V>>>>>"}          data
{SELECT A:A291..A:IV291;A:A291}
{DELETE-ROWS}
{PARSE A:A300;A:A300;"*****L************L***********L>>>***********L>>>"}          Wave(2) labels
{SELECT A:A301..A:IV301;A:A301}
{DELETE-ROWS}
{SELECT A:A300..A:D300;A:A300}
{STYLE-ALIGN-HORIZONTAL "RIGHT"}
{PARSE A:A302..A:A531;A:A302;"***V>>>>********V>>>>**********V>>>>*********V>>>>>"}          data
{SELECT A:A532..A:IV532;A:A532}
{DELETE-ROWS}
{PARSE A:A539;A:A539;"**L>>********L>>>*******L>>>*****L>>>******L>>>*******L>>>*******L>>>"}          labels
{SELECT A:A540..A:IV540;A:A540}
{DELETE-ROWS}
{SELECT A:A539..A:G539;A:A539}
{STYLE-ALIGN-HORIZONTAL "RIGHT"}
{PARSE A:A541..A:A580;A:A541;"*V>>>>******V>>>>******V>>>>*******V******V>>>>******V>>>>******V>>>>>"}          data
{SELECT A:A581..A:IV581;A:A581}
{DELETE-ROWS}
{PARSE A:A590;A:A590;"*****L************L***********L>>>***********L>>>"}          Wave(3) labels
{SELECT A:A591..A:IV591;A:A591}
{DELETE-ROWS}
{SELECT A:A590..A:D590;A:A590}
{STYLE-ALIGN-HORIZONTAL "RIGHT"}
{PARSE A:A592..A:A821;A:A592;"***V>>>>********V>>>>**********V>>>>*********V>>>>"}          data
{SELECT A:A822..A:IV822;A:A822}
{DELETE-ROWS}
{PARSE A:A829;A:A829;"**L>>********L>>>*******L>>>*****L>>>******L>>>*******L>>>*******L>>>"}          labels
{SELECT A:A830..A:IV830;A:A830}
{DELETE-ROWS}
{SELECT A:A829..A:G829;A:A829}
{STYLE-ALIGN-HORIZONTAL "RIGHT"}
{PARSE A:A831..A:A870;A:A831;"*V>>>>******V>>>>******V>>>>*******V******V>>>>******V>>>>******V>>>>>"}          data
{SELECT A:A871..A:IV871;A:A871}
{DELETE-ROWS}
{PARSE A:A877;A:A877;"**L>>******L>>>>>>>>>>>>>>>>>>>>>>>>*****L>>>>>>>>>>>>>>>>>>>>>>>>*****L>>>>>>>>>>>>>>>>>>>>>>>>>"}          end labels
{SELECT A:A878..A:IV878;A:A878}
{DELETE-ROWS}
{SELECT A:A877..A:J877;A:A877}
{STYLE-ALIGN-HORIZONTAL "RIGHT"}
{PARSE A:A879..A:A918;A:A879;"*V>>>>**************V>>>>>***********************V>>>>>***********************V>>>>>"}          end data
{SELECT A:A919..A:IV919;A:A919}
{DELETE-ROWS}
{EDIT-QUICK-MOVE A:D877..A:F918;A:B877..A:D918}
{EDIT-QUICK-MOVE A:G877..A:H918;A:E877..A:F918}
{EDIT-QUICK-MOVE A:J877..A:J918;A:H877..A:H918}
```

APPENDIX E. MIE CODE "MIESCAT6.FOR"

To simplify the data reduction process (i.e., finding the best combination of complex index of refraction m, geometric standard deviation σ_g, and Sauter mean diameter d_{32} for the measured transmittances) the Mie Code in Appendix B was further modified. Each modification resulted in the program getting assigned a new number such as "miescat4.for". Since the input data file and the compiled executable version usually also changed they were both given the new number. This particular program allows iteration starting values, step sizes, and the number of loops to be input in the data file for m and σ_g. The program outputs the current values of m and σ_g and the best fit d_{32} as well as the Sum of the Squared Deviations (SSD) value for the fit between the ln$T$ ratios and the $\bar{Q}$ ratios.

```
C
C
C               BY KENNETH CASHDOLLAR,  1976
C               REVISED BY THOMAS WELDON, JULY, 1977
C               BASED ON PROGRAM MICOEF BY C D LITTON AND Z J FINK
C               REVISED BY LT JOHN MANSER, USN 1994-1995 (PLOT
C                  FUNCTIONS REMOVED, UPDATED FOR MS-FORTRAN 4.1,
C                  DATA BLOCK WITH WAVES & T PUT INTO EXTERNAL FILE,
C                  DATA REDUCTION ITERATIONS ADDED)
C
C
C    "MIESCAT6.EXE" CALCULATES EXTINCTION COEFFICIENTS AND RATIOS FOR
C    LIGHT TRANSMISSION THROUGH DUST PARTICLES WITH COMPLEX REFRACTIVE
C    INDEX AND A LOG-NORMAL SIZE DISTRIBUTION AND OUTPUTS THE SUM OF
C    THE SQUARED DEVIATIONS BETWEEN THE QBAR AND LN(T) RATIOS
C
C
C**************  INPUT DATA FILE "MIESCAT6.DAT" FORMAT  *************
C
C
C         VARIABLE NAMES AS IN PROGRAM
C
C     ROW 1....T1,T2,T3
C     ROW 2....WAV(1),WAV(2),WAV(3)
C     ROW 3....NUMR,STEPR
C     ROW 4....NUMS,STEPS
C     ROW 5....RDUST,RMED
C     ROW 6....L2,L3,DS,DELDS
C     ROW 7....ND,SIGMA,SD32,SDL32
C
C        FORMATS AND VARIABLE DESCRIPTION
C
C     ROW ONE....F6.4(TRANSMITTANCE FOR WAVELENGTH 1),2X,F6.4(TRANSM
C                ITTANCE FOR WAVELENGTH 2),2X,F6.4(TRANSMITTANCE FOR
C                WAVELENGTH 3)
C     ROW TWO....F6.4(WAVELENGTH 1),2X,F6.4(WAVELENGTH 2),2X,F6.4
C                (WAVELENGTH 3) (ALL IN MICRONS)
C     ROW THREE..I3(NUMBER OF ITERATIONS ON RDUST),2X,F4.3(STEP SIZE
C                OF ITERATIONS).
C     ROW FOUR...I3(NUMBER OF ITERATIONS ON SIGMA),2X,F4.3(STEP SIZE
C                OF ITERATIONS).
C     ROW FIVE...2F6.3(COMPLEX REFRACTIVE INDEX OF DUST PARTICLES),
C                2X,F6.3(REFRACTIVE INDEX OF THE MEDIUM).
C     ROW SIX....2I3(L2,THE NUMBER OF INCREMENTS TAKEN AT A SET DELTA)
C                (L3, THE  NUMBER OF TIMES DELTA IS DOUBLED),2F6.3
C                (STAR DIAMETER AND INITIAL VALUE OF DELTA).
C     ROW SEVEN..I3(NUMBER OF INCREMENTS TAKEN FOR LOG-NORM),F4.2
C                (SIGMA),2F5.2(STARTING DIAMETER AND DELTA).
C
C
C*********************************************************************
C
C
      COMPLEX R,RDUST,RDUST1,DI,DELDI,RX,RINDX,DIS,DELIS
      COMPLEX COEFR,DPR(1000),XJR(1000),DJR(1000),PR(1000)
      DIMENSION XY(1000),WAV(3)
      DIMENSION DP(1000),XK(1000),XJ(1000),DJ(1000),P(1000)
      DIMENSION RAT1(100),RAT2(100),RAT3(100)
      DIMENSION RAT4(100),RAT5(100),RAT6(100),SSD(100)
      COMPLEX A(1000),B(1000),C(1000)
```

```
      COMPLEX ALPH,XH(1000),DH(1000),E(1000),DE(1000)
      COMMON/ADQ/DQ(500,2)
      COMMON ALLQ(100,4,3)
      COMMON/KPLT/RINDX(3),WAVL(3)
      COMMON DIAM32(100)
C
C
      OPEN (UNIT=1, FILE='MIESCAT6.DAT')
      READ (1,103)T1,T2,T3
      READ (1,103)WAV(1),WAV(2),WAV(3)
  103 FORMAT(F6.4,2X,F6.4,2X,F6.4)
      READ (1,104)NUMR,STEPR
      READ (1,104)NUMS,STEPS
  104 FORMAT(I3,2X,F4.3)
C      DO 8 NDATA=1,10
C      READ (1,105)NDAT
C  105 FORMAT(I3)
C      IF(NDAT.EQ.999) GO TO 9
      NDAT=001
C
C     RDUST IS COMPLEX REFRACTIVE INDEX OF DUST PARTICLES, WITH MINUS
C     RMED IS REAL REFRACTIVE INDEX OF MEDIUM
      READ (1,32)RDUST,RMED
   32 FORMAT(2F6.3,2X,F6.3)
      READ (1,34)L2,L3,DS,DELDS
   34 FORMAT(2I3,2F6.3)
      READ (1,12)ND,SIGMA,SD32,SDL32
   12 FORMAT(I3,F5.2,2F5.2)
      RDUST1=RDUST
      PRINT 18
   18 FORMAT(' EXP. TRANSMITTANCES:')
      PRINT 20,WAV(1),T1,WAV(2),T2,WAV(3),T3
   20 FORMAT(3('    T(',F6.4,')=',F6.4)/)
      PRINT 21
   21 FORMAT(' BEST LOG-NORMAL FIT VALUES:')
      PRINT 22
   22 FORMAT(8X,'M',11X,'SIGMAG',7X,'D32',10X,'SSD')
      DO 9 INDEX1=1,NUMS
      DO 8 INDEX2=1,NUMR
C     RX IS RELATIVE REFRACTIVE INDEX,     (N-IK)/M
      RX=RDUST/RMED
C     IMAGINARY PART OF R CHANGED TO POSITIVE TO CONFORM TO EXPANSION
C     FORMULA IN PROGRAM
      R=CONJG(RX)
      RINDX(1)=RX
      RINDX(2)=RX
      RINDX(3)=RX
C
C     L2*L3 = NUMBER OF SIZE INCREMENTS
C     INITIAL DIAMETER IS DS, INITIAL VALUE OF DELTA IS DELDS
C
C
C     INITIAL VALUE OF COMPLEX DIAMETER IS DIS
      DIS=CMPLX(0.0,DS)
      DELIS=CMPLX(0.0,DELDS)
C
C     INITIAL VALUES FOR ARRAY
      DO 51 K=1,3
      DO 52 J=1,2
      ALLQ(1,J,K)=0.0
```

```
      ALLQ(1,J+2,K)=0.0
      DO 53 I= 2,100
      ALLQ(I,J,K)=100.0
      ALLQ(I,J+2,K)=1.0
   53 CONTINUE
   52 CONTINUE
   51 CONTINUE
      DO 54 I=1,100
      DIAM32(I)=0.0
      RAT1(I)=0.0
      RAT2(I)=0.0
      RAT3(I)=0.0
   54 CONTINUE
      DO 4 NI=1,3
C
C       PRINT 106,NDATA
C  106 FORMAT(/' DATA SET NUMBER',I3)
C       PRINT 35
C   35 FORMAT(' MIE COEFFICIENTS FOR MONODISPERSE DUST PARTICLES')
C
C       PRINT 41,RDUST,RMED,RX
C   41 FORMAT(' RDUST=',2F7.4,/' RMED=',F7.4,/' REL. REF. INDEX=',2F7.4)
C       PRINT 104,R
C  104 FORMAT(' R=',2F7.4)
      WAVE=WAV(NI)
C       PRINT 30,WAVE
C   30 FORMAT(' WAVELENGTH =', F7.4,2X,'MICRONS'/)
C       PRINT 25
C   25 FORMAT(6X,'A',12X,'D',13X,'QABS',11X,'QEXT'/)
      WAVL(NI)=WAVE*10000.0
C
C
C     INITIAL VALUES SET
C
C     MAX VALUE FOR D IS (1000*WAVE)/(1.3*PI*RMED) = 244*WAVE/RMED
C     D IS REAL DIAMETER IN MICRONS,DELD IS INCREMENT
C     DI=I*D IS COMPLEX DIAMETER, DELDI IS INCREMENT
C     X IS REAL SIZE PARAMETER  X= PI*DIAMETER*RMED/WAVELENGTH
C     ALPH IS COMPLEX SIZE PARAMETER, ALPH=I*X
      D=DS
      DELD=DELDS
      DI=DIS
      DELDI=DELIS
C
C
C
      M=1
      DO 3 J=1,L3
      DO 2 I=1,L2
      X=3.14159*D/WAVE*RMED
      ALPH=3.14159*DI/WAVE*RMED
      XJ(1)= SIN(X)/X
      XJ(2)= SIN(X)/(X**2)- COS(X)/X
      XJR(1)=CSIN(R*X)/(R*X)
      XJR(2)=CSIN(R*X)/((R*X)**2)-CCOS(R*X)/(R*X)
      XH(1)=CEXP(ALPH)/ALPH
      XH(2)=((-CEXP(ALPH))/X)-((0.,1.)*CEXP(ALPH)/(X**2))
      DJ(1)= COS(X)/X- SIN(X)/(X**2)
      DJR(1)=CCOS(R*X)/(R*X)-CSIN(R*X)/((R*X)**2)
      DH(1)=CEXP(ALPH)/X+((0.,1.)*CEXP(ALPH)/(X**2))
```

```
      QEXT=0.0
      QSCA=0.0
C
C     L1 = ITERATIONS FOR SPHERICAL FUNCTIONS,  L1=1.3*X
      L1=1.3*X
      IF(L1.LE.10)  L1=10
      DO 1 L=1,L1
      CO=(FLOAT(L))/(2*L+1)
      COE=(FLOAT(L+1))/(2*L+1)
      COEF=(FLOAT(2*L+1))/X
      COEFR=(FLOAT(2*L+1))/(R*X)
      XJ(L+2)=COEF*XJ(L+1)-XJ(L)
      XJR(L+2)=COEFR*XJR(L+1)-XJR(L)
      XH(L+2)=COEF*XH(L+1)-XH(L)
      DJ(L+1)=CO*XJ(L)-COE*XJ(L+2)
      DJR(L+1)=CO*XJR(L)-COE*XJR(L+2)
      DH(L+1)=CO*XH(L)-COE*XH(L+2)
      P(L)=X*XJ(L+1)
      PR(L)=(R*X)*XJR(L+1)
      DP(L)=XJ(L+1)+X*DJ(L+1)
      DPR(L)=XJR(L+1)+(R*X)*DJR(L+1)
      E(L)=X*XH(L+1)
      DE(L)=XH(L+1)+X*DH(L+1)
      A(L)=((DPR(L)*P(L))-(R*PR(L)*DP(L)))/((DPR(L)*E(L))-(R*PR(L)*DE(L
     1)))
      B(L)=((R*DPR(L)*P(L))-(PR(L)*DP(L)))/((R*DPR(L)*E(L))-(PR(L)*DE(L
     1)))
      C(L)=A(L)+B(L)
      GAMMA=CABS(A(L))
      BETA=CABS(B(L))
      XK(L)=(FLOAT(2*L+1))*(2./(X**2))*((GAMMA**2)+(BETA**2))
      XY(L)=(FLOAT(2*L+1))*(2./(X**2))*(REAL(C(L)))
      QEXT=QEXT+XY(L)
      QSCA=QSCA+XK(L)
    1 CONTINUE
      QABS=QEXT-QSCA
      DQ(M,1)=D
      DQ(M,2)=QEXT
C      PRINT 22,X,DQ(M,1),QABS,DQ(M,2)
C   22 FORMAT(1X,F8.3,6X,F7.3,9X,F6.3,9X,F6.3)
C
C     D AND QEXT FOR MONODISPERSE PUT INTO PLOTTING ARRAY
C     EVERY FOURTH POINT CALCULATED IS PUT INTO ARRAY- ALLQ
C
      XM=M
      AREL=XM/4.0
      MINT=M/4
      XMINT=MINT
      IF (AREL.NE.XMINT) GO TO 60
      IF (D.GT.1.20) GO TO 60
C     NUMBER OF POINTS FOR PLOTS 1 AND 3 IS NPTS1
      NPTS1=MINT
      ALLQ(MINT+1,1,NI)=D
      ALLQ(MINT+1,3,NI)=QEXT
      ALLQ(MINT+1,1,NI)=D
      ALLQ(MINT+1,3,NI)=QEXT
   60 CONTINUE
C     INCREMENT SIZE PARAMETERS          D=DIAMETER
      D=D+DELD
      DI=DI+DELDI
```

```
      M=M+1
    2 CONTINUE
C       PRINT 36
   36 FORMAT (1H )
      DELD=2.0*DELD
      DELDI=2.0*DELDI
    3 CONTINUE
C       PRINT 106,NDATA
C       PRINT 235
C  235 FORMAT(' MIE COEFFICIENTS FOR LOG-NORMAL DUST DISTRIBUTION')
C       PRINT 236,SIGMA
  236 FORMAT (' SIGMA=',F4.2)
C       PRINT 237,RX
  237 FORMAT(' RELATIVE REFRACTIVE INDEX=',2F7.4)
C       PRINT 30,WAVE
      CALL QAVG(M,NI,SIGMA,NPTS2,SD32,SDL32,ND)
    4 CONTINUE
C       PRINT 106,NDATA
    7 CONTINUE
C       PRINT 500
C  500 FORMAT(' QBAR RATIOS FOR 3 WAVELENGTHS')
C       PRINT 236,SIGMA
C       PRINT 237,RX
C       PRINT 509,WAV(1),T1,WAV(2),T2,WAV(3),T3
C  509 FORMAT(' EXP. TRANSMITTANCES:',3(5X,'T(',F6.4,')=',F6.4))
C       PRINT 510,WAV(3),WAV(1),WAV(3),WAV(2),WAV(2),WAV(1)
C  510 FORMAT(/2X,' D32 ',3(5X,'QBAR(',F6.4,')/QBAR(',F6.4,')'),5X,'SUM
C     +OF SQUARED DEVIATIONS'/)
      K=ND+1
      DO 600 N=2,K
      RAT1(N)=ALLQ(N,4,3)/ALLQ(N,4,1)
      RAT2(N)=ALLQ(N,4,3)/ALLQ(N,4,2)
      RAT3(N)=ALLQ(N,4,2)/ALLQ(N,4,1)
      RAT4(N)=(RAT1(N)-LOG(T3)/LOG(T1))**2
      RAT5(N)=(RAT2(N)-LOG(T3)/LOG(T2))**2
      RAT6(N)=(RAT3(N)-LOG(T2)/LOG(T1))**2
      SSD(N)=RAT4(N)+RAT5(N)+RAT6(N)
C       PRINT 650,DIAM32(N),RAT1(N),RAT2(N),RAT3(N),SSD(N)
  600 CONTINUE
C  650 FORMAT(1X,F6.3,13X,F7.4,23X,F7.4,23X,F7.4,23X,F9.4)
C     PRINT 350,NDAT
C  350 FORMAT (/'************************** END OF DATA SET NUMBER',I3/)
      SMALLEST=2
      DO 700 N=2,K
      IF (SSD(N).LT.SSD(SMALLEST)) SMALLEST=N
  700 CONTINUE
      PRINT 701,RDUST,SIGMA,DIAM32(SMALLEST),SSD(SMALLEST)
  701 FORMAT (1X,2F7.4,'I',5X,F4.2,6X,F5.2,6X,F13.8)
      NDAT=NDAT+1
      RDUST=RDUST+STEPR
    8 CONTINUE
      RDUST=RDUST1
      SIGMA=SIGMA+STEPS
    9 CONTINUE
      END
C     ------------------------------------------------------------------
      SUBROUTINE QAVG(M,NI,SIGMA,NPTS2,SD32,SDL32,ND)
C
C                 BY KENNETH CASHDOLLAR, 1976
C
```

```
C     QAVG CALCULATES D32 AND QBAR FOR A GIVEN QEXT VS D AND
C     A GIVEN LOG-NORMAL SIZE DISTRIBUTION
C
C
C     INPUT DATA = ND,SIGMA,D32,DEL32
C
C
      COMMON ALLQ(100,4,3)
      COMMON/ADQ/DQ(500,2)
      COMMON DIAM32(100)
C     DQ(I,1)=D,  DQ(I,2)=QEXT
C     NI=WAVELENGTH OR REFRACTIVE INDEX CHANGE
C     ND IS NUMBER OF D32,QBAR CALCULATIONS
C     SIGMA IS THE GEOMETRIC STANDARD DEVIATION
C     D32 IS THE SURFACE WEIGHTED MEAN DIAMETER
C     DEL32 IS INCREMENT FOR D32
C     DIST IS SURFACE WEIGHTED LOG-NORMAL SIZE DISTRIBUTION
C     M IS THE MAXIMUM NUMBER OF POINTS IN Q-ARRAY FOR MONODISPERSE
C
C      PRINT 240
C 240 FORMAT(3X,'D32',8X,'DMIN',7X,'DMAX',5X,'NMBR',6X,'D10X',7X,'D32X'
C    1,7X,'QBAR'/)
C
      D32=SD32
      DEL32=SDL32
C
C     NUMBER OF POINTS FOR PLOTS 2 AND 4 IS NPTS2
      NPTS2=ND+1
      DO 17 NN=1,ND
      DMIN=D32/SIGMA**3.
      DMAX=D32*SIGMA**2.5
      AS=ALOG(SIGMA)**2.
      DG=EXP(ALOG(D32)-2.5*AS)
      QSUM=0.0
      DSUM=0.0
      XSUM=0.0
      DHOLD=0.0
      DNSUM=0.0
      XNSUM=0.0
      NMBR=0
      MM=M-2
      DO 13  N=1,MM
      IF (DQ(N,1).LT.DMIN) GO TO 13
      IF (DQ(N,1).GT.DMAX) GO TO 15
      IF (NMBR.GT.0) GO TO 242
      DMINZ=DQ(N,1)
  242 CONTINUE
      DD=DQ(N+1,1)-DQ(N,1)
      AA=(ALOG(DQ(N+1,1)/DG))**2/(2.0*AS)
      DIST=EXP(-AA)*DQ(N+1,1)/SQRT(6.2832*AS)
      QSUM=QSUM+(DIST*DQ(N+1,2)+DHOLD*DQ(N,2))*DD/2.0
      DSUM=DSUM+(DIST*DQ(N+1,1)+DHOLD*DQ(N,1))*DD/2.0
      XSUM=XSUM+(DIST+DHOLD)*DD/2.0
      XNSUM=XNSUM+(DIST/DQ(N+1,1)**2+DHOLD/DQ(N,1)**2)/2.0*DD
      DNSUM=DNSUM+(DIST/DQ(N+1,1)+DHOLD/DQ(N,1))/2.0*DD
      XHOLD=DQ(N+1,1)
      DHOLD=DIST
      NMBR=NMBR+1
   13 CONTINUE
   15 CONTINUE
```

```
      QBAR=QSUM/XSUM
      D32X=DSUM/XSUM
      D10X=DNSUM/XNSUM
      ALLQ(NN+1,2,NI)=D32X
      ALLQ(NN+1,4,NI)=QBAR
      DIAM32(NN+1)=D32
C       PRINT 241,D32,DMINZ,XHOLD,NMBR,D10X,D32X,QBAR
C  241 FORMAT(1X,3(F6.3,5X),I3,5X,2(F6.3,5X),F7.4,5X)
      D32=D32+DEL32
   17 CONTINUE
      RETURN
      END
```

APPENDIX F. LINEAR INTERPOLATION IN LOTUS 1-2-3 RELEASE 4

A formula was written to perform linear interpolation in Lotus® 1-2-3® Release 4 for Windows™. The formula used the diameter value in column B (cell address B10 below) to choose the correct extinction coefficient Q from a separate 1-2-3 file named "qext.wk4". The file "qext.wk4" had a named range QEXT containing seven columns of data: diameter and six columns of Q's for different wavelengths and indices of refraction. The formula below contains the offset for the first column of Q's.

```
@INDEX(<<qext.wk4>>$QEXT,1,@MATCH(B10,<<qext.wk4>>$QEXT,1))+((
@INDEX(<<qext.wk4>>$QEXT,1,@MATCH(B10,<<qext.wk4>>$QEXT,1)+1)-
@INDEX(<<qext.wk4>>$QEXT,1,@MATCH(B10,<<qext.wk4>>$QEXT,1)))/(@
INDEX(<<qext.wk4>>$QEXT,0,@MATCH(B10,<<qext.wk4>>$QEXT,1)+1)-@I
NDEX(<<qext.wk4>>$QEXT,0,@MATCH(B10,<<qext.wk4>>$QEXT,1)))*(B10
-@INDEX(<<qext.wk4>>$QEXT,0,@MATCH(B10,<<qext.wk4>>$QEXT,1))))
```

Linear interpolation can best be described by an example. Suppose d_1 and d_2 are increasing diameters with corresponding extinction coefficients Q_1 and Q_2. Then the Q for a diameter d between d_1 and d_2 is:

$$Q = Q_1 + \left(\frac{Q_2 - Q_1}{d_2 - d_1} * [d - d_1] \right) \tag{F.1}$$

The reader is directed to the User's Guide for further information and the @function help in the software for an explanation of @INDEX and @MATCH.

APPENDIX G. DATA PRINTOUTS, PLOTS, AND TABLES

MALVERN Series 2600 SB.00 Master Mode 07 Mar 1995 1:57 pm

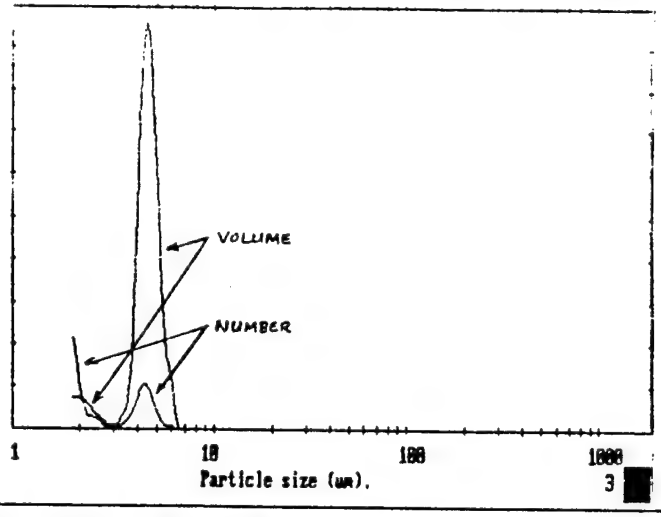

2048 pia ldr487 / 3/ 0/0.00/1.00/
PS-1, small motor, Dt=0.239", 6" nozzle to beam plume measurement
100 mm lens, 50 sweeps, starting 1 sec after Pc=100 psia 000001197

MALVERN Series 2600 SB.00 Master Mode 07 Mar 1995 1:57 pm

Upper	in	Lower	Under	Upper	in	Lower	Under	Upper	in	Lower	Under	Span 0.91
				57.7	0.0	49.8	100	9.82	0.0	8.47	100	
				49.8	0.0	43.0	100	8.47	0.0	7.30	100	D(4,3)
				43.0	0.0	37.0	100	7.30	0.0	6.30	100	3.77µm
				37.0	0.0	32.0	100	6.30	5.3	5.43	94.7	
188	0.0	162	100	32.0	0.0	27.5	100	5.43	23.4	4.68	71.3	D(3,2)
162	0.0	140	100	27.5	0.0	23.8	100	4.68	35.8	4.05	35.5	2.59µm
140	0.0	121	100	23.8	0.0	20.5	100	4.05	10.4	3.48	25.1	
121	0.0	104	100	20.5	0.0	17.7	100	3.48	1.0	3.02	24.1	D(v,0.9)
104	0.0	89.8	100	17.7	0.0	15.3	100	3.02	0.5	2.60	23.6	5.17µm
89.8	0.0	77.5	100	15.3	0.0	13.2	100	2.60	1.7	2.23	21.9	
77.5	0.0	66.8	100	13.2	0.0	11.4	100	2.23	2.7	1.93	19.2	D(v,0.1)
66.8	0.0	57.7	100	11.4	0.0	9.82	100	1.93	19.2	0.50	0.0	1.23µm
Source = Data:Input				Beam length = 77.0 mm				Model indp [3, 0]				D(v,0.5)
				Log. Diff. = 4.963								4.32µm
Focal length = 100 mm				Obscuration = 0.8622				Volume Conc. = 0.0022%				
Presentation = pia				Volume distribution				Sp.S.A 2.3136 m²/cc.				Shape OFF

2048 pia ldr487 / 3/ 0/0.00/1.00/
PS-1, small motor, Dt=0.239", 6" nozzle to beam plume measurement
100 mm lens, 50 sweeps, starting 1 sec after Pc=100 psia 000001197

MALVERN Series 2600 SB.00 Master Mode 07 Mar 1995 1:57 pm

Upper	in	Lower	Under	Upper	in	Lower	Under	Upper	in	Lower	Under	Span 0.91
				57.7	0.0	49.8	100	9.82	0.0	8.47	100	
				49.8	0.0	43.0	100	8.47	0.0	7.30	100	D(4,3)
				43.0	0.0	37.0	100	7.30	0.0	6.30	100	3.77µm
				37.0	0.0	32.0	100	6.30	0.1	5.43	99.9	
188	0.0	162	100	32.0	0.0	27.5	100	5.43	0.8	4.68	99.0	D(3,2)
162	0.0	140	100	27.5	0.0	23.8	100	4.68	2.0	4.05	97.0	2.59µm
140	0.0	121	100	23.8	0.0	20.5	100	4.05	0.9	3.48	96.1	
121	0.0	104	100	20.5	0.0	17.7	100	3.48	0.1	3.02	96.0	D(v,0.9)
104	0.0	89.8	100	17.7	0.0	15.3	100	3.02	0.1	2.60	95.9	5.17µm
89.8	0.0	77.5	100	15.3	0.0	13.2	100	2.60	0.6	2.23	95.3	
77.5	0.0	66.8	100	13.2	0.0	11.4	100	2.23	1.4	1.93	93.9	D(v,0.1)
66.8	0.0	57.7	100	11.4	0.0	9.82	100	1.93	93.9	0.50	0.0	1.23µm
Source = Data:Input				Beam length = 77.0 mm				Model indp [3, 0]				D(v,0.5)
				Log. Diff. = 4.963								4.32µm
Focal length = 100 mm				Obscuration = 0.8622				Volume Conc. = 0.0022%				
Presentation = pia				Number distribution				Sp.S.A 2.3136 m²/cc.				Shape OFF

2048 pia ldr487 / 3/ 0/0.00/1.00/
PS-1, small motor, Dt=0.239", 6" nozzle to beam plume measurement
100 mm lens, 50 sweeps, starting 1 sec after Pc=100 psia 000001197

Figure 10. Malvern Data from PS-1 Firing 3/7/95.

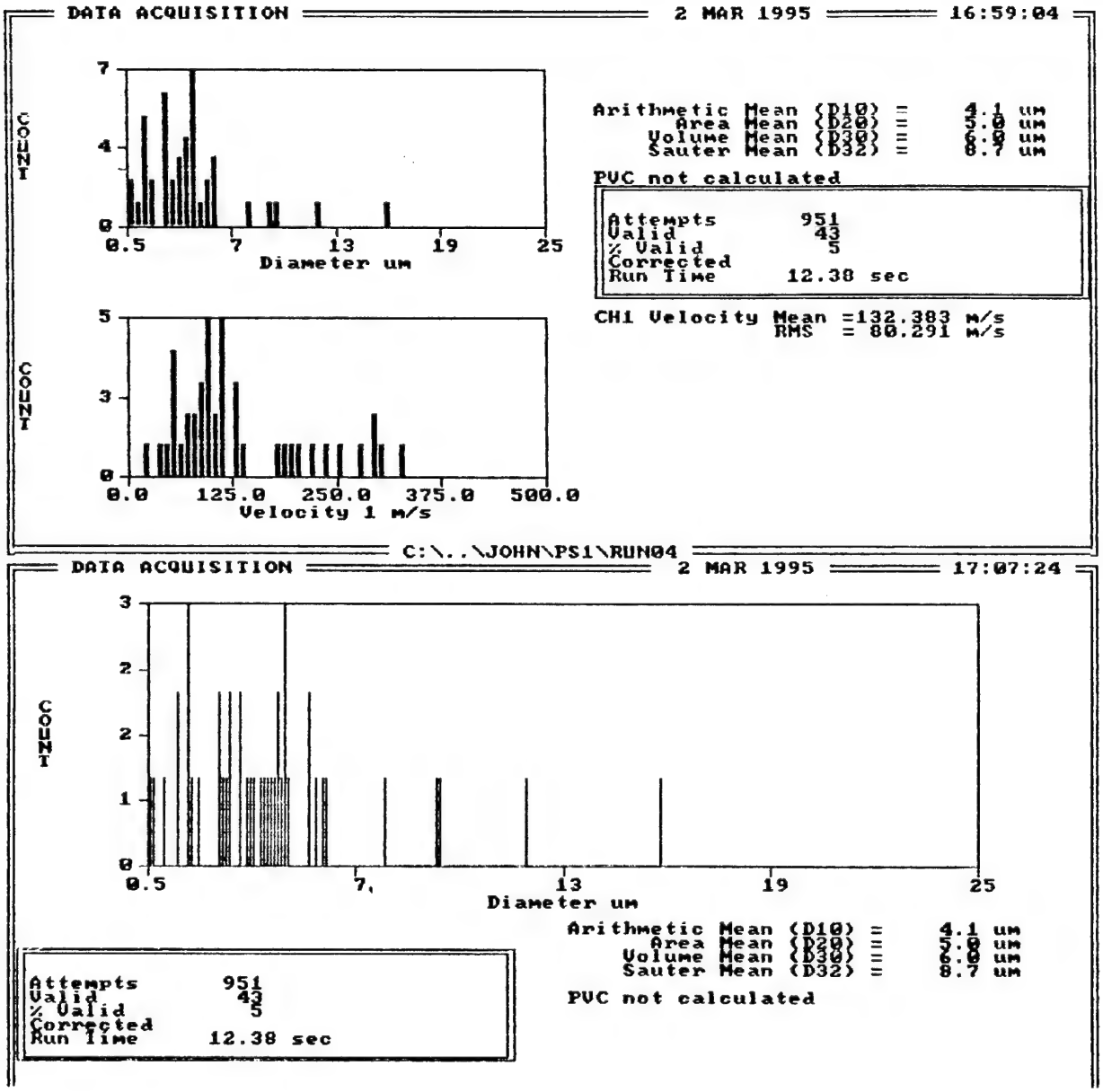

Figure 11. PDPA Data from PS-1 Firing 3/2/95.

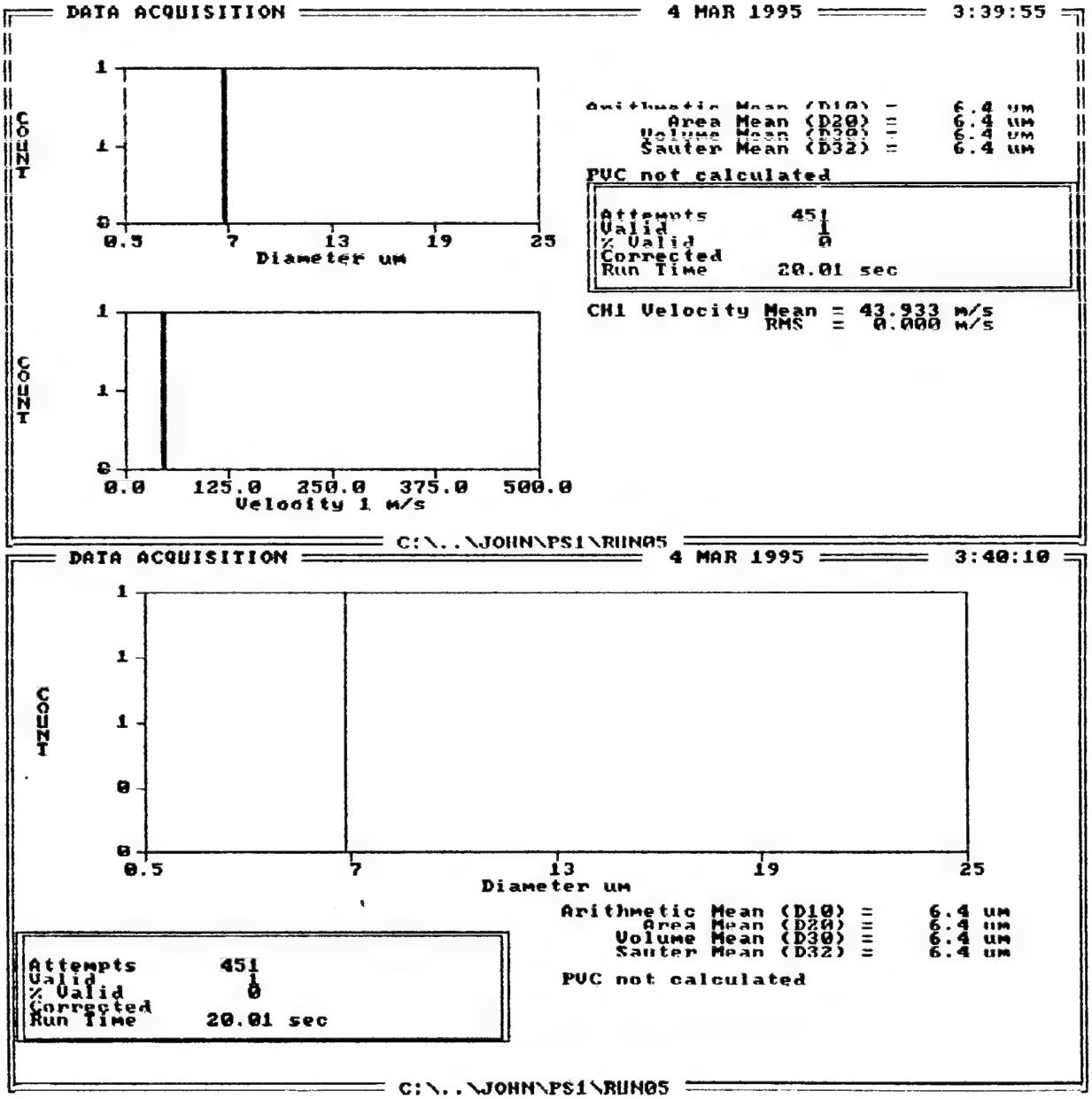

Figure 13. PDPA Data from PS-1 Firing 3/4/95.

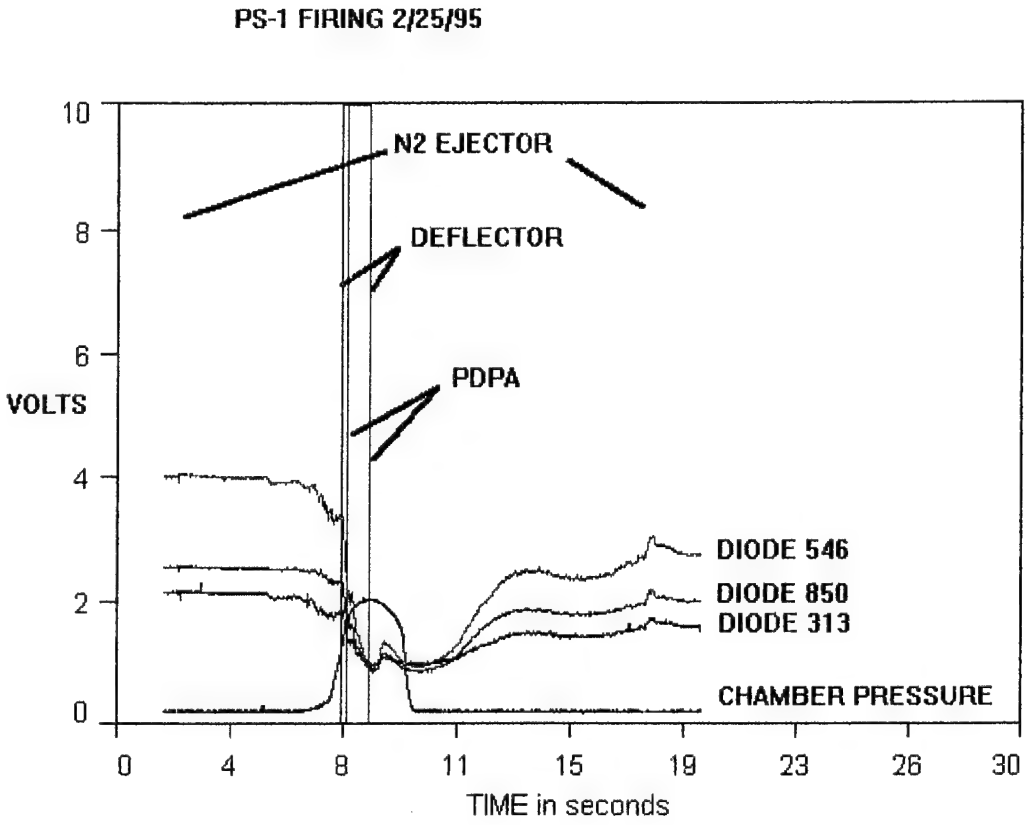

Figure 14. LABTECH Notebook Data Acquisition Program Plot of PS-1 Firing 2/25/95.

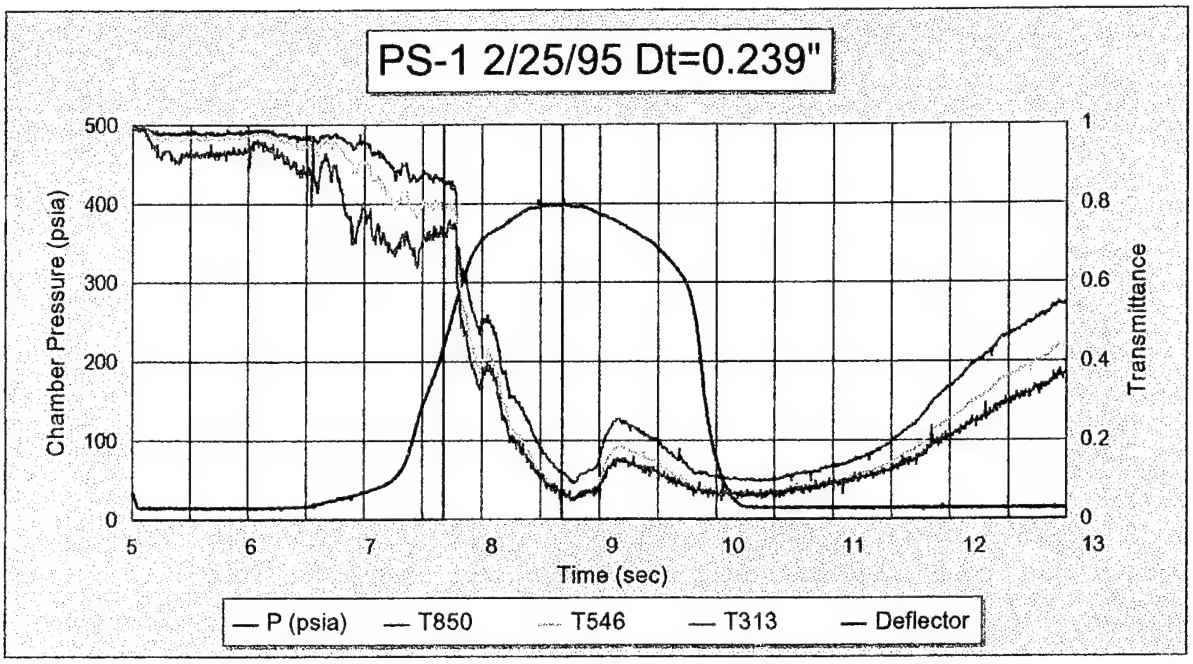

Diode Outputs (v)

	0.8500	0.5461	0.3130
0-2 sec	2.5443	4.0226	2.1436
8.78-8.82 sec	0.8406	0.8894	0.9525
no light	0.6600	0.7131	0.8822
T	0.0958	0.0533	0.0557

Figure 15. Normal Plot of PS-1 Firing 2/25/95.

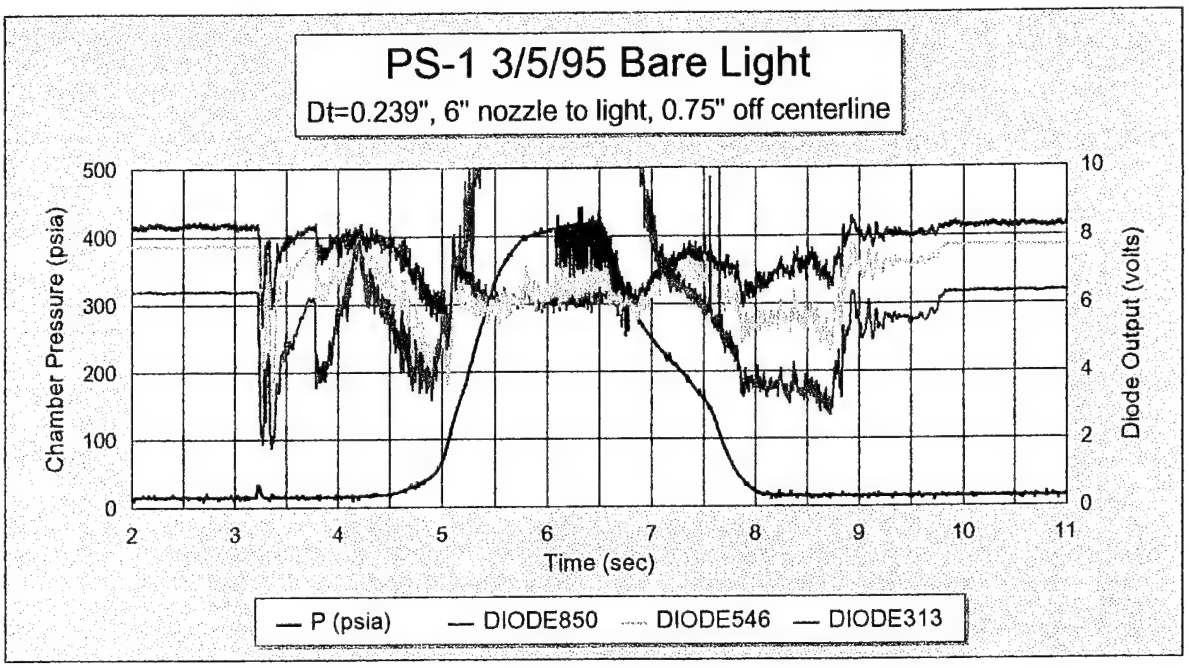

	Diode Outputs (v)		
	0.8500	0.5461	0.3130
0-2 sec	8.3110	7.7200	6.3999
5.4-6.9 sec	6.1475	6.2676	9.9938
no light	0.6270	0.6700	0.8060
T	0.7184	0.7940	1.6425

Figure 16. Bare Light (No Probe) PS-1 Firing 3/5/95.

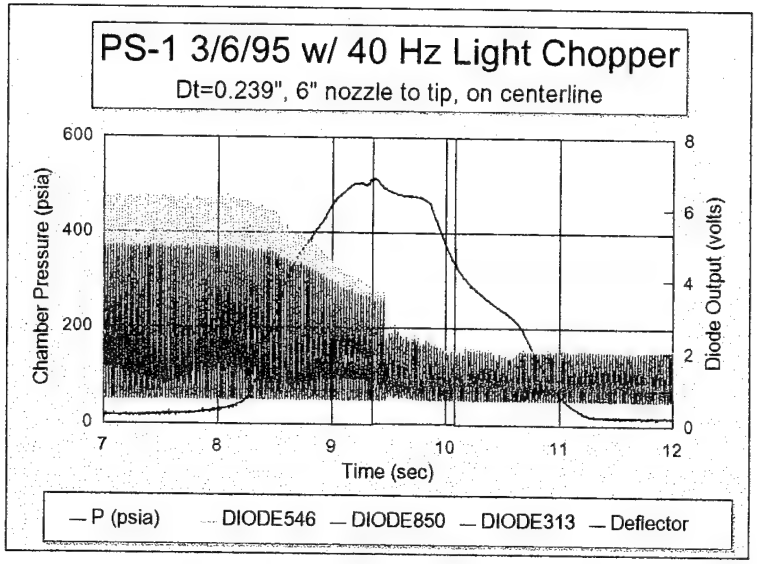

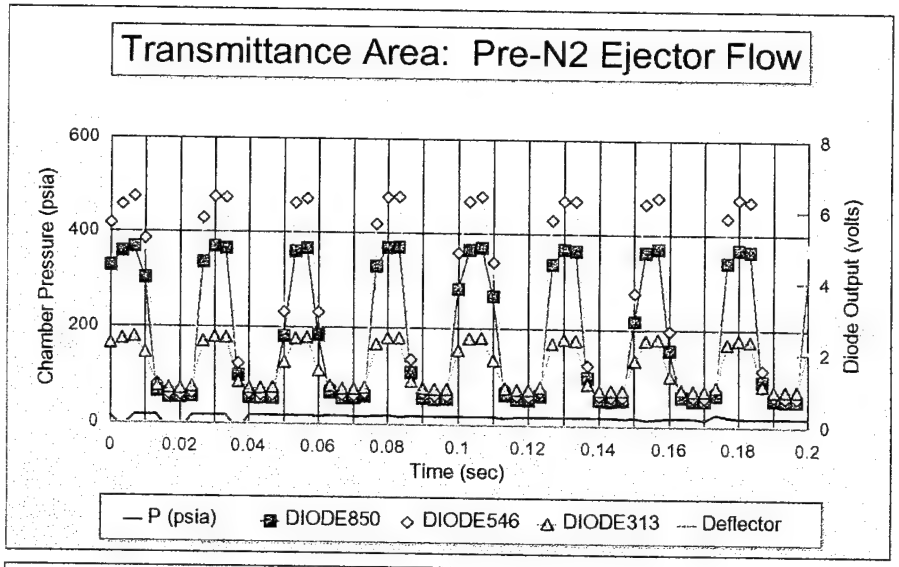

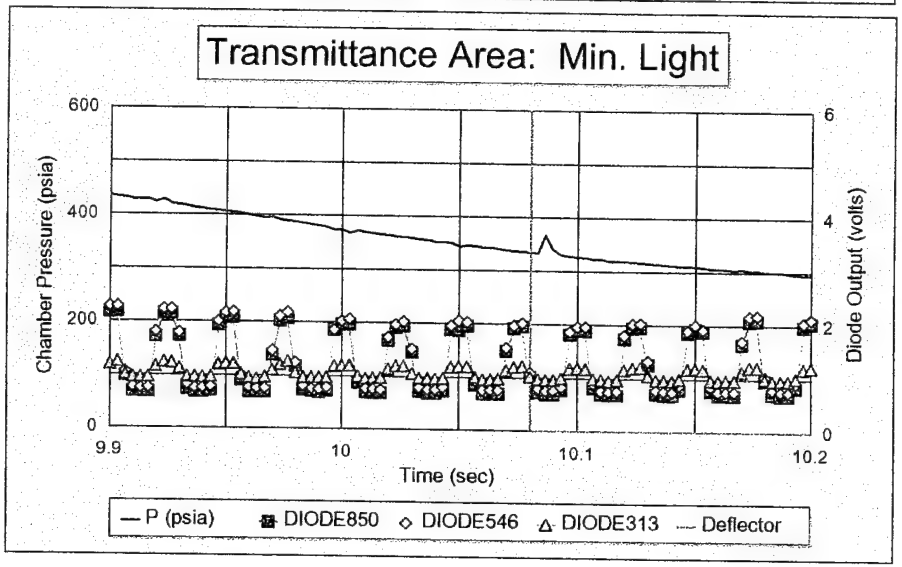

Diode Outputs (v)

	0.8500	0.5461	0.3130
0-0.2 sec	4.9280	6.3397	2.3840
10.0767 sec	1.9531	2.0117	1.2061
no light	0.6740	0.7420	0.9630
T	0.3007	0.2268	0.1711

Figure 17. PS-1 Firing 3/6/95.

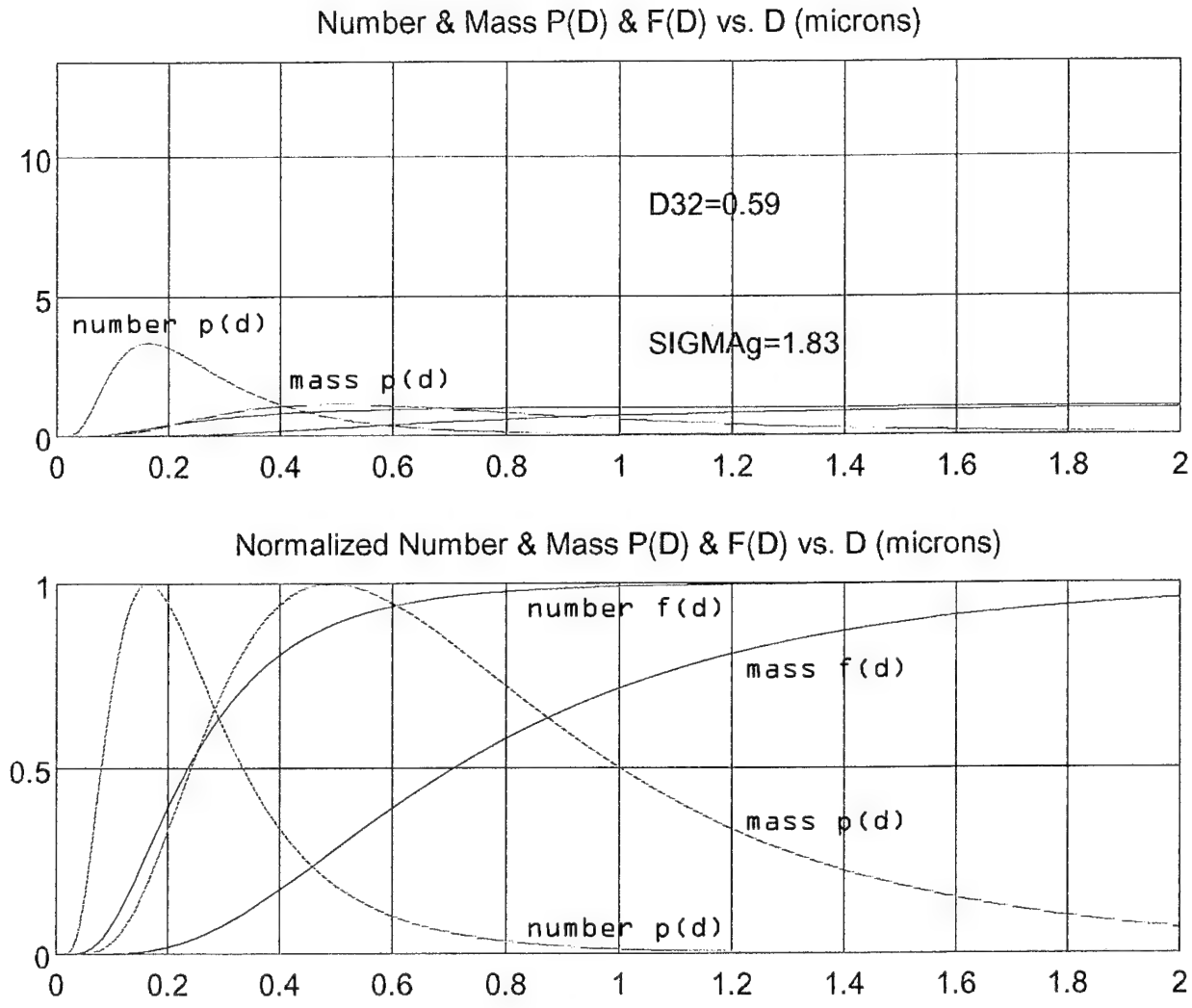

Figure 18. MATLAB Distribution Plots for "Small Particles".

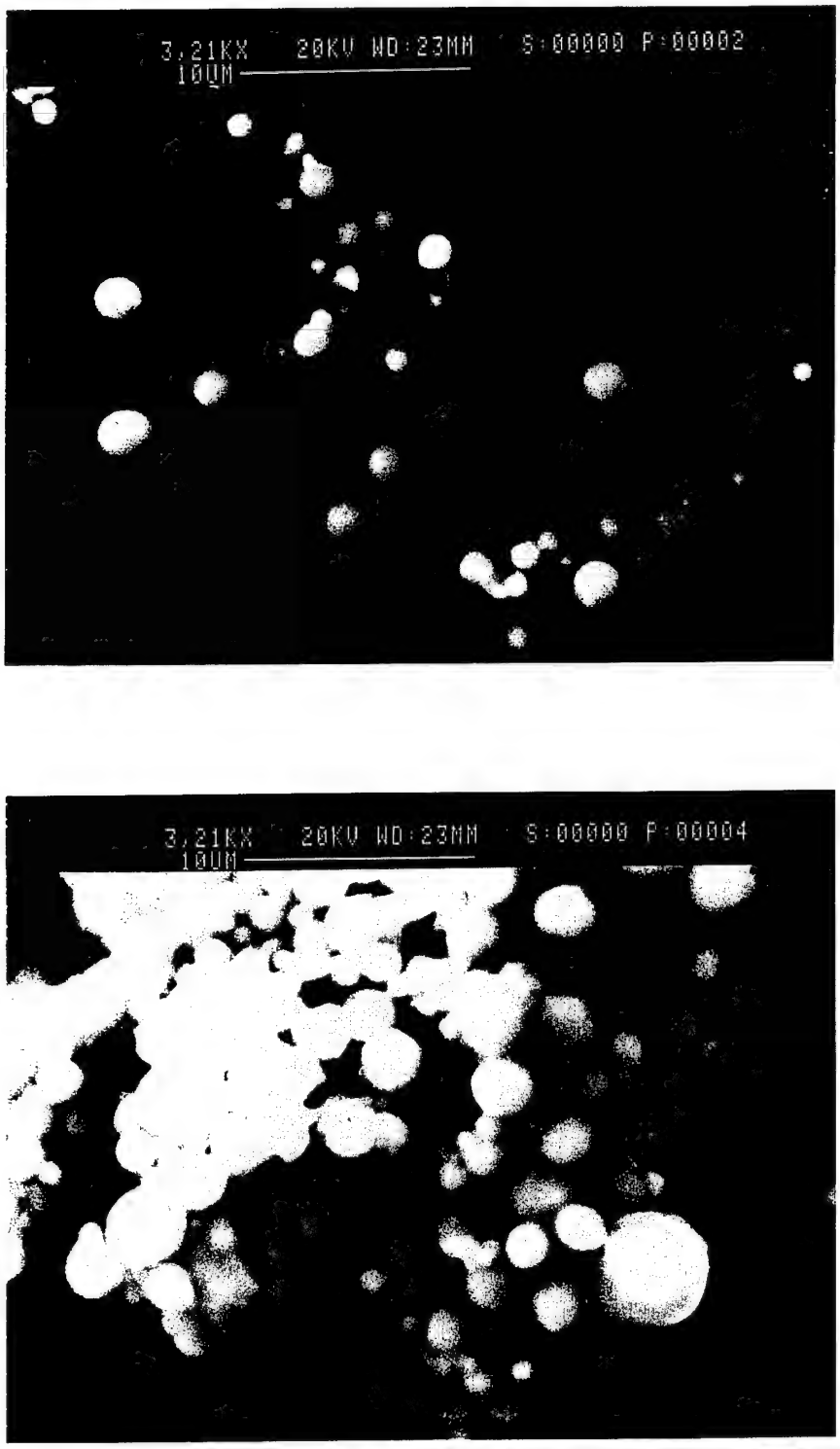

Figure 19. Scanning Electron Microscope Pictures of Al_2O_3 Collected in the Probe.

LIST OF REFERENCES

1. Price, E. W. et al., "The Al and Al_2O_3 Droplet Cloud in Solid Rocket Motors", presented at the 31st JANNAF Combustion Subcommittee Meeting: Sunnyvale, CA, October 19, 1994.

2. Reed, R. A., and Calia, V. S., *Review of Aluminum Oxide Rocket Exhaust Particles*, AIAA-93-2819, AIAA 28th Thermophysics Conf., Orlando, FL, July 6-9,1993.

3. Salita, Mark, *Characterization of Al_2O_3 Particulate Formed During Combustion of SRB Propellant (TP-H1148)*, Doc. No. TWR-18456, Morton Thiokol, Inc., Space Division, Brigham City, UT, September 13, 1988.

4. Blomshield, Fred S., et al., "Shuttle Redesigned Solid Rocket Motor Aluminum Oxide Investigations", presented at the 31st JANNAF Combustion Subcommittee Meeting: Sunnyvale, CA, October 19, 1994.

5. Salita, Mark, *Some Effects of Particle Size-Averaging on Rocket Motor Performance Prediction*, CPIA 17th PSS Meeting Minutes: Denver, Colorado, March 8-9, 1984.

6. Kerker, Milton, *The Scattering of Light*, Academic Press, Inc.: New York, NY, 1969, pp. 351-359.

7. Orr, Clyde Jr. and J. M. Dallavalle, *Fine Particle Measurement*, MacMillan Co.: New York, NY, 1959, pp. 25-35.

8. R. D. Cadle, *Particle Size Determination*, Interscience Pub., Inc.: New York, NY, 1955, pp. 27-49.

9. Hines, William W., *Probability and Statistics in Engineering and Management Science*, 2nd Edition, Wiley: New York, NY, 1980.

10. Miller, Irwin, *Probability and Statistics for Engineers*, Prentice-Hall, Inc.: Englewood Cliffs, NJ, 1977, pp. 114-117.

11. Conversation with Prof. Dave Herscovici, Department of Mathematics, Naval Postgraduate School, Monterey, CA, September 8, 1994.

12. Cashdollar, Kenneth L. et al., "Three Wavelength Light Transmission Technique to Measure Smoke Particle Size and Concentration", *Applied Optics,* Vol. 18, No. 11, June 1, 1979, pp. 1763-1769.

13. Vaughn, John K., *Measurement of Submicron Al_2O_3 Particles in Rocket Plumes*, Master's Thesis, Naval Postgraduate School, Monterey, CA, December, 1992.

14. Netzer, David W., Classnotes from "AA3852 Launch Vehicle Propulsion", Naval Postgraduate School, Monterey, CA, Fall, 1994.

15. *Oriel Corporation Catalog*, Vol. 2: Stratford, CT, 1994.

16. *Laser Doppler Velocimeter User's Manual*, Aerometrics: 550 Del Rey Ave., Sunnyvale, CA 94086, 1993.

17. *System 2600 Instruction Manual*, Malvern Instrument Ltd., Version IM026 Issue 2.2, November, 1991.

18. Laredo, David, et al., "Motor and Plume Particle Size Measurements in Solid Propellant Micromotors", *Journal of Propulsion and Power*, Vol. 10, No. 3, May - June, 1994.

19. Laredo, David, and Netzer, David W., "The Dominant Effect of Alumina on Nearfield Plume Radiation", *J. Quant. Spectrosc. Radiat. Transfer*, Vol. 50, No. 5, 1993, p. 519.

20. Kim, H. O., et al., "Measurement of Submicrometer Al_2O_3 Particles in Plumes", *Applied Optics*, Vol. 32, No. 33, Nov. 20, 1993.

21. Holman, J.P., *Experimental Methods for Engineers*, McGraw-Hill, Inc.: New York, NY, 1966, pp. 37-39.

INITIAL DISTRIBUTION LIST

1. Defense Technical Information Center — 2
   Cameron Station
   Alexandria, VA 22304-6145

2. Library, Code 52 — 2
   Naval Postgraduate School
   Monterey, CA 93943-5101

3. Prof. David W. Netzer, Code AA/Nt — 1
   Naval Postgraduate School
   Monterey, CA 93943-5002

4. Prof. Oscar Biblarz, Code AA/Bi — 1
   Naval Postgraduate School
   Monterey, CA 93943-5002

5. Chairman, Code AA — 1
   Department of Aeronautics and Astronautics
   Naval Postgraduate School
   Monterey, CA 93943-5002

6. Chairman, Code SP — 1
   Space Systems Academic Group
   Naval Postgraduate School
   Monterey, CA 93943-5002

7. Captain Thompson — 1
   Office of the Chief of Naval Operations
   Code N63, Room 4E679 The Pentagon
   Washington, DC 20350-2000

8. Commander, Naval Space Command — 1
   ATTN: N112
   5280 4th Street
   Dahlgren, VA 22448-5300

9. LT John Manser 2
c/o Rev. & Mrs. William Johnson
34 Aberdeen Lane
Southampton, NY 11968